THE DETERMINATION OF BORON USING ^{11}B(p, α)^{8}Be NUCLEAR REACTION

BY

AZWIHANGWISI IREN MABUDA

Thesis presented in fulfillment of the requirements for the degree

MAGISTER SCIENTIAE

In the Department of Physics

University of the Western Cape.

Supervisor: Dr W.J Przybylowicz

Materials Research Group

iThemba LABS, Somerset West

Co-supervisor: Prof D. Knoesen

University of the Western Cape

Department of Physics

November 2008
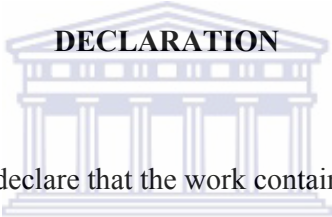
DECLARATION

I, the undersigned, hereby declare that the work contained in this thesis is my own

original work and that I have not previously in its entirety or in part submitted it at

any other university for a degree.

Signature: ………………….…   Date: ………………..…

ACKNOWLEDGEMENTS

Firstly, I, the author would like to give thanks to God the Almighty that by His grace and love I completed this thesis. I would also like to extend my sincere appreciation to the following people:

- Dr W. Przybylowicz, my supervisor, many thanks for your guidance and all the support you gave me throughout this joint work.

- Prof D. Knoesen, my Co-supervisor and the Department of Physics at University of the Western Cape for allowing me to register with you.

- Dr R. Bucher, how can I forget your contribution; you were such an inspiration in most times. Thank you for the long hours you spent on my thesis, your positive comments & patience are much appreciated.

- Thanks to all the iThemba LABS technicians, Karl Springhorn, Lawrence Ashworth, Nieldane Stodart, Colin Doyle and Solomon Marsh, for the maintenance of the experimental equipments.

- Dr Manyala thanks for your words of encouragement, many helpful discussions and all the support you gave me.

- Materials and Research Group people at iThemba LABS without you this journey would have been difficult, your kindness and support I won't forget it.

- Mandla Msimanga, Philip Sechogela, Mpho Makgale and Praise Sibuyi guys you such a blessing, I'm grateful for everything you did for me in this thesis.

- Mavhungu's family, I won't forget your encouragement, prayers and all the support you gave me throughout my studies, thank you.

- Mr J. Maselesele and family you have been so kind to me, thank you for your love and support.

- To all my friends, especially Alson Biyela, Suzan Bvumbi, Daphney Singo, Joele Mira and Tshifhiwa Madiba I appreciate all the goodness I find in you in my everyday life.

- To my family, my grandmother Miss Nyamukamadi Mabuda and Aunt Ndivhudzannyi Mabuda ndi livhuwa thikhedzo yavho, lufuno lwavho, na dzithabelo dzavho uri ndi kone u khunyeledza uno mushumo.

I dedicate this thesis to my late mother Elinah Mabuda who always encouraged me to further my studies and to my late grandfather Mr. Thavhaliyawa Joseph Mabuda who always wanted to see the completion of my studies, rest in peace.

ABSTRACT

Mabuda Azwihangwisi Iren[1, 2]

1. *iThemba LABS, Material Research Group, P.O.Box 722, Somerset West, 7129*

2. *University of the Western Cape, Department of Physics, Private BagX 17, Bellville 7535*

Determination of trace quantities of boron is required in various studies of materials and in geology. Using $^{11}B(p, \alpha)^8Be$ nuclear reaction with focused proton beam of 670 keV energy is one of the few microanalytical techniques capable of achieving detection limits in the 5-10 ppm range. The set-up for the determination of boron with high sensitivity was developed at iThemba LABS nuclear microprobe (NMP) facility by using a PIN photodiodes detector. The trace elements such as boron and lithium were analyzed using the nuclear reaction analysis (NRA) method.

This project aims at performing microanalysis of boron by NRA method and reaching the developmental phase in which routine, non-destructive boron analyses would be possible at detection limits below 5 ppm. A ^{228}Th source was used for energy calibration of the detector. Five set of standards and unknown samples with a wide range of boron concentrations were analyzed in order to demonstrate the effectiveness of the $^{11}B(p, \alpha)^8Be$ reaction by NRA technique. The standards were used to calibrate the boron yield with respect to their concentration in order to determine the boron concentration of the unknown specimen from the calibrated curve. The determination of the detection limit was also addressed. The concentrations of boron from Mts+Tu 950 glass samples were ranging between 0.17-1.05 wt % and the detection limit of 8.6 ppm for the minimum counts of 100 for 1μC accumulated charge was obtained.

Contents

List of figures

List of tables

CHAPTER 1

1.1 Introduction

Boron (B) is a chemical element with atomic number 5. It is found in sedimentary, volcanic, plutonic and metamorphic environments. B is a major industrial material that has been widely used in ceramics, glasses, insulation, soaps and fuel technology [1]. It is well-known although not very abundant element in the Earth's crust [2]. Skogby *et al*. [3] noticed that B may be a more significant component in geological processes in several rock-forming minerals than believed before. Boron has two naturally occurring isotopes: ^{10}B and ^{11}B with natural abundance of 19.8% and 80.2% respectively and there is a fundamental advantage in using methods based on the more abundant isotope [4].

The detection of trace quantities of boron is important in various studies of materials and metallurgical, biological as well as in geological analyses [5]. The determination of boron depth profile in materials can be obtained by secondary-ion mass spectrometry (SIMS) [6]. However, with SIMS there are problems related to ion beam mixing during the analysis and the loss of information about the surface that results from the time taken to achieve the equilibrium sputtering conditions [6]. Laser ablation inductively coupled plasma mass spectrometry (LA-ICP-MS) can be used to control the ion implantation process from ^{11}B$^+$ dopant ion and to find the deposited dose [7]. This technique is also used for analysis of boron isotopes ($\delta\,^{11}$B) at the nanogram level. LA-ICP-MS does not require any chemical separation of boron prior to analysis [8]. Nuclear reaction analysis (NRA) using the ^{11}B(p, α)^{8}Be reaction offers the advantage of an isolated α peak well above the incident protons energy and high cross-section [9]. This nondestructive

technique is capable of measuring low concentrations of boron and allows achieving a distinct determination of the boron elemental profile. The quantitative determination of boron with its lateral and in-depth distributions can be achieved using the NRA technique [10]. The ^{11}B(p, α)^{8}Be* reaction with proton energy of 670 keV is one of the most attractive nuclear reaction for boron analysis. This reaction is preferred for its sensitivity to determine the more abundant boron isotope ^{11}B, it has a large cross section of 300 mb, it is almost free from interferences with other nuclear reactions and allows relative quick measurements [10; 11].

Boron plays an important role in medical sciences due to ^{10}B(n, α)^{7}Li neutron capture reaction. Boron neutron capture therapy (BCNT) is a novel technique for cancer treatment based on the resultant short range α-particles that kill the cancerous cells. B is important in the nuclear power industry because of its high neutron absorption cross section. It is also used in pressurized water reactors (PWRs) as a primary coolant system in the form of boric acid to control the reactivity in the core [12]. Boron compounds, boric acid is used as a mild antiseptic and insecticide for cockroaches, and borax as a cleaning flux in welding and as water softener [1].

1.2 Scope of investigation

The purpose of this study was to perform microanalysis of boron by the NRA method and to reach the phase in which routine, non-destructive boron analyses would be possible at detection limits below 5 ppm. The boron measurements were done with a proton ion beam and are based on the detection of the α- products from the ^{11}B(p, α)^{8}Be* nuclear

reaction, which is the 3α-reaction emitted after the interaction of the proton beam with the target material. The 3α-particles reaction has a broad resonance around 650 keV, which means the surface concentration is not the only one that is measured. The measured yield depends on the proton stopping power folded with the cross section **[13].**

A detector consisting of four large PIN diodes was used to capture the α-particles emitted from the above reaction. The obtained spectra were analyzed with the GeoPIXE software package. All the experiments were performed at the iThemba LABS nuclear microprobe facility. The Scanning Electron Microscopy (SEM) method was used for the image morphology and characterization of the minerals in the samples before performing nuclear microprobe (NMP) measurements. The positions of the samples were obtained using the PIXE technique with the proton beam energy of 3 MeV. The samples were then analyzed with the proton beam of 670 keV using the NRA technique. The calibration curve of the PIN diodes detector from boron yield with the set of standards was obtained. This was done to achieve the concentrations of boron from the unknown samples and to obtain the detection limits.

CHAPTER 2

Ion beam interaction with materials

2.1 General introduction to boron analysis

Light elements such as boron and lithium because of their small mass and the ability of boron to form volatile compounds, are likely to be developed in the last stage of magmatic differentiation [14]. These elements and their isotopic abundance can be used as tracers for petrological, thermodynamical and geological evolution of the rocks that host them in magmatic series. The nuclear microprobe implemented with ion beam analysis techniques is a useful method for the determination of such elements in solids [14]. Their concentration in volcanic rocks remains at the level of few ppm [15]. Boron behaves as an incompatible element in igneous systems and is concentrated in melt by crystal fractionation. For this reason boron is likely to be enriched in felsic and silicate differentiation of magmatism [16]. On the other hand, the quantitative measurement of B in many other applications, such as in biological, medical and metallurgical samples are important [5].

One efficient way of analyzing boron is by (p, $\alpha\gamma$) reaction. However in the analysis of organic samples such as teeth, liver, kidney etc. this method fails due to the presence of matrix effects for i.e.> 1.5 MeV [17]. The $^{11}B(p, \gamma)$ reaction at 163 keV bombarding energy with H^{2+} ions offers a good depth resolution and a good sensitivity while $^{11}B(\alpha, \alpha)$ which is easier and quicker to use can also be used for B analysis [18]. The $^{11}B(p, \alpha)^{8}Be$ reaction is widely used at 660 keV with high cross-section of 300 mb, but it does not provide depth profiling of boron, while $^{11}B(p, \alpha_0)^{8}Be$ reaction can be used to achieve the

depth resolution of boron **[10]**. The ^{11}B(p, α)^{8}Be reaction offers a more attractive alternative method as it reduces matrix effects because of low proton bombarding energy required **[17]**. Compared with other reactions, this reaction is almost free from interference with other reactions and allows quick measurements with very good sensitivity. This reaction is used in the nuclear microprobe in the field of material science. Boron cannot be analyzed easily if both low detection limits and good lateral resolution are required **[19]**. However by using the NRA method, the quantitative determination of boron as well as its lateral and in-depth distributions can be obtained **[10]**.
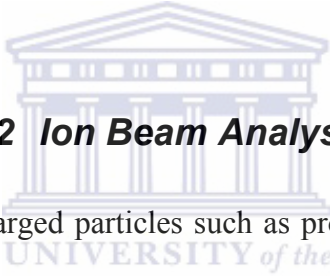
2.2 Ion Beam Analysis

In ion beam analysis (IBA) charged particles such as protons, alpha or heavier ions are focused on a target resulting in various interactions between the atoms in the target and the charged particles in the beam. The interactions usually take the form of Coulomb interactions, excitations or nuclear reactions. The radiation that comes out from the interaction is detected and its properties such as energy of scattered ions and secondary radiation are measured yielding information on structure of the target and distribution of the elements in the target **[50]**. The important advantages of the IBA methods are the relative speed and low cost for comparable accuracy to that of conventional techniques. Because of the use of a microbeam, only small samples are required. Even though a microbeam diameter of 1 μm can be produced today, geological IBA often requires much larger ion beam spots to attain results in reasonable time without destroying the sample by radiation damage **[20]**.
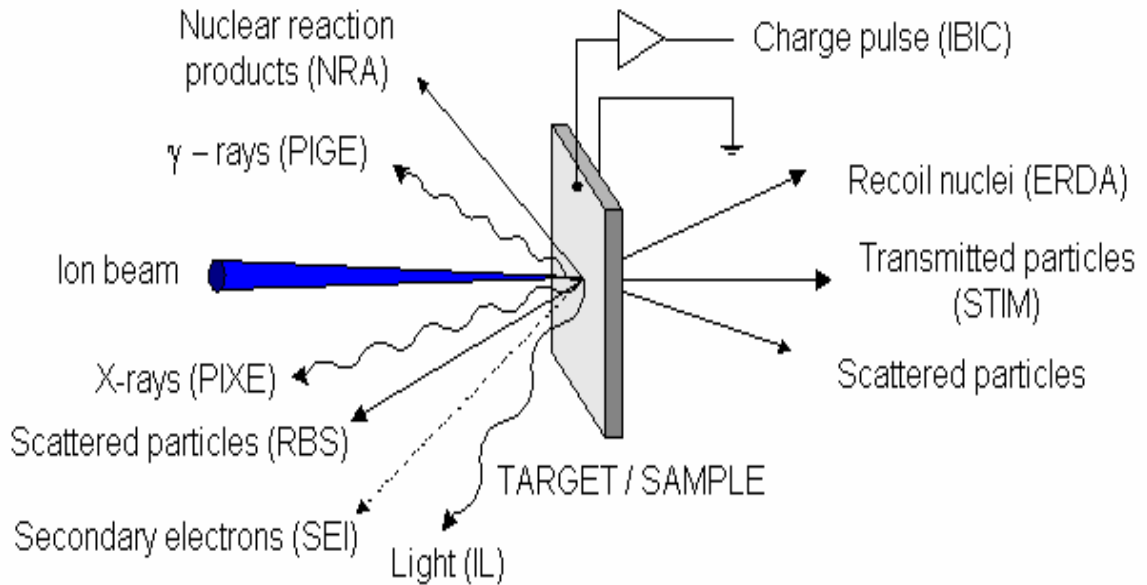
Fig. 2.1: Types of analytical technique possible at iThemba LABS NMP **[51].**

2.3 Analytical Techniques

After the incident ion beam enters the target, most of the individual particles penetrate the specimen in roughly their incident direction, gradually losing energy until they stop at a depth near the range of that particular matrix (see Fig 2.1). A very significant aspect of all the analytical techniques is the magnitude of the cross section that each target atom offers for producing the analytical signal emitted X-ray, charged particles, etc in the direction of the detector. As a general rule, the greater the cross section of the process being used for the analysis, the better **[21]**. The following analytical techniques are routinely used at the Material Research Group of iThemba LABS:

- Particle Induced X-ray Emission (PIXE)

- Rutherford Backscattering Spectrometry (RBS)

- Nuclear Reaction Analysis (NRA)

- Elastic Recoil Detection Analysis (ERDA)

In the present study, NRA technique has been used for α-particles detection from $^{11}B(p, \alpha)^8Be$ nuclear reaction.

2.3.1 Particle Induced X-ray Emission

Particle-induced X-ray emission (PIXE) is a method in which X-ray emission is used for elemental analysis. For PIXE analysis, the accelerated ions of sufficient energy (usually MeV protons) produced by an ion accelerator, will cause inner shell ionization of atoms in a specimen. Outer shell electrons drop down to replace inner shell vacancies, however only certain transitions are allowed. X-rays of a characteristic energy of the element are emitted. A Si(Li) X-ray detector is used to record and measure the emitted radiation and the intensities are then converted to elemental concentrations. The GeoPIXE software package is used for PIXE analysis and quantitative imaging. For point analysis, GUPIX software can be used [22]. PIXE is a multi-elemental technique with high sensitivity and detection limit across a wide range of atomic numbers. It is a powerful and non-destructive elemental analysis technique now used routinely by geologists, archaeologists and art conservators. It has the ability to cope with very tiny specimens as low as 0.1 mg and has high speed [23].

2.3.2   Rutherford Backscattering Spectrometry

Rutherford backscattering spectrometry (RBS) is a method of analysis and based on the detection of the charged particles elastically scattered by the nuclei of the analyzed sample. It allows a separation of atomic masses of the elements and to determine the profile distribution as a function of the detected energy. RBS is a method based on the Rutherford experiment that led to the discovery of the nucleus of an atom. It is a powerful tool for determining elemental composition, useful for example in characterization of thin films. Alpha particles are the most commonly used type of ion beams, accelerated to energies between 1 and 4 MeV. These particles are next focused at few micrometers on the sample to be analyzed in a vacuum chamber [50]. A schematic view of RBS analysis is shown in the Fig. 2.2 below.
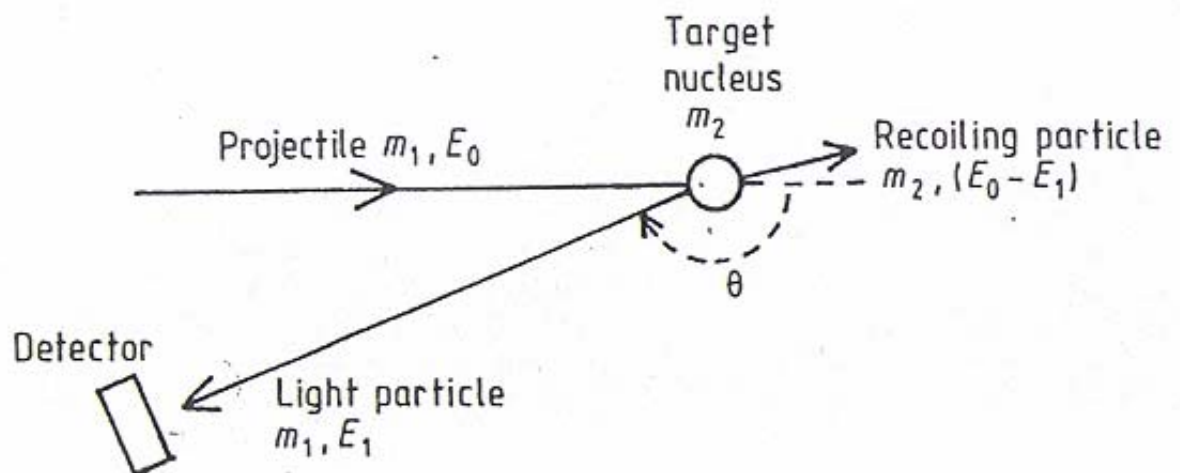
Fig. 2.2: A schematic view of RBS analysis [21].

2.3.3 Nuclear Reaction Analysis

NRA is an analytical technique involving a nuclear reaction between the incident beam and a target nucleus. When the energy of the incident particle approaches or exceeds the Coulomb barrier, i.e. the potential barrier caused by charge repulsion, nuclear reactions can occur, which results in the emission of α-particle [52]. The energy of the incident particle must be greater than

$$E = \frac{zZ}{\left[\sqrt[3]{a} + \sqrt[3]{A} \ \right]} \text{MeV} \qquad (2.1)$$

where z is the atomic number of the projectile, Z is atomic number of the target nuclei, a and A are the atomic weights of the projectile and target nuclei respectively [21].
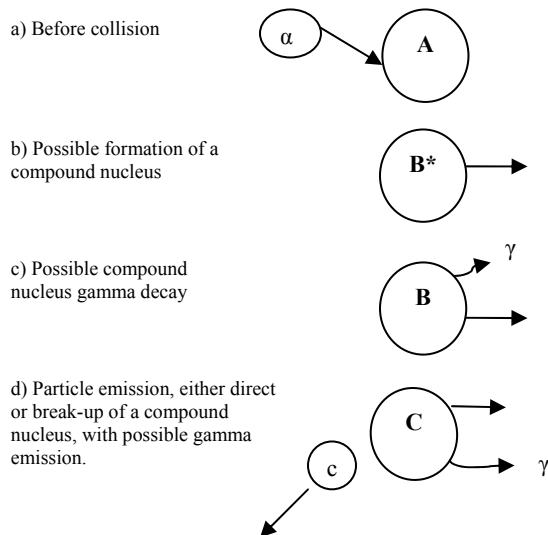
Fig. 2.3: An illustration of different types of reaction used in NRA. Small letters indicate light particles and capitals the heavier particles. The asterisk indicates an excited nucleus [21].

Fig. 2.3 shows that NRA can have different types of nuclear reactions. When a projectile α succeeds to penetrate the Coulomb barrier, a direct or a compound nucleus A reaction can be formed B*. The compound reaction can be produced by the protons and neutrons of the projectile α and target nuclei A. Fig. 2.3 pictures in (a) combined as in part (b) to form B, (c) illustrate the gamma ray emission and (d) shows the break-up of the compound nucleus to light and heavy particles c and C. When the compound nucleus reaction is formed, it will either loose its internal energy or break up into two particles [21]. NRA makes possible analysis of the lightest elements such as B and Li. NRA makes use of fast coincidence criteria, high time resolution and multiparameter techniques for identification [24]. Most of the light elements have a fairly high nuclear reaction probability when bombarded with protons with energies of few MeV. NRA is a very powerful technique that allows quantitative analysis; it provides good depth resolution and high sensitivity under well-chosen conditions. With microprobe facilities, it enables the determination of elemental surface distributions. Although, it provides chemical information, it is complicated and expensive [4]. NRA emerges to be effective method for the study of the boron depth profile in surface and other materials. Its sensitivity to ^{11}B(p, α)^{8}Be reaction is higher than that attained by other nuclear reactions [10]. This method is assumed to be free from matrix effect due to the stopping power and straggling caused by electron density variations. The nuclear microprobe boron analysis using this method has been in the past used for the characterization of thin films of interest to medicine, materials sciences and biological samples [3].

NRA can have different secondary radiation products such as charged particles, neutrons, gamma rays and sometimes beta decay prior to gamma rays [21].
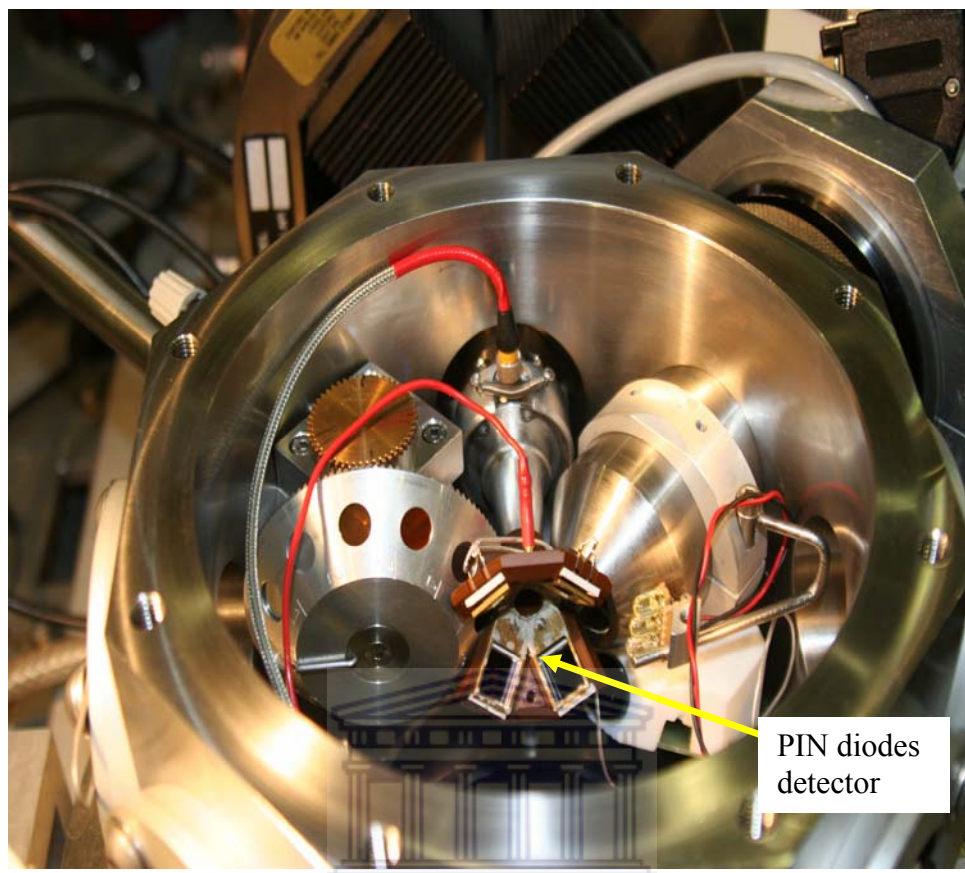
Fig. 2.4: The set-up for NRA technique with the PIN diodes detector at iThemba LABS**.**

2.3.3.1 NRA for charged particle detection

The most important difficulty in performing useful NRA with microbeams is to get enough signals with the relatively small cross sections in order to achieve a respectable level of sensitivity. This places an optimum for NRA on detecting the comparatively weak signal as efficiently as possible. The best way is to have a detector with a large solid angles of about 0.2 sr with 100% efficiency. The largest solid angle are usually achieved when an annular detector is used, mounted around the path of the incident beam. The most popular incident ions have been deuterons which give (d, p) reactions with several important light elements. One of this reactions used in microbeam work is

$^{10}B(d, p_o)^{11}B$ which is free from elemental interference because of its high amount of energy released in a nuclear reaction (Q value) **[21]**.

2.3.3.2 NRA for neutron detection

There are limited microbeam measurements with neutrons, since neutrons are much less convenient to detect than charged particles. The most suitable neutron detector is a liquid scintillator with capability to discriminate against gamma rays. Once neutrons of given energy are detected in this detector, they produce a roughly rectangular spectrum from maximum depending on the neutron energy down to zero. Fig. 2.5 shows the type of spectrum obtained when two neutron energies are present. This figure indicates that any counts in the upper part of the spectrum could come from certain elements; due to poor neutron energy resolution, microbeam (neutron) analyses have only involved reactions with high Q values **[21]**.
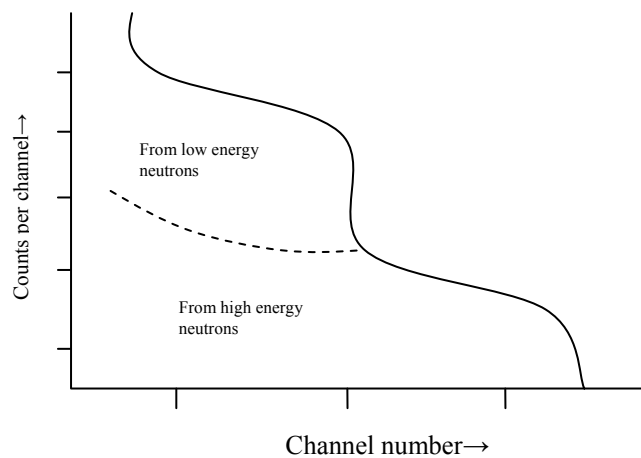
Fig. 2.5: The type of spectrum produced in a liquid scintillator by neutrons of two different energies **[21].**

2.3.3.3 NRA for gamma detection

Particle-induced gamma ray emission (PIGE) is a method based on the detection of prompt γ-rays emitted from the exited nuclei that are in excited state following a charged particle induced nuclear reaction. The energy of the γ-ray is a measure of the nature of the isotope and the intensity (counts). It is rapid, nondestructive and is generally used in the analysis of light elements from hydrogen through chlorine. Because it is based upon specific nuclear reactions, the sensitivity of PIGE varies greatly from isotope to isotope [16]. An example of NRA reaction with gamma ray emission is illustrated in Fig. 2.3 (c) and may be written as A(a, bγ)B, where "a" represent arrange of different ions. Beams of different ions, protons, deuterons, tritons, ^{3}He and ^{4}He have been used to perform NRA with gamma ray detection [21]. In order to do a sensitive analysis for a particular element, the beam must interact strongly with the element of interest, giving a gamma-ray which is free from interference from other gamma rays of similar energy [21].
The nuclear reactions mostly used in PIGE analysis of boron are [16].

$$^{10}\text{B}(p, p'\gamma)^{10}\text{B} \qquad\qquad \text{with} \quad E\gamma = 718 \text{ keV}$$

$$^{11}\text{B}(p, p'\gamma)^{11}\text{B} \qquad\qquad \text{with} \quad E\gamma = 2125 \text{ keV}$$

$$^{10}\text{B}(p, \alpha\gamma)^{7}\text{Be} \qquad\qquad \text{with} \quad E\gamma = 429 \text{ keV}$$

2.3.4 Charged Particle Activation Analysis

Charged particle activation analysis (CPAA) is an analytical method for determining the elemental concentration of trace elements in bulk of the sample. It provides excellent detection limits and accuracy **[25]**. CPAA is a powerful and very convenient method for the determination of light elements. It is based on the product of artificial radioactive nuclei, often positron emitters easily detectable by their annihilation radiation **[4]**. Its advantages are: solid samples are not dissolved before irradiation; surface contamination can be removed after irradiation so that only the bulk concentration is determined, and the method is not subject to reagent blank error. Its disadvantage is that it is complex and costly, less suitable for liquid samples, and the heating of the sample occurs during irradiation **[25]**. Compared to NRA, this technique cannot produce depth profiling and scanning **[53]**.
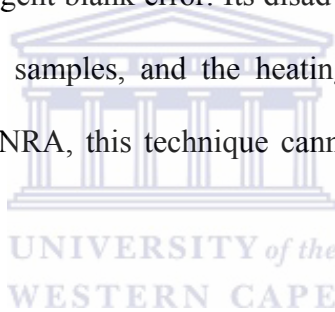
2.3.5 Elastic Recoil detection Analysis

Elastic recoil detection analysis (ERDA) is an analytical technique which uses the same elastic scattering between projectile and target nucleus as RBS, with the essential difference that in this case it is the energy of the recoiling target nucleus that is measured. The kinematics of elastic collision allows the recoil event to occur only in the forward hemisphere. For useful measurements the projectile should have a higher mass than the target nucleus. The figure below shows the geometry of ERDA.
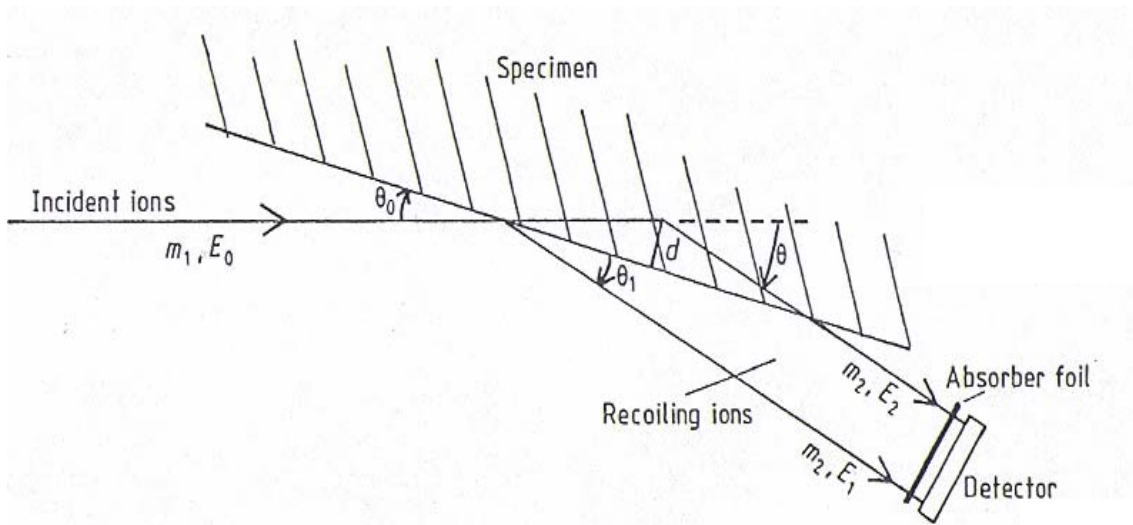
Fig. 2.6: A schematic view of a typical arrangement for ERDA analysis **[21].**

For an incident particle of mass m and energy E_0 the energy of the nucleus of mass m_R recoiling at angle θ is

$$E_R = E_0 \, \frac{4m/m_R}{1+m/m_R} \cos^2 \theta \qquad (2.2)$$

Which can be simplified as

$$E_R = E_0 \frac{4mm_R}{(m+m_R)^2} \cos^2 \theta \qquad (2.3)$$

where k is a quantity known as the kinematic factor

2.4 Other techniques for boron analysis

2.4.1 Secondary ion mass spectroscopy

Secondary ion mass spectroscopy (SIMS) is an analytical technique capable to provide a boron profiling view as a function of depth. The beam of a primary ion bombards the surface, causing ions (anions and captions), atoms and molecules to be ejected from the surface. The energy of the primary ions can be of the order of a few 100 eV to 10 s of keV, more than enough to eject atoms and molecules from the surface layers. The actual depth of interaction is usually a few nm. As the beam moves across the surface it sputters a hole deeper into the sample (see Fig. 2.7). Continuous detection of these sputtered secondary ions allows SIMS to create a depth profile of the surface and underlying layers to a depth of 10 microns with a depth resolution of 2-5 nm **[54]**.

It has high spatial resolution and high sensitivity. SIMS is characterized by considerable matrix interference effects. Therefore it requires the use of a standard of the same composition as the analyzed specimen and the determination of a calibration curve based on data for the range of phases **[26]**. The SIMS technique provides a unique combination of extremely high sensitivity for all elements from Hydrogen to Uranium detection limit down to ppb level for many elements, high lateral resolution imaging down to 40 nm, and a very low background that allows high dynamic range more than 5 decades. This technique is "destructive" by its nature sputtering of material. It can be applied to any type of material insulators, semiconductors, metals that can stay under vacuum **[55]**. The variation in secondary ion yield between different matrixes represents a complication. It is difficult to establish the sputtering rate and the range of the sputter ions. SIMS has

been extensively used for the investigation of boron concentration in semiconductors, since it probably offers the lowest detection limits [4].
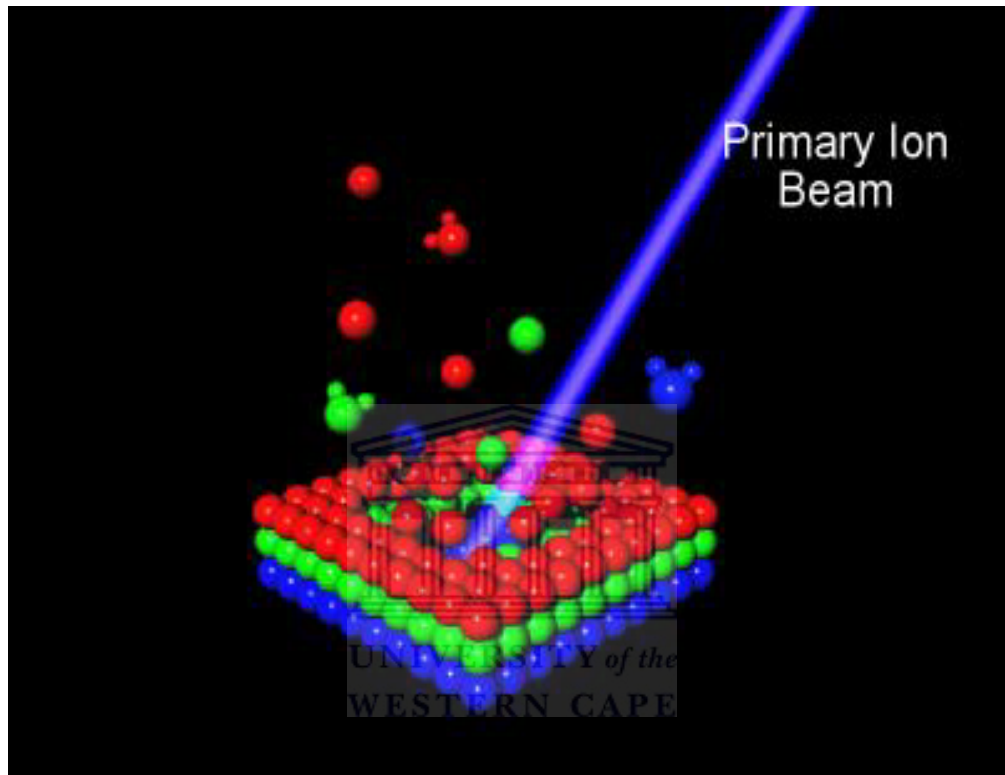
Fig. 2.7: A schematic diagram showing the primary ion beam beam penetrating through the sample [54].

2.4.2   Laser ablation ICP-MS

Laser ablation inductively coupled plasma-mass spectrometry (LA ICP-MS) is a microanalytical technique for the determination of trace elements in solid materials. It is applicable in many fields of studies such as geochemistry, materials science, forensics and environmental studies. LA ICP-MS combines the micrometer-scale resolution of a

laser probe with the speed, sensitivity and multi-element capability of ICP-MS, and rivals other microbeam techniques such as the proton microprobe and secondary ion mass spectrometry. It is mostly useful for in-situ analyses of trace elements for applications requiring the understanding of the spatial variation of elemental content within the sample.
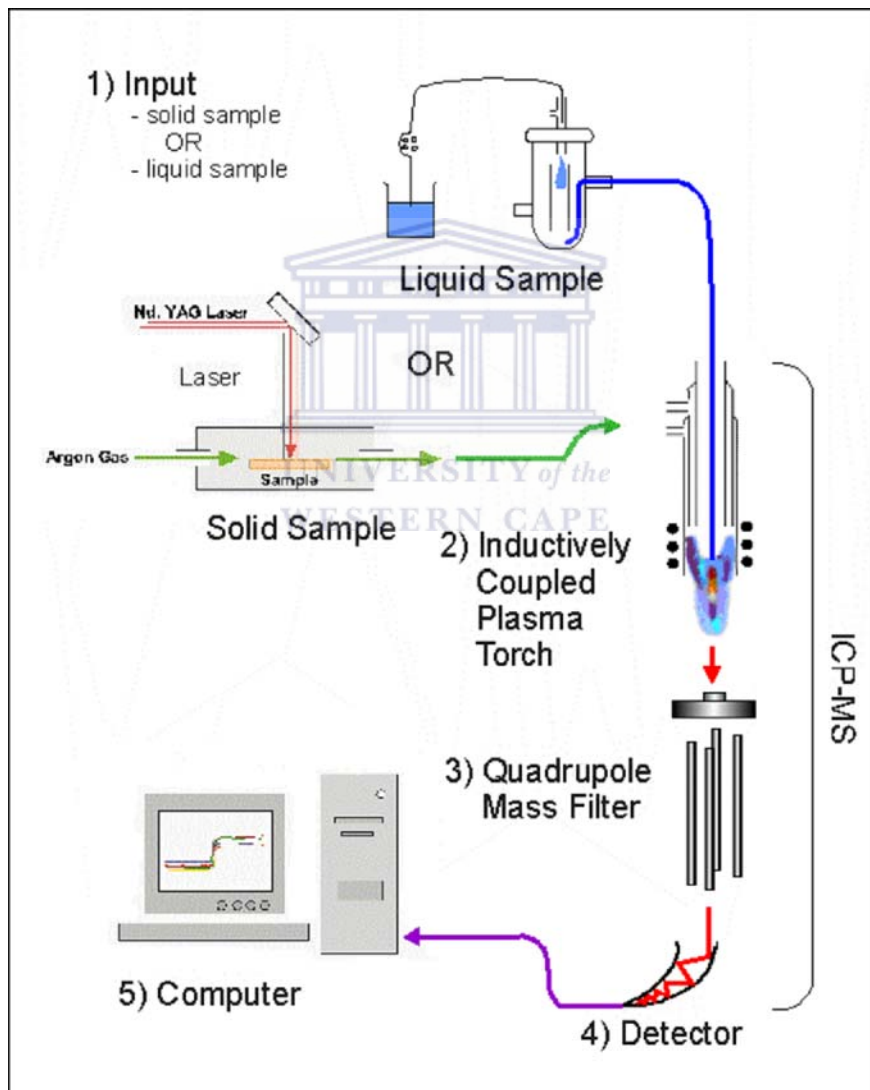
Fig. 2.8: Schematic view of LA-ICP-MS **[56].**

Compared to some other microbeam techniques, it has low spatial resolution, requires well-characterized, homogeneous standards, and requires prior knowledge of initial standard concentrations in samples and standards [57]. This method can be used for total dose measurements, to help monitor and to control the ion implantation process [7]. It also has fewer limits of sample size, low probability of contamination, little to no sample preparation and little matrix interference [27].

2.5 Comparison of nuclear methods with SIMS

The nuclear probes are considered to be either near surface or bulk-oriented and not highly sensitive to the surface composition. They sample the complete volume of minerals when a fine particles sample is irradiated with neutrons or they may explore up to depth of between 5 and 100 μm in thin section when irradiated with high energy charged particles [16]. In contrast the SIMS technique, samples a depth of less than 1 μm at the surface of a thin section. They are nearly free of matrix interference effects, while SIMS requires considerable care to ensure that the accuracy of the measurements is not affected by the sample matrix. In SIMS the secondary ion yield is dependent upon the type and energy of the bombarding beam, the composition and the surface topology of the target material. For the analysis of boron in minerals the sample is nearly transparent to nuclear probe, the resulting analytical signal, or both. Therefore, matrix interference effects are negligible and the conversion of the analytical signal into absolute boron concentration is simple [16]. The possibility to focus a charged particle beam makes them also suitable for lateral analysis [26]. The disadvantages of the nuclear methods are that

only some of the nuclear methods can be used as microprobe techniques. The number of facilities at which they may be performed is limited **[16]**.

2.6 Scanning Electron Microscopy

Scanning Electron Microscopy (SEM) is a microscopy which is able to produce high resolution image of a sample surface. It uses an electron beam rather than light. SEM has a large depth of field, which allows a large amount of the sample to be in focus at one time**. [58].**
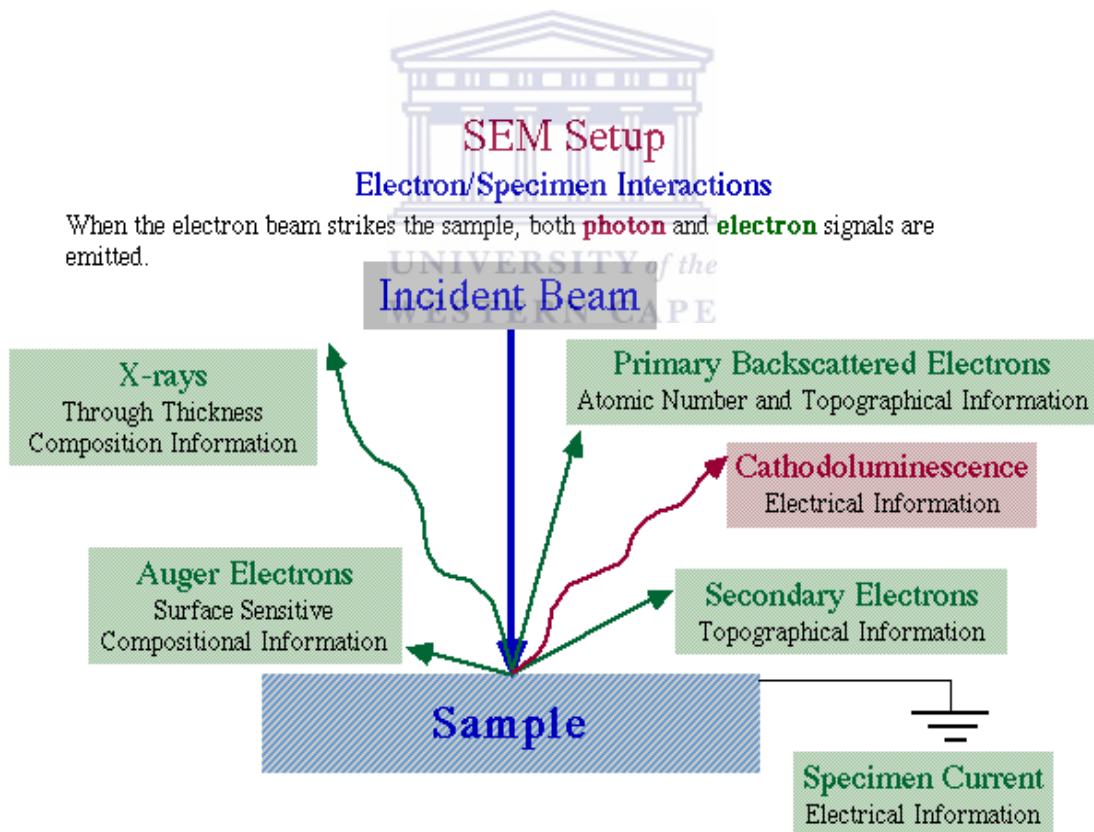
Fig. 2.9: The setup of Scanning Electron Microscope **[59].**

In use the column is always kept in vacuum. If the sample is in a gas filled environment, an electron beam cannot be generated or maintained because of a high instability in the beam. The transmission of the beam through the electron optic column would also be delayed by the presence of other molecules which could come from the sample or the microscope itself. The molecules could form compounds and condense on the sample. This would lower the contrast and obscure details in the image. **[59]**

2.6.1 SEM process
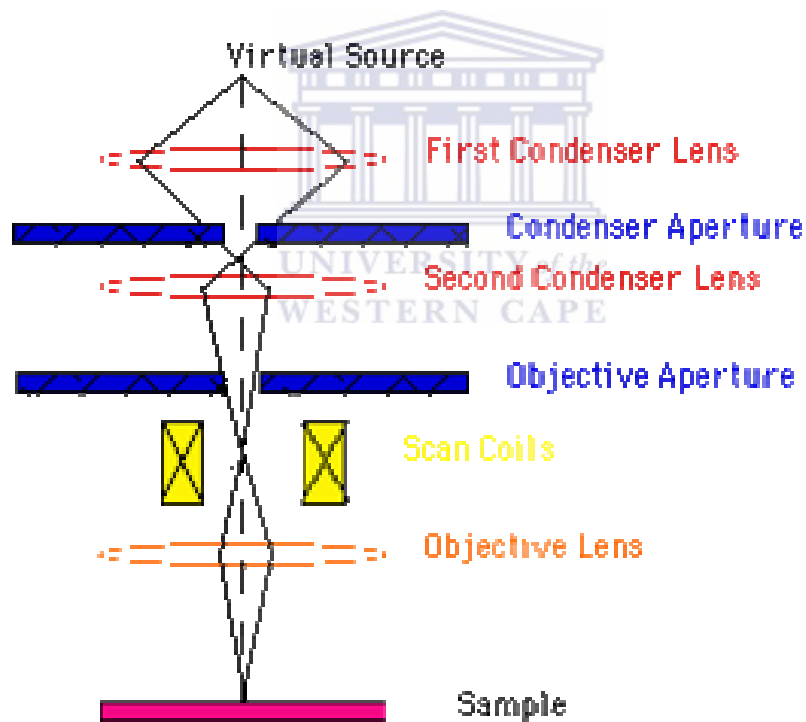
Fig. 2.10: The schematic of typical SEM functions **[60].**

2.6.2 How does a SEM function?

Considering the diagram on Fig. 2.10 above, the electron beam is generated by an electron gun which is represented by Virtual Source at the top that produces a stream of monochromatic electrons. The beam is condensed by the first condenser lens. It works in combination with the condenser aperture to eliminate the high-angle electrons from the beam. The second condenser lens forms the electrons into a thin, rigid, consistent beam and is usually controlled by the "fine probe current knob". The scan coils then scan the beam in a grid fashion, dwelling on points for a period of time determined by the scan speed. The final Objective lens focuses the scanning beam onto the preferred part of the specimen. When the beam strikes the sample and stays for a few microseconds, interactions occur inside the sample and are detected with various instruments. Before the beam moves to the next point these instruments count the number of interactions and display a pixel on a Cathode-ray tube (CRT) whose intensity is determined by this number. This process is repeated until the grid scan is finished and then repeated, the entire sample can be scanned 30 times per second [60].

2.7 Previous analysis of boron by CPAA

The determination of boron concentration and depth profiles by NRA are essential but difficult tasks in semiconductor, metallurgical and biological materials analysis [5]. One of the difficulties is the occurrence of several very broad resonances with a widespread overlap so that the compound ^{12}C formed at any given proton energy must normally be considered as superposition of states [28]. Depth profiles has been studied by the

^{11}B(p, α)^{8}Be reaction in semiconductors **[5]**. Boron and lithium can be detected using different types of ion beam techniques such as (p, α) and (n, α) reactions and particle induced gamma-ray emission (PIGE). The (p, α) reactions are the most appropriate IBA methods of determining B and Li concentration due to less interferences in comparison with other nuclear reaction analysis methods, higher sensitivity, and higher detection limit **[20]**. The ^{10}B (n, α)^{7}Li reaction is a very sensitive method that allows the determination of boron depth profile. In comparison with (p, α) method, PIGE **[29]** and alpha induced gamma-ray emission (AIGE) normally have 10-100 times lower sensitivities than (p, α) method under practical conditions **[17]**. The PIGE technique is particularly suitable for the analysis of light elements in thick geological and biological targets **[30]**.

IBA techniques used in this study are multi-elemental, non-destructive and appropriate for the determination of trace element contents **[31]**. In most cases it has been shown that the yield of the α product using the resonance at 660 keV proton energy, the technique can be successfully used in the nuclear microbe as far as the minimum detection limits is concerned **[19]**. Therefore the (p, α) nuclear reaction is a more attractive alternative, reducing matrix effect because of low proton energy needed. The optimum proton energy for boron analysis can be expected to be ≤1.0 MeV which is sufficient to induce a nuclear reaction which produces α- particles. When analyzing boron there is an interference of 0.2% of ^{18}O and 0.37% of ^{15}N natural abundances from ^{18}O(p, α)^{15}N and ^{15}N(p, α)^{12}C reactions respectively **[20]**. However, they can be neglected since their abundances are low in comparison with that of boron and their cross sections are small

compared to that of boron **[11]**. Boron has been analyzed from the tumour seeking substances by Boron Neutron Capture Therapy (BNCT) using $^{11}B(p, \alpha)^8Be$ reaction **[19; 32]**. The sensitivity of this nuclear reaction analysis was found to be about 0.01 ppm, if interference from other reaction is negligible **[5]**.

For the ^{11}B analysis, reactions induced by protons have the largest cross sections and the minimum competing interferences with the semiconductor matrices **[4]**. Beckman *et al.* **[33]** published the first measurement of the cross section of $^{11}B(p, \alpha)^8Be$ reaction. The authors claimed that experimental error was 30%, but they also accepted that the inconsistency between the proton backscattering yield and the Rutherford cross-section was as large as 50% **[33]**. Other authors published the accurate integral cross-section of $^{11}B(p, \alpha)^8Be$ reaction at 667 keV with the experimental error of 8%. Their integral cross-section at this energy was 50% higher than Beckman measurements **[5]**. This result corresponds to the findings of Vollmer *et al.* who obtained the same experimental error of 8% **[11]**. For analysis of light elements ($Z \leq 9$), for which NRA was very convenient, detection limits obtained with nuclear microprobe analysis are lower than 50 ppm **[34]**. Rio *et al.* **[15]** achieved a minimum detection limit of 10 ppm for B with the same reaction at $E_p = 700$ keV.

Analysis of B can also be performed from the energy spectrum of α-particles which covers the range between 0-6 MeV (see Fig. 2.11) **[17]**. The results from Mayer *et al.* **[9]** show that the elastic cross sections have absolute error of $\pm 6\%$, while **[35; 36]** cite an error of $\pm 7\%$. Hålenius *et al.* **[26]** estimate the errors of B concentrations in their samples with statistical error of the order of 5-10% and their main systematic error is induced by uncertainties in life-time corrections. The actual cross-section of the

^{11}B(p, α)^{8}Be in the energy range 0.4 to 1.6 MeV was achieved for the first time with the experimental error of 3.3% by Jiarui *et al.* [5]. Boron analysis using NRA methods have been used for characterization of thin films of interest to medicine and material sciences [4] or biological samples [19].
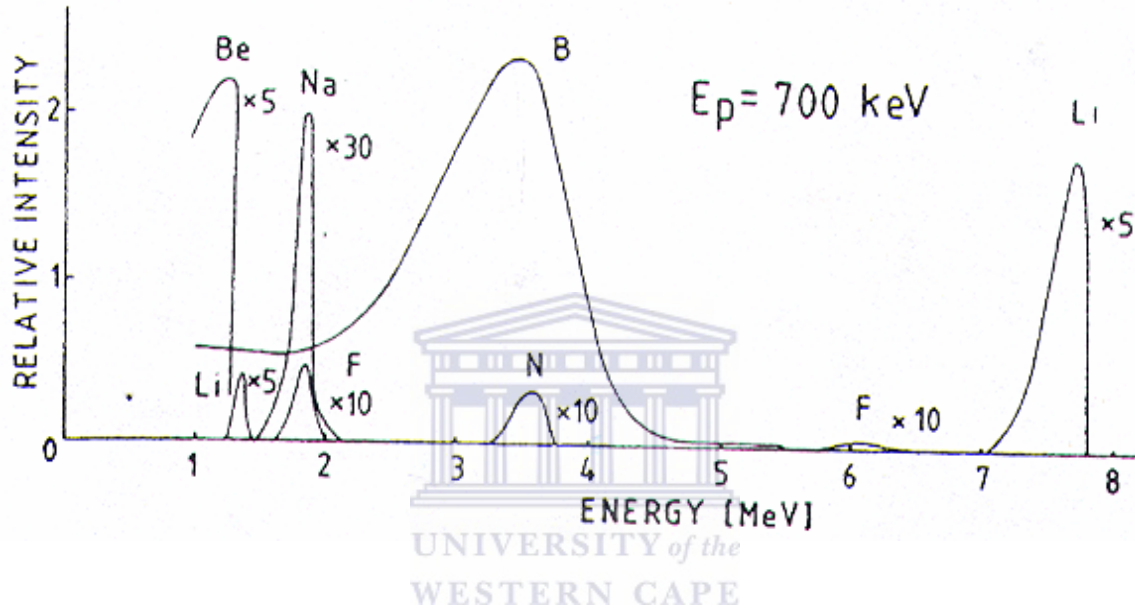
Fig. 2.11: The schematic illustration of energy range in which B can be determined [17].

Lightowlers and Collins [37] discovered three sources of systematic errors in their nuclear measurements: the cross calibration of the standards, the calculated stopping powers and the validity of assumptions. The reaction of proton with ^{11}B nucleus has four exit channels Vollmer *et al.* [11]:

$$^{11}B+p \rightarrow {}^{12}C^* \rightarrow {}^8B+\alpha_0 \rightarrow \alpha_{01}+\alpha_{02}+\alpha_0 \qquad (2.4)$$

$$^{11}B+p \rightarrow {}^{12}C^* \rightarrow {}^8B^*+\alpha_1 \rightarrow \alpha_{11}+\alpha_{12}+\alpha_1 \qquad (2.5)$$

25

$$^{11}B+p \rightarrow {}^{12}C^* \rightarrow \alpha_2 + \alpha_3 + \alpha_4 \qquad (2.6)$$

$$^{11}B+p \rightarrow {}^{12}C^* \rightarrow {}^{12}C + \gamma \qquad (2.7)$$
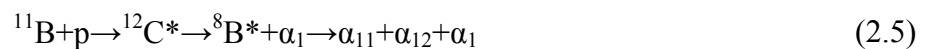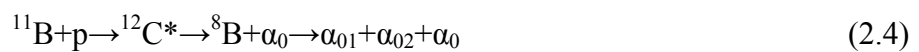
The reaction given by Eq. 2.6 is more attractive due to the huge cross-section at 660 keV [5] and in most of the studies it has been considered for B analysis. Fig. 2.12 gives a schematic representation of the different possible reactions between protons and ^{11}B at low energies. The ones which are underlined with thicker solid lines are more interesting and used for analytical applications [4].
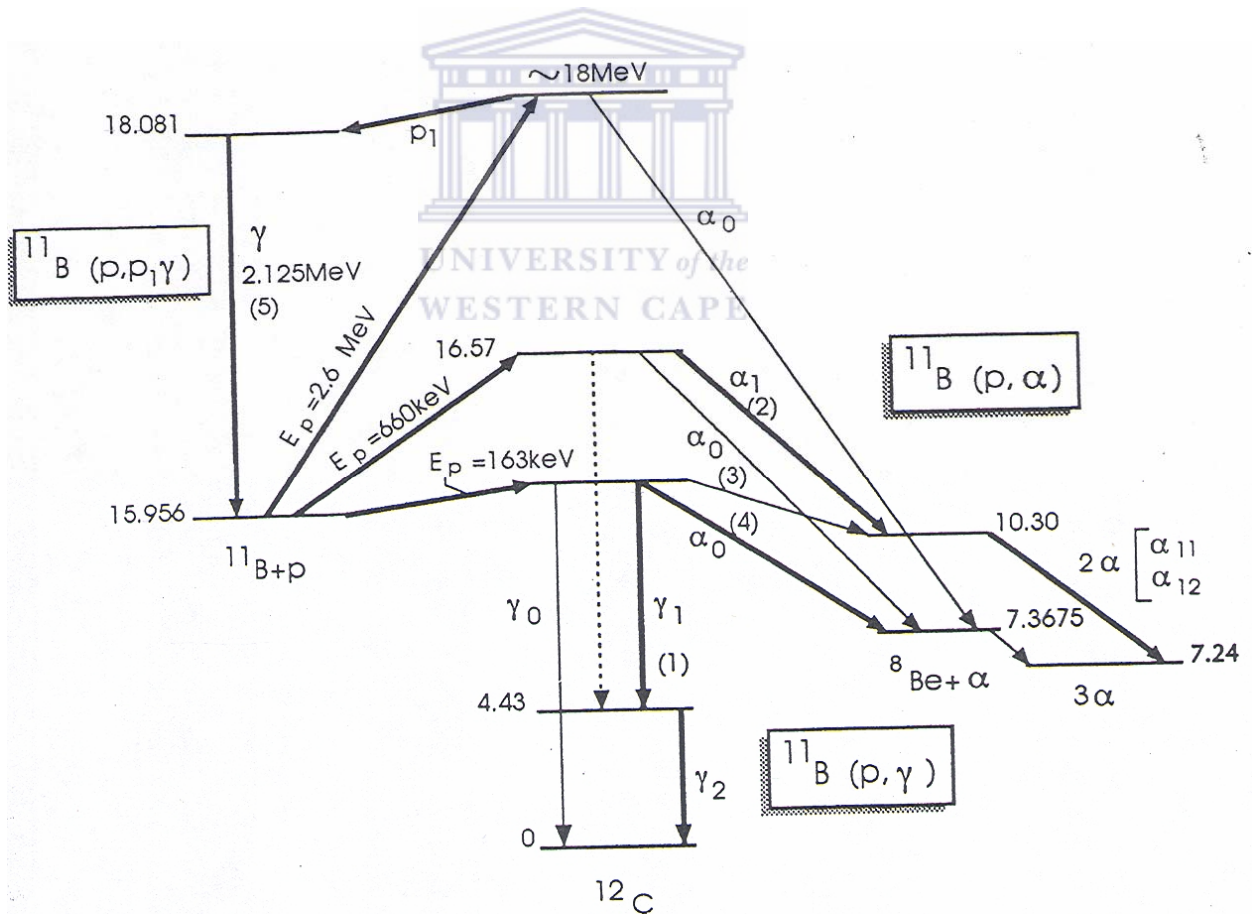
Fig. 2.12: The schematic representation of $^{11}B(p, \alpha)^8Be$ nuclear reaction [4].

The simultaneous determination of the two stable isotopes, ^{10}B and ^{11}B, was done through the measurement of proton induced gamma-ray. These have the advantage that the data obtained for each isotope is independent of any errors that may have been involved in the determination of the other isotope. Also the total boron content may be obtained without assuming a natural isotopic composition [38]. For the natural isotopic composition the use of gamma-rays induced on ^{11}B was preferred even though the yield per atom is less than that for ^{10}B. The results show that the relative standard deviation of the method is of the order of 3%, but the amount of inhomogeneity of the sample may be reviewed by the size of which this value is exceeded [38].

Olivier *et al* [39] determined B analysis in ore with deuterons of 2.7 MeV using prompt proton spectrometry method. The most possible reactions yielding prompt charged particles when stable nuclei are bombarded with deuterons of few Mev are (d, p) and

(d, α) reactions. The number of counts obtained was normalized to unit percent of boron as obtained from irradiation with 0.1 mC current. The mean number of counts from BN was used as calibration values for all these analyses. Boron counts observed from the same target but irradiated with different beam intensity showed a standard deviation of ±3.23% for a beam current between 0.3 and 1.0 μA. Higher beam current results in a decrease in B count, caused by the loss of deposited material associated with the higher temperature involved [39]. The relative error of the determination for low boron glass sample and significant difference between the mean values determined by this method and known B content seems to imply that the reported value of 0.22% is rather high. Authors suggested that the value 0.19% would have to be used to bring these results into line with those of the other samples [39].

The proton-induced prompt spectrometry method was also used to determine lithium in ores by Olivier *et al* [40]. The sample was irradiated with 4.5 MeV proton beam from the Van de Graaf accelerator. The gamma-ray spectra were obtained from the proton irradiation of the samples and detected with Ge(Li) detector. The determination of lithium was achieved by homogeneous spiking of the ore with five different B compounds of known composition. The aim was to demonstrate, how, by spiking lithium ores with suitable boron compounds and measuring the yields of Li and B prompt gamma-rays the Li concentration can be determined. The advantage of this method is that once the ranges of the analyte samples have been determined all analyzable elements can be determined without further spiking. Furthermore, if the sample contains an appropriate element of known concentration, this element can replace the spike for determining other components [40].

Boron content of steel samples was determined by measuring α-particles emitted from $^{11}B(p, \alpha)^{8}Be$ reaction at the bombarding energy of 1.110 MeV. The emitted α-particles were detected by SSB detector. The calibration curve found by irradiating a number of standardized steel was in the range of 1-140 ppm. Pure materials and standard steels were all irradiated in the form of solids with thicknesses greater than the range of particles in the respective materials [41].

CHAPTER 3

Experimental methods

3.1 Sample preparation

The samples investigated in this study were NIST 611, NIST 612, pure B, BN, tourmaline standard and Mts+Tu 950 thick glass samples. They were coated with a carbon layer to prevent the charge build up. The coatings were done for the preparation of the nuclear microprobe analysis of boron.
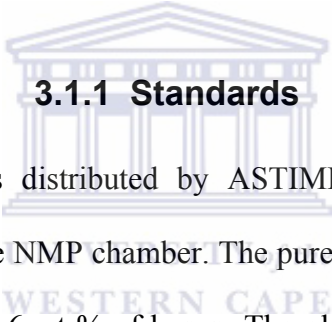
3.1.1 Standards

The set of standard materials distributed by ASTIMEX, B and BN standards are permanently mounted inside the NMP chamber. The pure boron has 99.9% concentration of boron while BN contains 43.6 wt % of boron. The glass standards from the National Institute of Standards and Technology, NIST 611, NIST 612 were also used for calibration purposes. These standards are widely used as potential microanalytical reference materials. The concentration of boron in these standards is 0.0351 wt % and 0.0032 wt % respectively [42]. Tourmaline standard contains 3.27 wt % of boron [3].

3.1.2 Tts-Tu 950 samples

Mts+Tu 950 is a thick glass material which contain low boron concentration. It is named Mts+Tu 950 because it is a mixture of an Australian metasediment from the Mt Stafford area and it consists of tourmaline and water. It has melted substantially at pressures

around 0.3 GPa and temperature above 900° C. The boron content in these glasses was not known. Therefore the concentration and the distribution of this element were established using the method developed in this thesis.

3.2 Methods

3.2.1 Scanning electron microscopy

Imaging of the samples and analysis of the phase compositions were accomplished using a Leo® 1430VP Scanning Electron Microscope at the Stellenbosch University before the nuclear microprobe measurements. Prior to imaging or any other analysis the samples were sputter-coated with either gold or carbon depending on the application. In this study it was a carbon layer as mentioned above. The sample to be viewed was mounted on a small stub with double sided carbon tape so that it could be better handled when mounting it on the SEM stage. The stub was placed on the SEM stage in a chamber under high vacuum. The beam was then switched on with energy of 30 keV. The image can then be viewed on the SEM screen. The electron beam can be focused to produce a sharp image and the magnification of the image can be set as required. The brightness and contrast can be adjusted to produce a clear image. The image can be saved in digital formats such as Tiff, Bitmap or Jpeg. The sample surface was characterized by backscattered electron (BSE) and/or Secondary electron images using an Oxford Instruments® 133KeV detector and Oxford INCA software.

3.2.2 Nuclear Microprobe Analysis

3.2.2.1 Introduction

The NMP at iThemba LABS was installed at the 0° beam line of the single ended 6MV Van de Graaf accelerator in 1991. The facility has been successfully used in the analysis of a wide variety of materials from the fields of archaeology, biology, geology, materials science and medicine. The ion beam analysis for this study was performed in this facility. NMP at iThemba LABS consists of three main parts [22]:

- Accelerator

- Ion beam line and focusing system and

- The experimental chamber
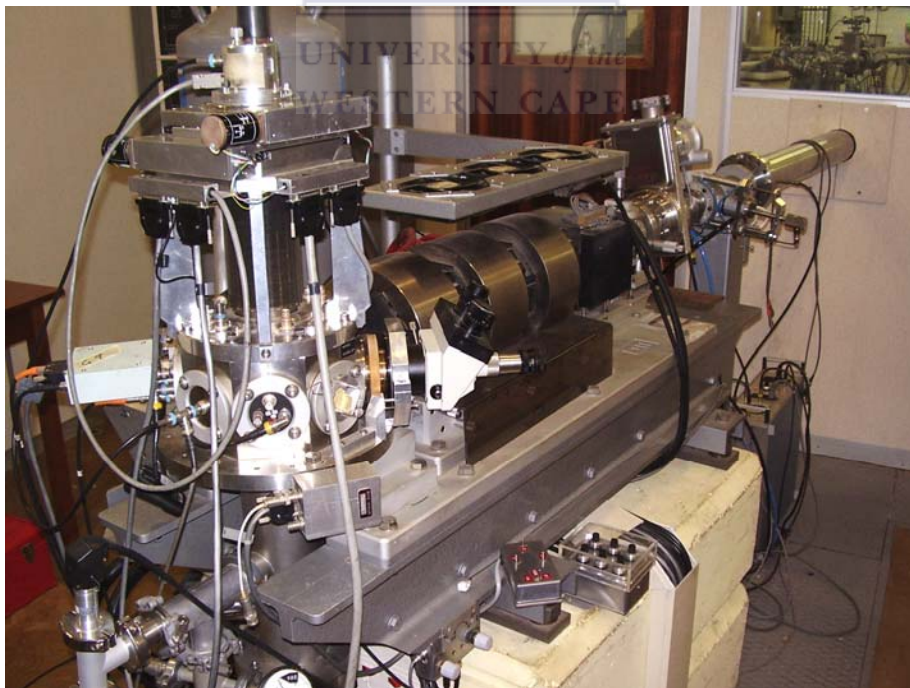
Fig. 3.1: iThemba LABS, Material Research Group, nuclear microprobe setup.

3.2.2.2 Accelerator

The accelerator used for the experiments at the Materials Research Group (MRG), iThemba LABS is a single ended 6 MV Van de Graaff accelerator manufactured by High Voltage Engineering in 1962. It accelerates the ions vertically downwards, and the energy stabilization and beam deflection are made by a 90º analyzing magnet. It remains the essential instrument that anchors the activities of the MRG. In the configuration used at present, ion beams are generated using the duoplasmatron source. The only ion beams used are protons or alpha particles [22]. The ions can be accelerated to the potential between 0.6 and 4.5 MV. Boron analysis in this study requires proton beam of 670 keV, close to the lowest possible potential, far from the optimum condition for this accelerator was used. Figure 3.2 below shows the layout of the Van de Graaf accelerator and NMP at iThemba LABS
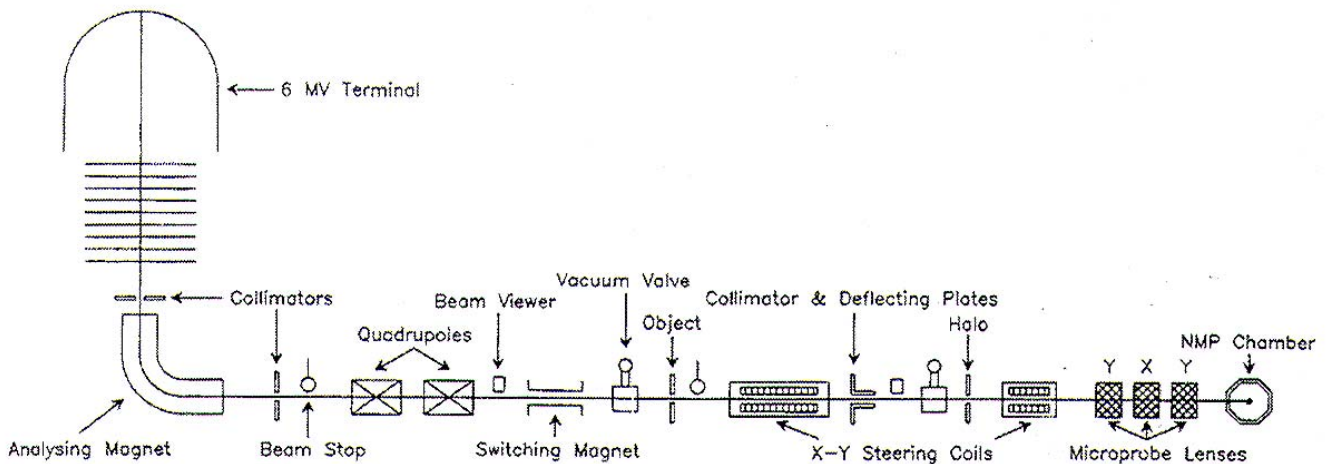

Fig. 3.2: A schematic of the Van de Graaf accelerator and layout of NMP at iThemba LABS **[22].**

3.2.2.3 Ion beam line and focusing system

The probe forming the focusing system of a nuclear microprobe normally consists of a set of a slits and focusing lenses (triplet, quadruplets) which are optimized in order to produce an ion probe with energy of several MeV and a micrometer beam spot with a current between 100-200 pA. After the analyzing magnet, the ions travel through the energy stabilization slits situated in front of the main beamstop. The ions pass through a quadrupole doublet for focusing the beam at the object slits. Before the object slit the beam passes through a switching magnet with a narrow entrance port in the y direction of 1.2 mm. This magnet is used to direct the beam to other beam lines besides the microprobe line which is situated at an angle 0 degree. This narrow entrance and additional circular water-cooled collimator protect object slits from damage. Beam focusing is done by the standard Oxford triplet of magnetic quadrupoles. Further standard features include the Oxford scanning coils **[22]**.

3.2.2.4 The experimental chamber

The microprobe target chamber is a modified version of the standard Oxford Microbeam chamber. The focused beam from the accelerator is directed into this chamber. The samples are mounted and positioned on the target ladder which is placed in front of the detector. The movement of the ladder and the target position are viewed through an optical microscope at an angle of 45°. Stepper motors control the movement of the sample in X, Y and Z axes **[22]**. Equipments in the chamber includes X-ray detector, an annular Si surface barrier (SSB) detector, channeltron electron detector for secondary

electron imaging, electron suppression ring in front and behind the target and the optical microscope. The nuclear microprobe chamber can be realigned to accommodate what was originally not mounted. For example the detectors like PIN photodiodes can be mounted for the specific measurements and removed thereafter. The α-particles emitted from the interaction between the proton beam and the samples are detected by the PIN photodiodes detector. This detector has electron suppression ring to measure the current. Fig. 3.3 below presents a picture of the NMP chamber.
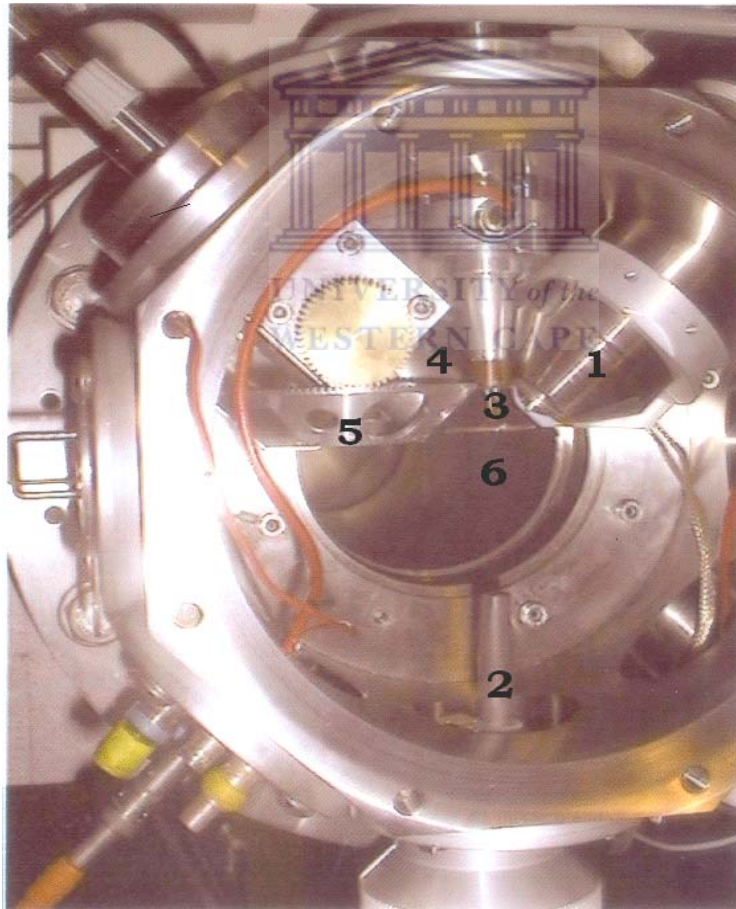

Fig. 3.3: The features inside the experimental chamber (1).Microscope, (2) Faraday cup, (3) the direction where the silicon surface barrier detector is placed, (4) Si (Li) detector, (5) Filter wheel, (6) Sample stage.

3.2.2.5 Experimental conditions

The usual proton bombarding energy used at iThemba LABS nuclear microprobe is 3 MeV. Hence, it is easy to focus the beam using this bombarding energy. To obtain the position of the samples we used PIXE technique with this proton energy. Thereafter, we focused the proton beam of 670 keV for boron measurements. The beam spot size was 3×3 μm^2 and the beam current was kept in the low range between 100-200 pA in order to keep the flux low in the detector and to avoid pile-up. The shaping time of this detector was 1.5 μs with the coarse and fine gain of 30 and 0.4 respectively. The nuclear reaction used was $^{11}B(p, \alpha)^8Be^*$. The α-particles emitted from this reaction were detected by a PIN photodiodes detector placed in the chamber and mounted into a half spherical geometry. The signal from the detector was amplified, shaped, digitized, and lastly stored with co-ordinates for beam position in the sequence, event by event. The amplified signal was taken to the ADC and thereafter stored in the computer. The obtained results were analyzed using NRA method and GeoPIXE software package [43].

3.2.2.6 Data acquisition

The iThemba LABS NMP uses XSYS system for data acquisition. This system allows the use of complex arrays of data, with event by event storing capability, the use of multi-parameter systems and multiple windows. The event handling is facilitated by the high level EVAL language code. This is completed with the VAX computer network which facilitates full multi-tasking and background processing. The XSYS system is linked to VAX via a CAMAC crate. The PIXE and NRA spectra were analyzed using the

GeoPIXE software and the RBS data by RUMP package **[44]**. For standard RBS measurements up to ten samples can be loaded in the experimental chamber. A silicon detector for RBS at an angle of 176º detects the backscattered alphas from the sample **[22].**

3.2.2.7 GeoPIXE software

GeoPIXE software is used for quantitative processing of PIXE/SXRF spectra. It produces elemental images from list-mode data, and has tools for image exploration, spectra extraction for quality control, and for multi-layered targets, using a new efficient PC graphical user interface. The GUI interface allows interactive spectrum fitting, list-mode sorting and quantitative image projection using dynamic analysis (or simple energy windows, or regions of interest), and quantitative analysis of arbitrary regions and line projections of images (all elements simultaneously). The windows are linked and correspond with each other to provide an efficient interactive analysis and imaging environment **[61]**. This software package allows the analysis of thin and thick target X-ray spectra, with complete thick target corrections for beam stopping power, X-ray attenuation and secondary fluorescence. The major advantage of using this software is the dynamic analysis (DA) capability of on-line elemental mapping **[43]**.

3.3 PIN photodiodes detector

The Hamamatsu S3590-02, PIN photodiodes detector consists of four large area PIN diodes for particle detection which can also be used as light sensors. It is a semiconductor that generates current or voltage when the P-N junction in the semiconductors is

illuminated by light. These diodes show excellent linearity with respect to incident light, have low internal noise, extensive spectral response, and are mechanically strong [62].

The advantages of using PIN diodes instead of an annular surface barrier detector are that they are not expensive when compared to the surface barrier and their feasibility of optimizing the solid angle. Their disadvantages are the prior energy resolution and degradation due to light, even though good energy resolution is not very important in the case of the ^{11}B(p, α)^{8}Be nuclear reaction. These diodes are connected in parallel and mounted on an insulating banking. The so-called active surface of each diode is about 100 mm^2. Therefore, the geometrically optimized arrangement of large area PIN photodiodes constructed by Sziki *et al.* was used as shown in Fig. 3.4 [45].
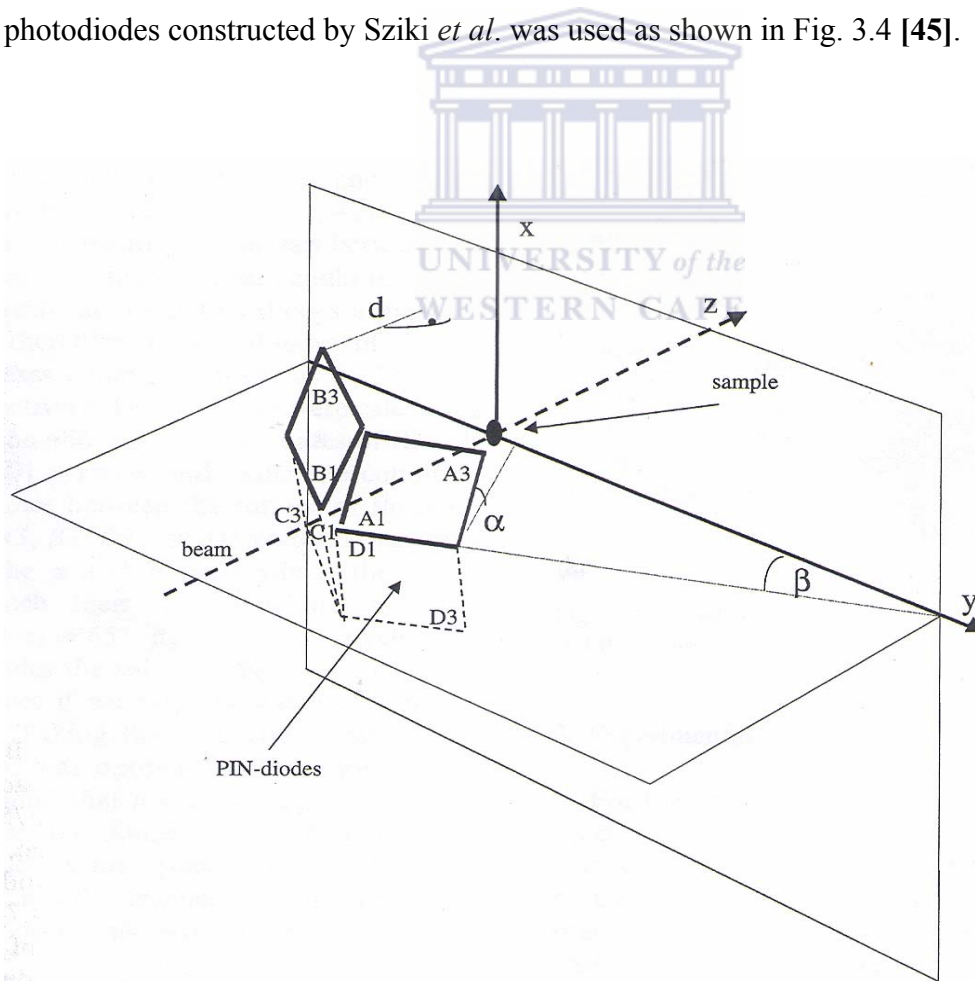

Fig. 3.4: Schematic view of PIN diodes detector [45].

3.4 Minimum detection limits

Minimum detection limits (MDL) is anticipated to estimate the lowest concentration of analyzed element that can be measured. This low concentration limit is of interest in forensic drug testing, where the presence or absence of trace elements such as B may be the critical reference. MDL is one of the most important parameters in trace element analysis that since it can be related to the accuracy of the technique. MDL for given peak is given by [46]:

$$MDL = 3\sqrt{N_B} \qquad (3.1)$$

where N_B is the summed background below the peak. In case where the background is very low i.e. below 10 counts, the MDL is conventionally set to 10 counts. The SI unit of MDL is ng/cm^2. It depends on the experimental parameters, the measurement duration and the detector quality [21].

Following an experimental observation, one must decide whether or not that which was being required was, in fact, detected. A well-known hypothesis testing, such a binary (qualitative) decision is subjected to two kinds of error: deciding whether the substance is present or not (α, error of the first kind), and contrary, failing to decide that it is present when it is (β, error of the second kind). The maximum acceptable value for the α, together with the standard deviation, σ_0, of the net signal $\mu_S = 0$ establish the critical level, L_C, upon which decisions maybe based. Operationally, an observed signal, S, must exceed L_C to yield the decision, detected [47]. The critical level is given as

$$L_C = k_\alpha \sigma_0 \qquad (3.2)$$

and the detection limit,

$$L_D = L_C + k_\beta \sigma_D \qquad (3.3)$$

where k_α and k_β are abscissas of the standardized normal distribution corresponding to probability levels, 1-α (which correspond to the decision, not detected) and 1-β (which correspond to the decision, detected). Neither a binary decision, based upon L_C, nor an upper limit (if not detected), nor a wide confidence interval (if detected) may be considered satisfactory for quantitative analysis. Therefore, for $\mu_S = L_Q$, the determination limit, the standard deviation, σ_Q, must be but a small fraction of the true value. Determination limit is defined as

$$L_C = k_Q \sigma_Q \qquad (3.4)$$

where L_Q is a true value of the net signal, μ_S, having a standard deviation, σ_Q.

The levels L_C, L_D and L_Q are determined entirely by the error-structure of the measurement process, the risks, α and β, and the maximum acceptable relative standard deviation for quantitative analysis. L_C is used to test an experimental result, whereas L_D and L_Q refer to the capabilities of measurement process itself **[47].**

In order to make a decision, detected or not detected, one require to know only the net number of counts resulting from the experiment, and the critical number of counts, L_C. Limits for the qualitative and quantitative analysis and upper limits or confidence intervals for actual results, however, are of value only when expressed in terms of the physical quantity of interest, such as grams or atoms. The connection is simply made by means of the relevant calibration factor. For instance, the detection limit, L_D, may be related to the minimum detectable mass, m_D (g), by means of equation 3.5 below,

$$L_D = Km_D \qquad\qquad (3.5)$$

where K represents an overall calibration factor relating the detector response to the mass present. Even though the constant, K, is not involved directly in the statistics of the detection limit, its role is fundamental, and it must be included when choosing between experimental procedures or in optimizing a given procedure [47].

CHAPTER 4

Results and discussions

4.1 Sample images from microscopes

### 4.1.1 Optical light microscope images

The optical microscopy images of Mts+Tu 950 (glass) samples were taken (see Appendix) before the nuclear microprobe measurements and used to find the position of the specimen when focusing the beam on the sample in the nuclear microprobe chamber. The measurements with this technique were not very helpful compared to SEM imaging, since this technique shows only the position of the sample in the glass and not the composition of the samples.
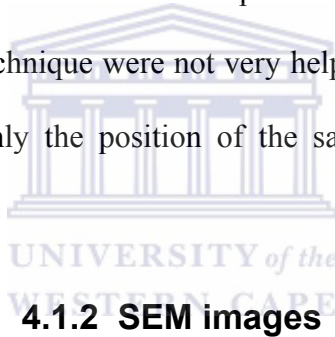
4.1.2 SEM images

Imaging using scanning electron microscopy (SEM) has been performed before nuclear microprobe studies. Fig. 4.1 shows a typical SEM image of the Mts+Tu 950 (glass) sample. This sample is divided into three parts Fig. 4.1 (A-C). The sample contains different types of minerals such as plagioclase, quartz, tourmaline, zircons and ilmenite. Some types contain fewer crystals and uneven surface than others. Images were obtained at low magnification (from 80 X to 115 X), since the main aim was to register the position and the shape of specimens rather than to identify small details. However, it was possible to reveal some details such as the presence of holes within the sample. These images were helpful in the selection of areas for nuclear microprobe analysis
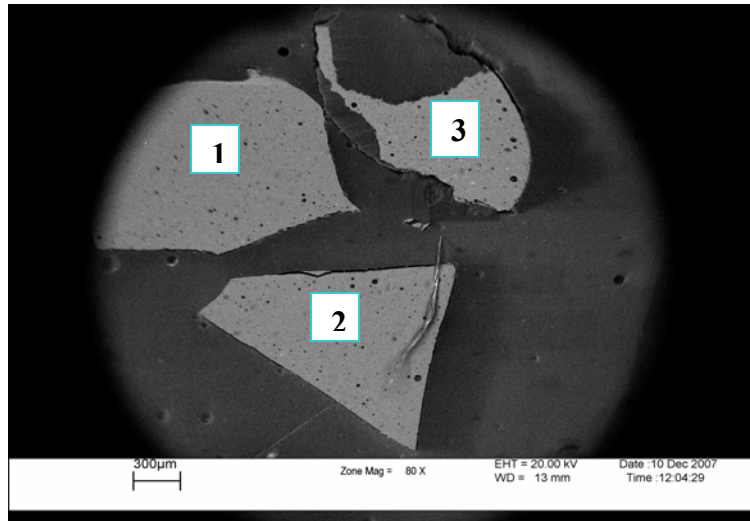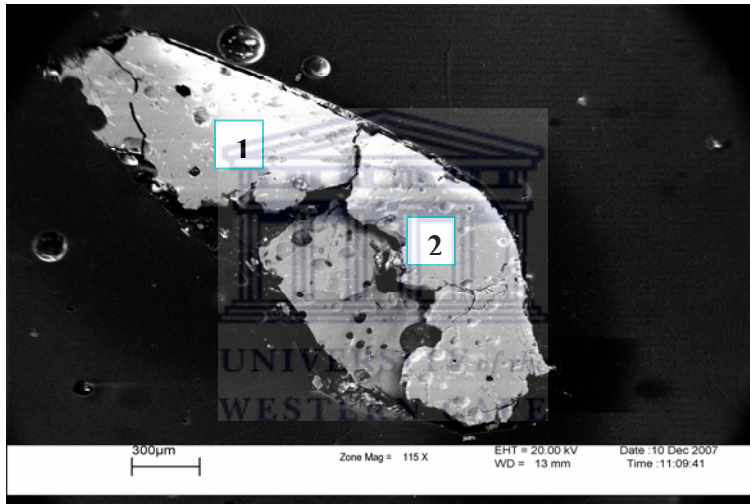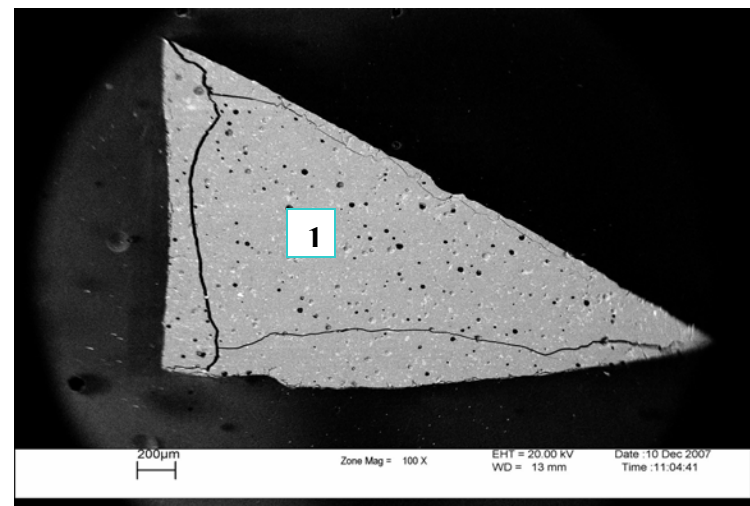
Fig. 4.1: SEM images from Mts+Tu 950 (glass) samples.
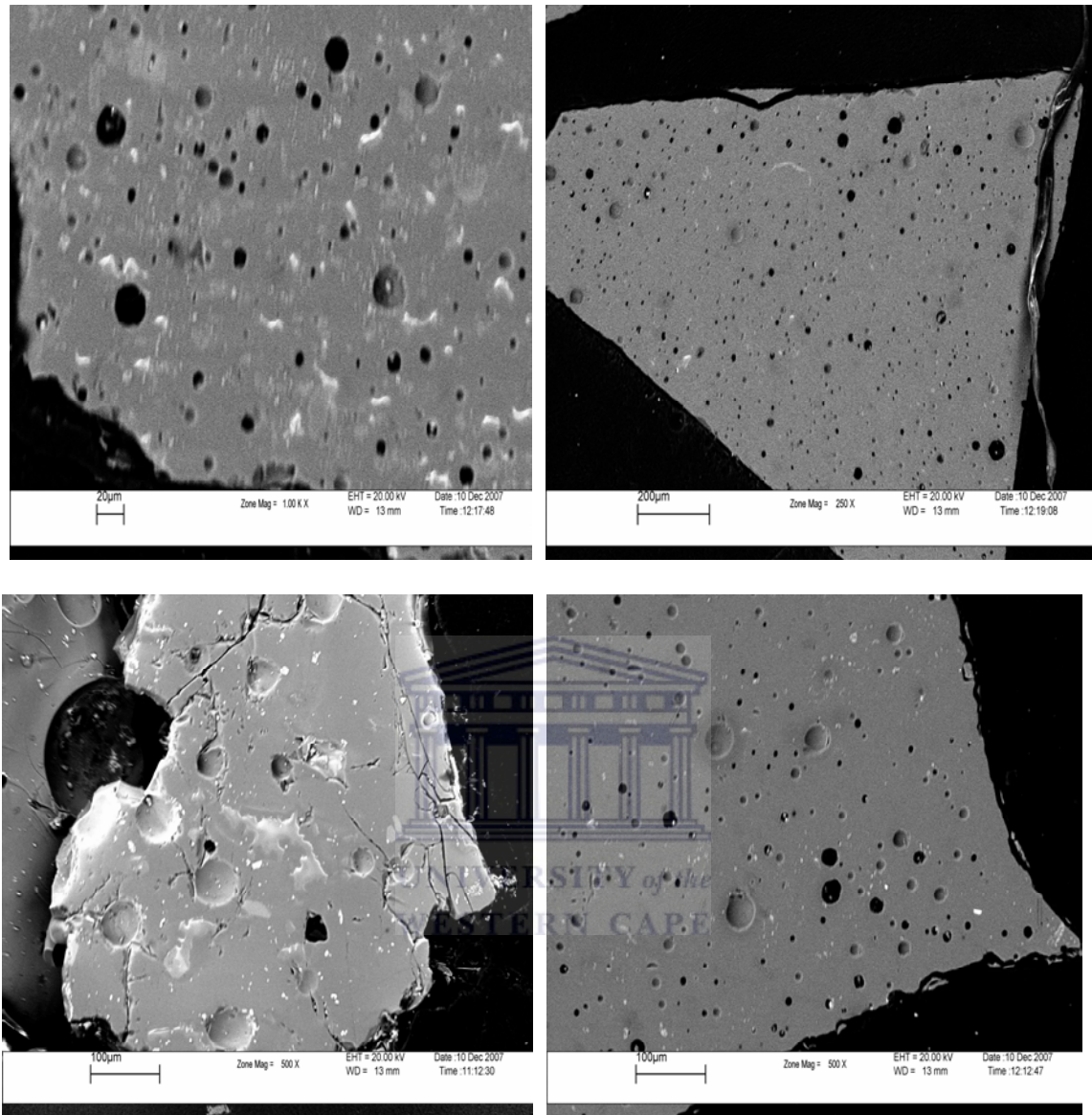
Fig. 4.2: SEM images from Mts+Tu 950 (glass) samples at higher magnification.

4.2 NMP measurements of boron

Mookodi **[48]**, in the course of his MSc. thesis investigation, performed the measurements using the same set of PIN photodiode detector with an absorber Al foil in front of the diodes to stop the backscattered protons and without the Al foil. It was found

that there were noise problems observed in the NRA energy spectrum. When using the Thorium source (^{228}Th), with no Al foil showed better resolution. The presence of Al foil reduces the resolution of the detector. In the same work it was noticed that even the (Al foil) absorber had an effect on the resolution of the PIN detector. Although his results have shown that the absorber was not the only source of the signal noise, they have not identified its origin either.

In the present study we have noticed that the electronic noise could as well be originating from the turbo-molecular pump or be due to earth loops. The photodiodes showed spectra with lot of distortions when used with an Al foil but much improved detector resolution was seen when there was no absorber used. These led to the conclusion that the absorber itself has an effect on the resolution of the detector. As a result an attempt was made to eliminate additional electronic noise by putting an insulator (rubber) between the turbo-molecular pump and the scattering chamber, in order to improve the resolution of the detector. However, during the last measurements the insulator was not as helpful as it was in the beginning as we experienced higher noise again. Since Mookodi's measurements without absorber were good, we then decided to perform the measurements without Al foil in this study.

4.2.1 Energy calibration

The PIN diodes detector was initially tested for its resolution and for the electronic noise in the chamber. The ^{228}Th source was used as a reference for energy calibration for the detector. It is characterized by known energy peaks ranging from 5.3405 to 8.7844 MeV.

To check the level of the noise in the chamber, the calibration was performed both with and without the insulator between the chamber and the turbo-molecular pump.

4.2.1.1 Energy calibration without insulator

The PIN diodes detector and the ^{228}Th source were placed in the nuclear microprobe chamber. They were placed on a cardboard with an open gap to help the turbo molecular pump to maintain a high vacuum. The chamber was evacuated with the turbo-molecular pump on to the desired pressure. A high level of noise ~ 50 mV was noted during the measurements process. We have anticipated that the noise levels could be from the turbo-molecular pump and also from the electronic modules. Fig. 4.3 shows the energy calibration spectrum obtained in this condition with a visible high noise level.
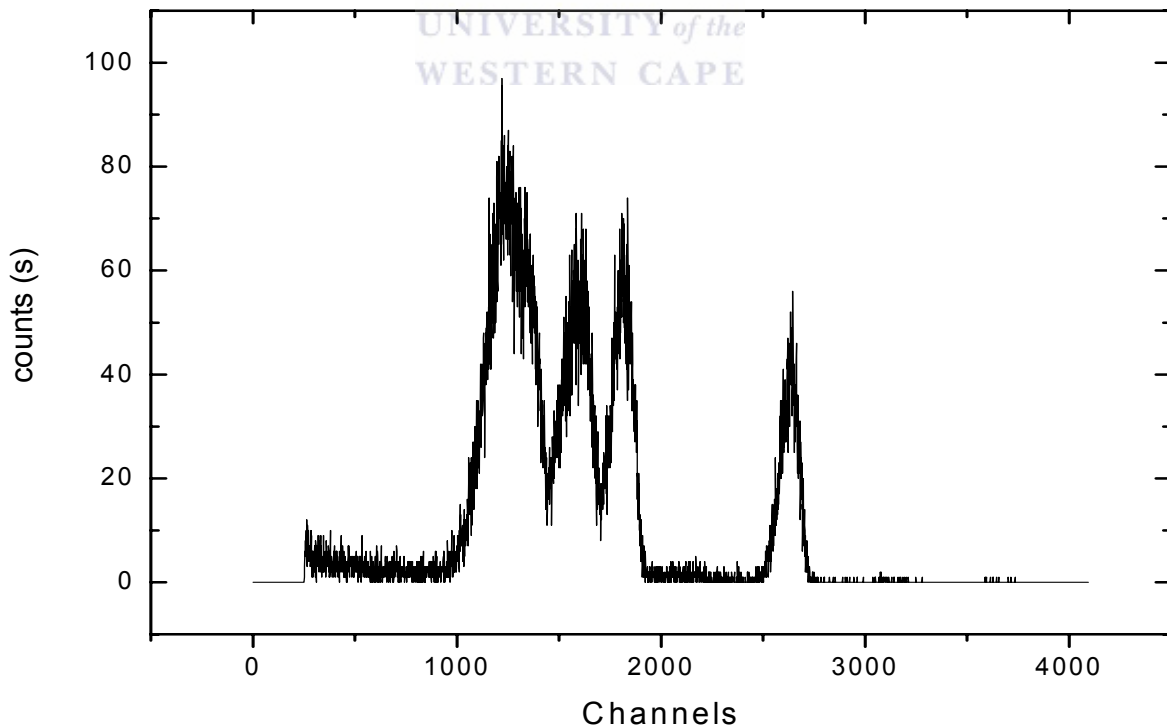

Fig. 4.3: Poor energy resolution from ^{228}Th spectrum without insulator.

4.2.1.2 Energy calibration with insulator

The test was made with the same ^{228}Th source placed inside the experimental chamber. The obtained calibration spectrum is shown on Fig. 4.4 and shows a better resolution of the detector than the one obtained without the insulator (Fig. 4.3). The insulator has somehow reduced the noise level. This led to the conclusion that some of the noise could come from the turbo-molecular pump. The measurements of pure B and BN standards were carried out after this test. The spectrum obtained from the pure boron standard is presented on Fig. 4.5.
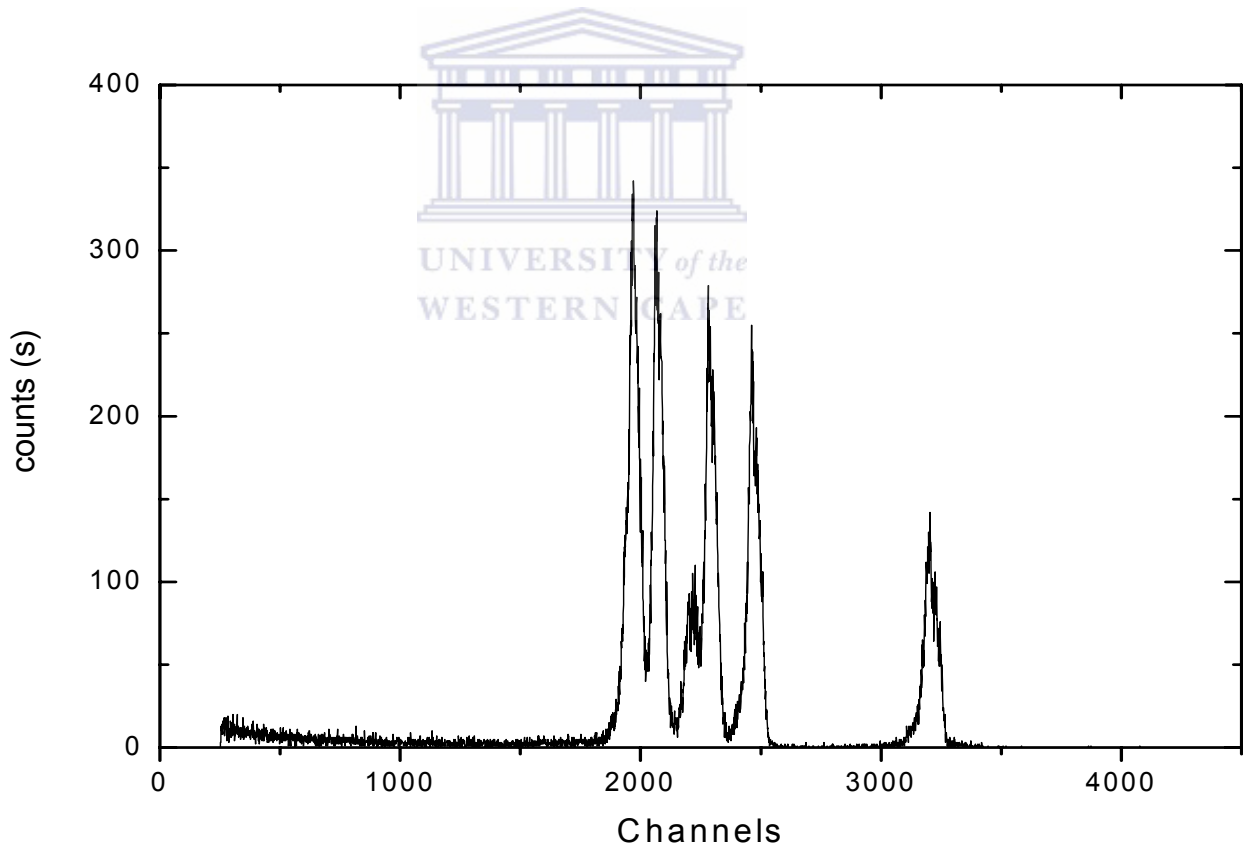

**Fig. 4.4:** Improved energy resolution from ^{228}Th spectrum with insulator.
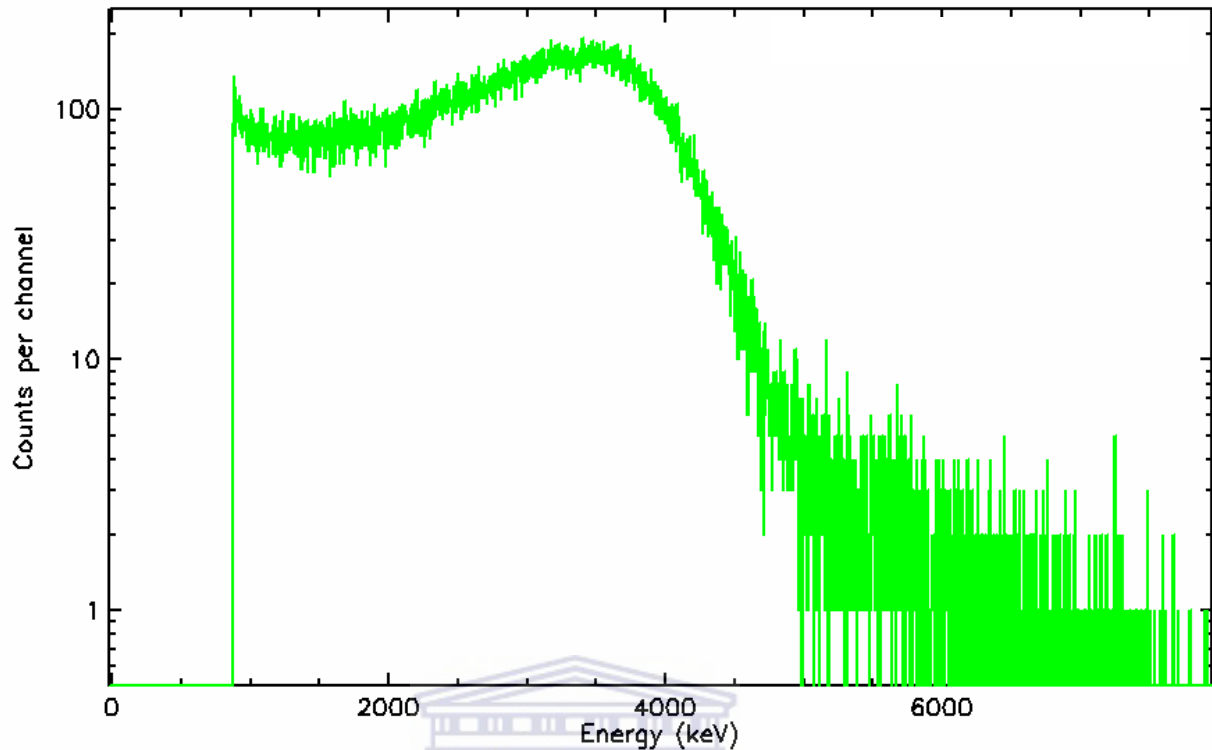
Fig. 4.5: The energy spectrum obtained from a pure boron standard target using a PIN diodes detector.

4.2.1.3 Energy calibration after the realignment of the set up

To be able to focus the microprobe at 670 keV it was necessary to do the realignment of the whole microprobe beam line experimental set-up, including the realignment of the bending magnets, collimators and objects slits for beam focusing. After realigning the whole experimental set-up, we obtained a very good focused beam. However, we noticed again some electronic noise signal in the experimental chamber which was most probably due to the proximity of the turbo-molecular pump.

Fig. 4.6 shows the poor calibration energy spectrum obtained from the [228]Th source after realignment of the experimental setup. Despite the significant noise in the counts of the

energy spectrum, we proceeded with the measurements of the samples. Since the energy spectrum of the measured samples shows a very broad energy distribution, a good (Fig. 4.4) or poor (Fig. 4.6) detector resolution will not significantly change the energy spectrum profile of the measured samples, as can be seen for pure boron sample (see Fig. 4.5). Therefore, the energy resolution of the PIN diodes is not a critical issue in the determination process of boron concentration. The broad energy distribution observed in the energy spectrum is mainly due to the scattering of alpha particles.
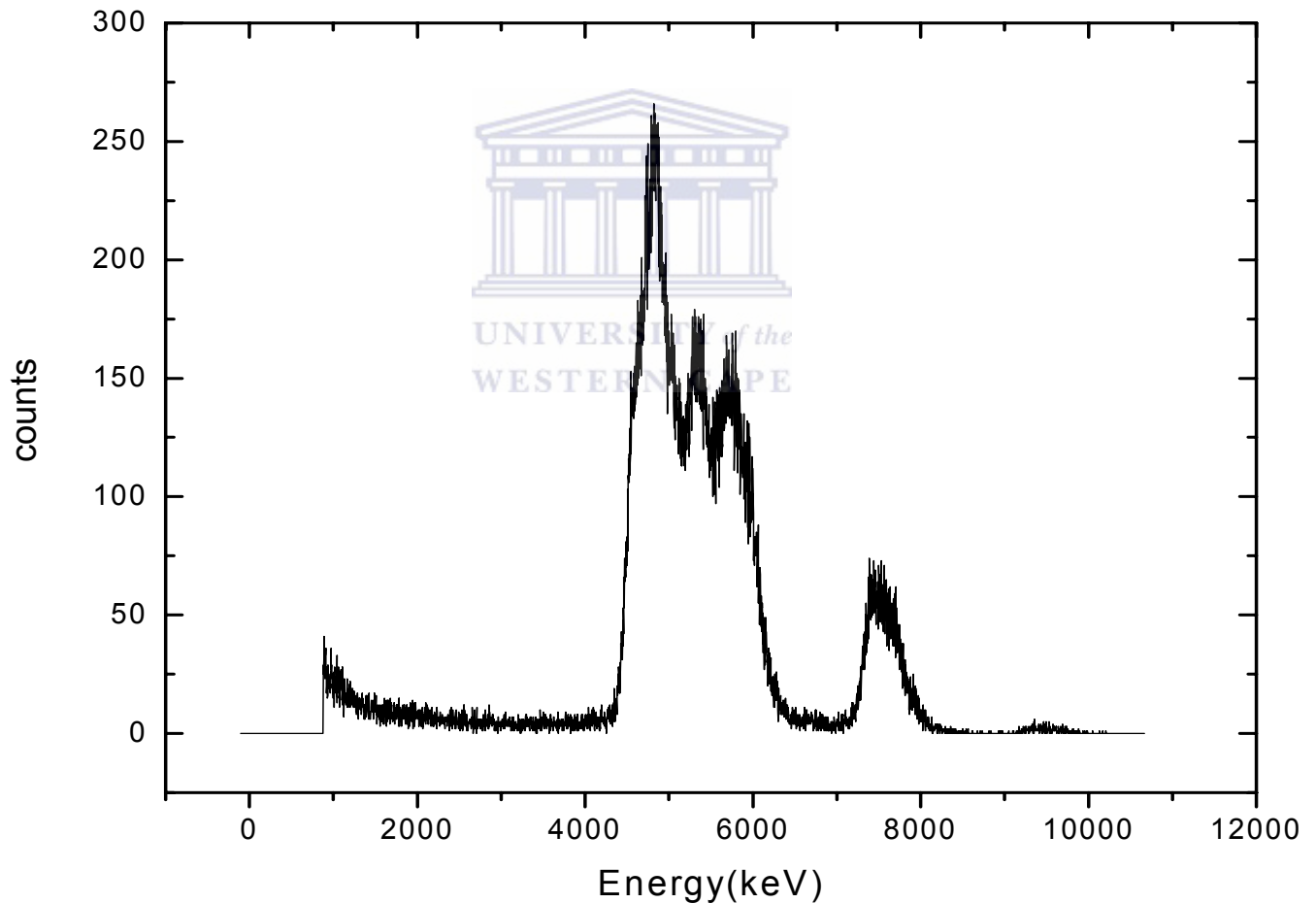

**Fig. 4.6:** Poor energy spectrum from ^{228}Th with insulator, after realignment of the experimental setup.
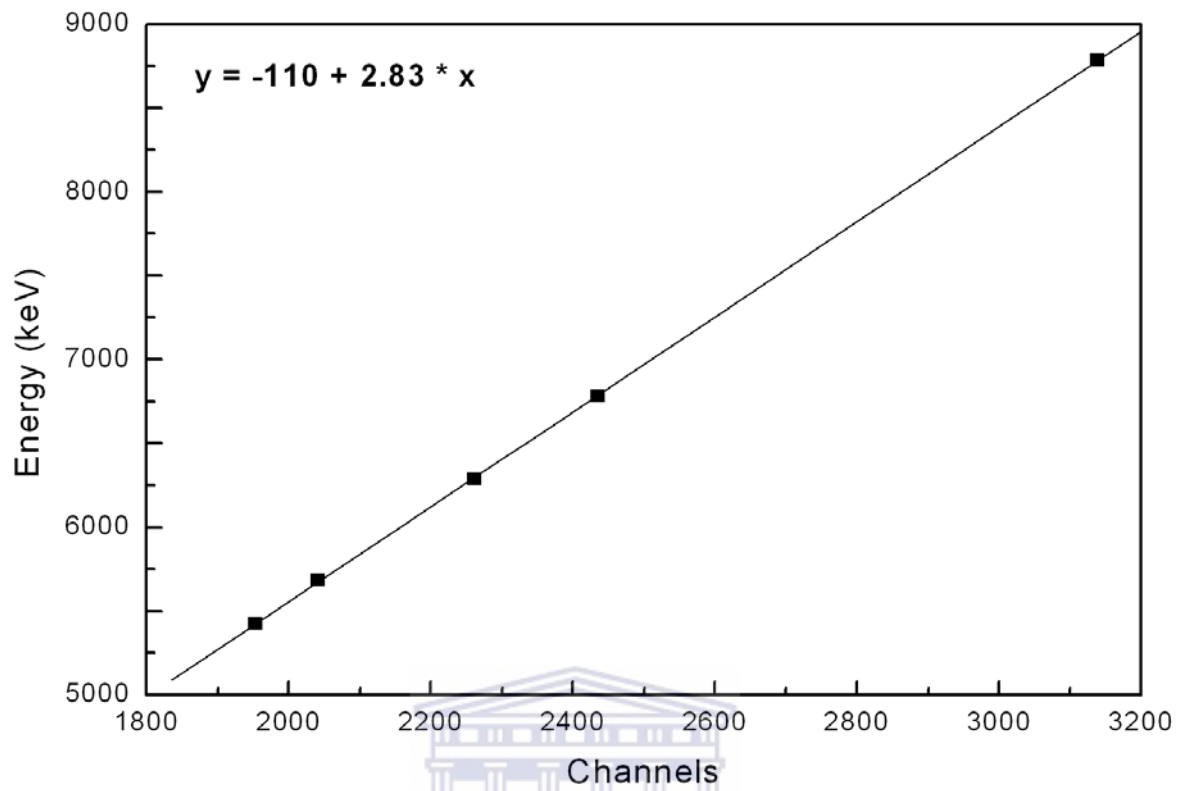
Fig. 4.7: Energy calibration of PIN diodes detector with ^{228}Th source.
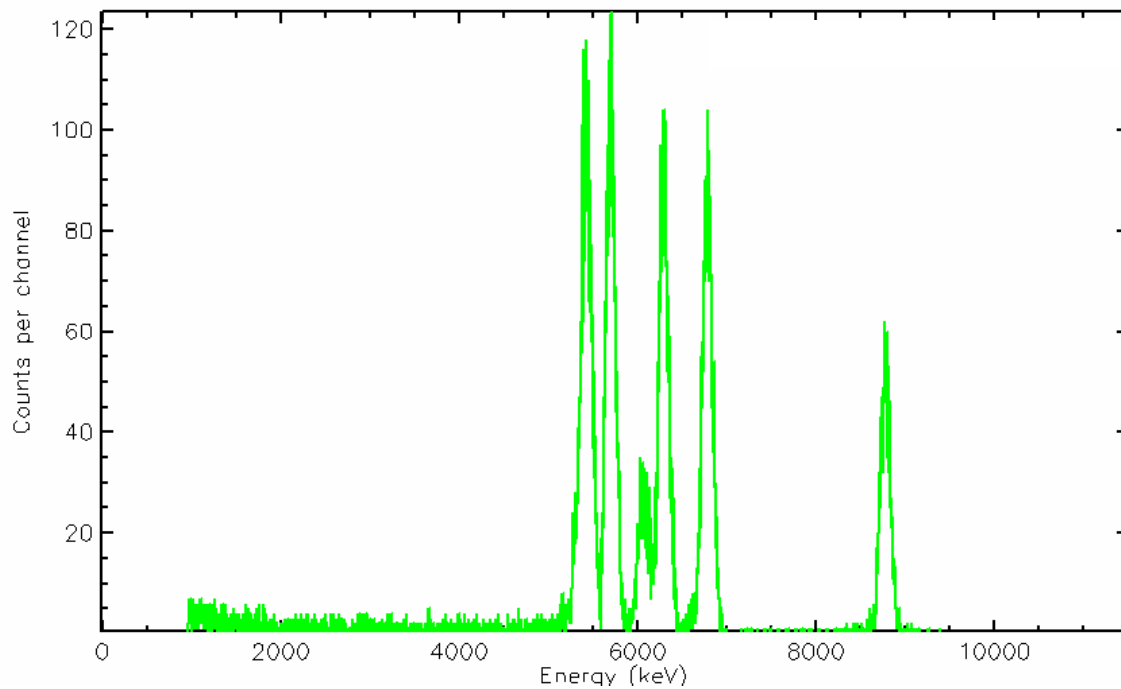

Fig. 4.8: Energy spectrum of ^{228}Th source before realignment of the experimental setup.

The energy calibration curve with good linear correlation obtained with the source is illustrated in Fig. 4.7 and its energy spectrum in Fig. 4.8 obtained before realignment of the setup. The slope of the energy calibration curve allows the correction between energy and channel numbers. The uncertainty is ±30 keV and ±0.01 keV/channel for the intercept and the slope respectively.

4.2.2 PIN diodes calibration and measurements

The PIN diodes detector was calibrated for boron measurements in the low concentration region with the glass standards from the National Institute of Standards Technology (NIST), the set of standard materials distributed by ASTIMEX, B and BN standards and tourmaline standard. The boron concentration in these standards is presented in Table 4.1. They cover a broad range of boron concentration.

Table 4.1: The boron concentration (wt %) from the standards.

Mineral	B conc. (wt %)
B	99.9
BN	43.6[a]
Tourmaline	3.27[b]
NIST 611	0.0351[c]
NIST 612	0.0032[c]

[a] Calculated value, [b] Obtained by **[3]**, [c] Obtained by **[42].**

A linear correlation curve was observed between the experimental yields data from ^{11}B(p, α)^{8}Be reaction and the boron concentration values in different standards (Fig. 4.9). The maps (Figs. 4.22-4.30) from both the standards and the glass samples were obtained by scanning the proton beam over the samples. The gates were set from the obtained maps in order to select the true region of boron as indicated by map (a), (b) and (c) from the above mentioned figures. We then extract the region of interest (see Fig. 4.22b) using GeoPIXE software and these represent the boron yield per charge.

The linear trend obtained using the five mentioned standards shows that the data for BN is found slightly above the linear trend which may be related to the carbon layer around the BN which is now partly destroyed. This results in possibly poor metallic contact between BN and the sample holder and hence might affect the charge measurements. The other cause of the BN result being located above the trend line might be because the proton beam could have caused damage of the graphite coating around BN standard during long exposure. The concentration of boron from the unknown sample can be obtained from the linear fit.

In order to calculate the detection limit we assume that the smallest measurable signal is 100 counts per 1μC or 10^{-4} pC. From the slope and intercept of the linear best fit, we can calculate the corresponding concentration by the use of equation 4.2. Since the detection limit must be positive, the value of the intercept becomes a critical parameter (Eq.4.3). Ideally, the intercept is expected to be zero, but unless the measured data are perfectly aligned, the intercept will always be different from zero. The calibration curve in Fig. 4.9 shows a fairly good linear relationship, the point of BN is however a bit away from the fit line. The parameters for the best fit are shown in column 2 of Table 4.2. The intercept is

far bigger than the smallest measurable signal given by y_0, so that the detection limits become negative. We can however estimate the best possible detection limit that can be achieved by our facility, by assuming a perfect linear relationship between the various standards. We therefore assume the intercept to be equal to zero and the only relevant parameter for the detection limit is the slope m = 0.116 counts/pC/wt % of the calibration curve.

Table 4.2: The coefficient of the linear equation for calibration curve comparison with all the standards and the two points plot.
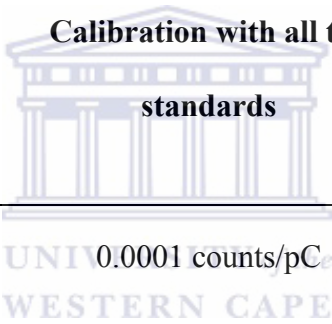
Parameters	Calibration with all the standards	Two points Calibration
y_0	0.0001 counts/pC	0.0001 counts/pC
c	0.02 counts/pC	0.00 counts/pC
m	0.116 counts/pC/wt %	0.1156 counts/pC/wt %

$$y = mx + c \qquad (4.1)$$

$$x = \frac{y_0 - c}{m} \qquad (4.2)$$

$$y_0 - c > 0 \qquad (4.3)$$
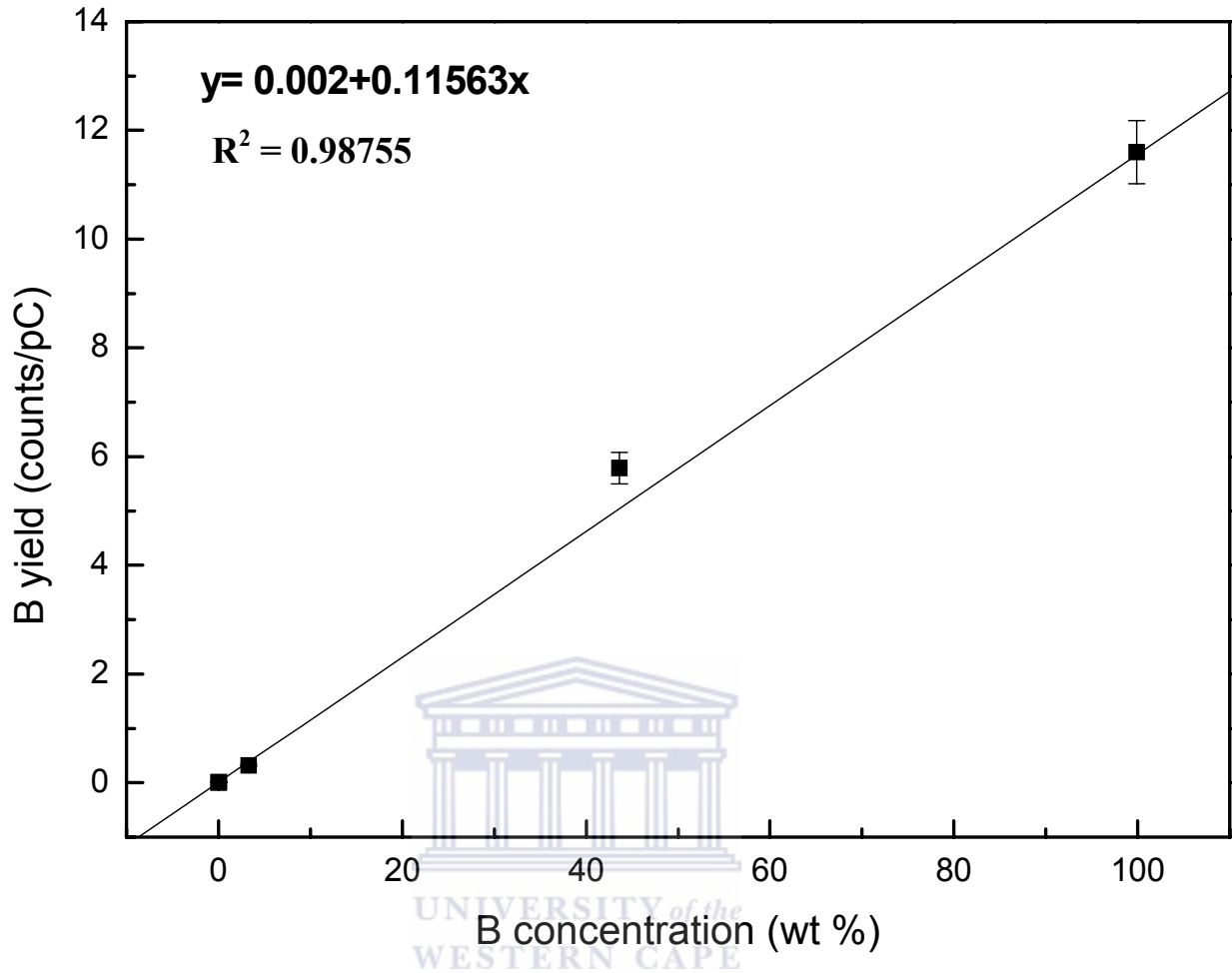
Fig. 4.9: The calibration curve of the boron yield (counts/μC) versus the B concentration (%).

The concentration in low content Boron samples should be weighted according to the low concentration boron standards (NIST 611,612 and Tourmaline). Since the boron yield is proportional to the boron concentration we expect a low boron yield for the unknown samples. The uncertainty of the intercept was $0.00155 \pm 9.0 \times 10^{-5}$ counts/pC in Fig. 4.9 and $0.01832 \pm 4.2 \times 10^{-4}$ counts/pC in Fig. 4.10; the values are in acceptable range.
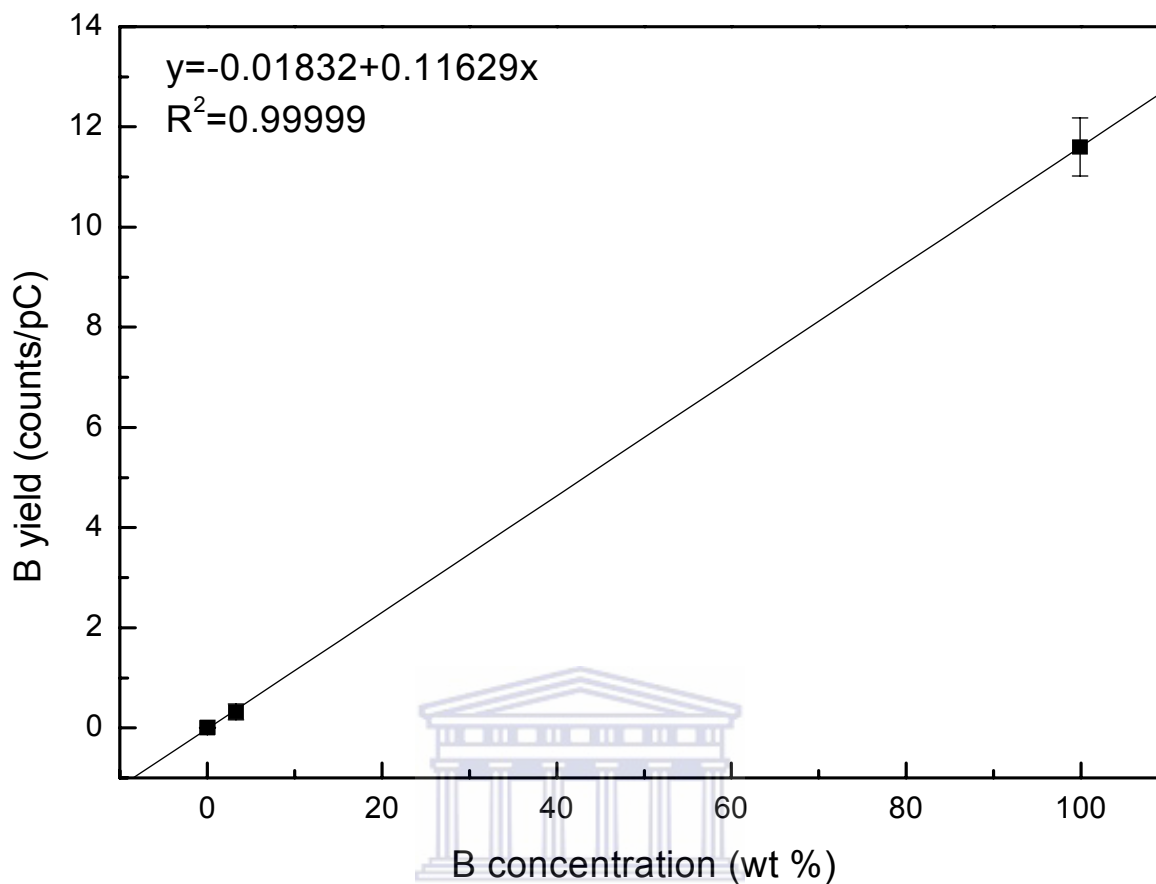
Fig. 4.10: The calibration curve of the boron yield (counts/μC) versus the B concentration (%).

Table 4.3: NMP acquired data for B using NRA from set of standards**.**

Mineral	Area (counts)×10^4	Charge(μC)	B yield (counts/μC) ×10^5
B	13.94±0.0343	0.012±0.0001	116±0.31
BN	16.15±0.0402	0.028±0.0001	57.95±0.14
Tourmaline	2.78±0.0167	0.086±0.0001	3.13±0.001
NIST 611	0.24±0.0049	0.349±0.0001	0.068±0.001
NIST 612	0.12±0.0034	0.691±0.0001	0.018±0.0006

The energy spectrum of a pure boron standard sample is shown by the energy spectrum in Fig. 4.11. The counts in the broad peak between the energy 3500-4500 keV are the α-particles emitted from the $^{11}B(p, \alpha)^{8}Be$ reaction. They have been used in the analysis because they have higher energy than the elastically scattered ion beam. Fig. 4.11 shows a clear spectrum which gave a positive outlook confirming that the NMP facility at iThemba LABS can detect light elements such as boron.
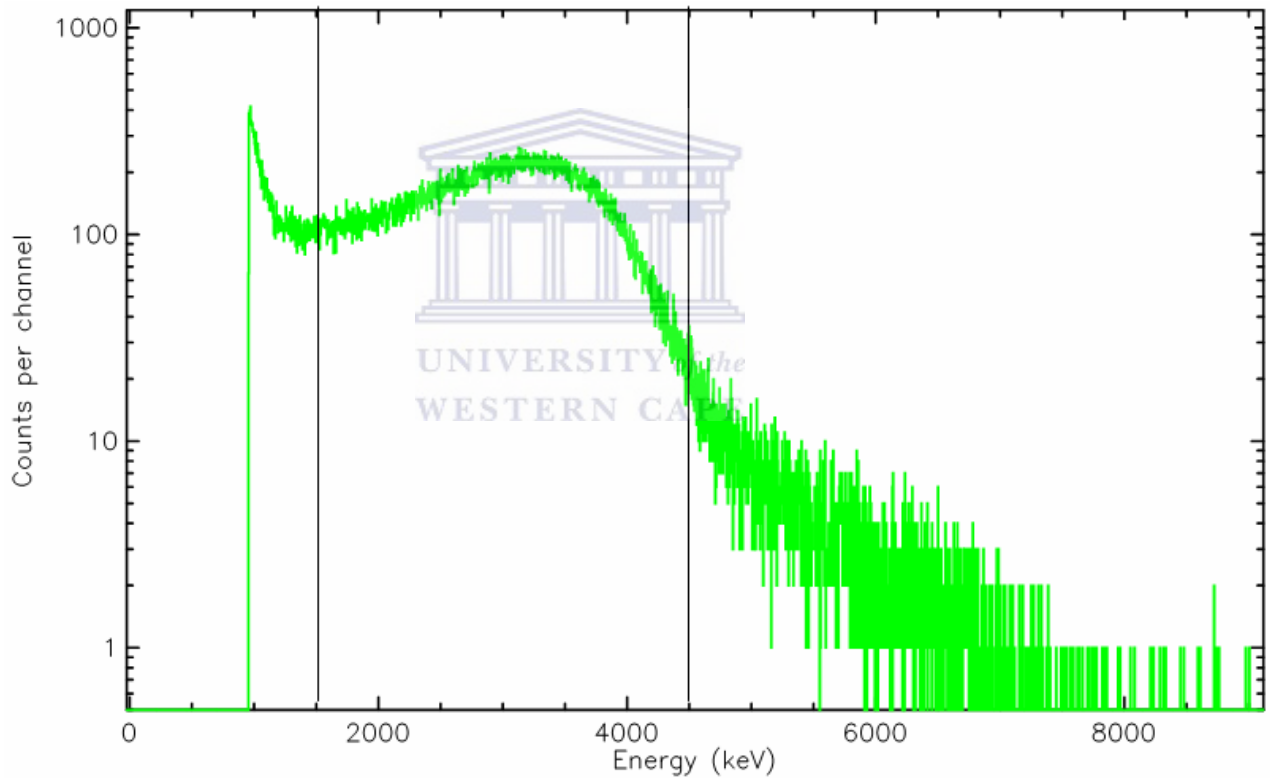

Fig. 4.11: The energy spectrum from the PIN diodes obtained from a pure boron standard as target.

The two following NRA steps were systematically applied in all the measurements.

1. Boron events were identified in the energy window between 3500-4500 keV (see Fig. 4.11).

2. The ratio between the number of B events and the number of charge events within the selected area determines the boron yields. The B yield for the different standards are summarized in the Table 4.3.

The possible interferences could be coming from O and N (see Fig. 2.11) but are considered negligible because their yields are less than the boron by a factor of 10^3 **[17].** Figs. 4.11-4.13 show typical measurements of the three standards of the highest concentration of boron as taken from pure boron, BN and tourmaline samples.
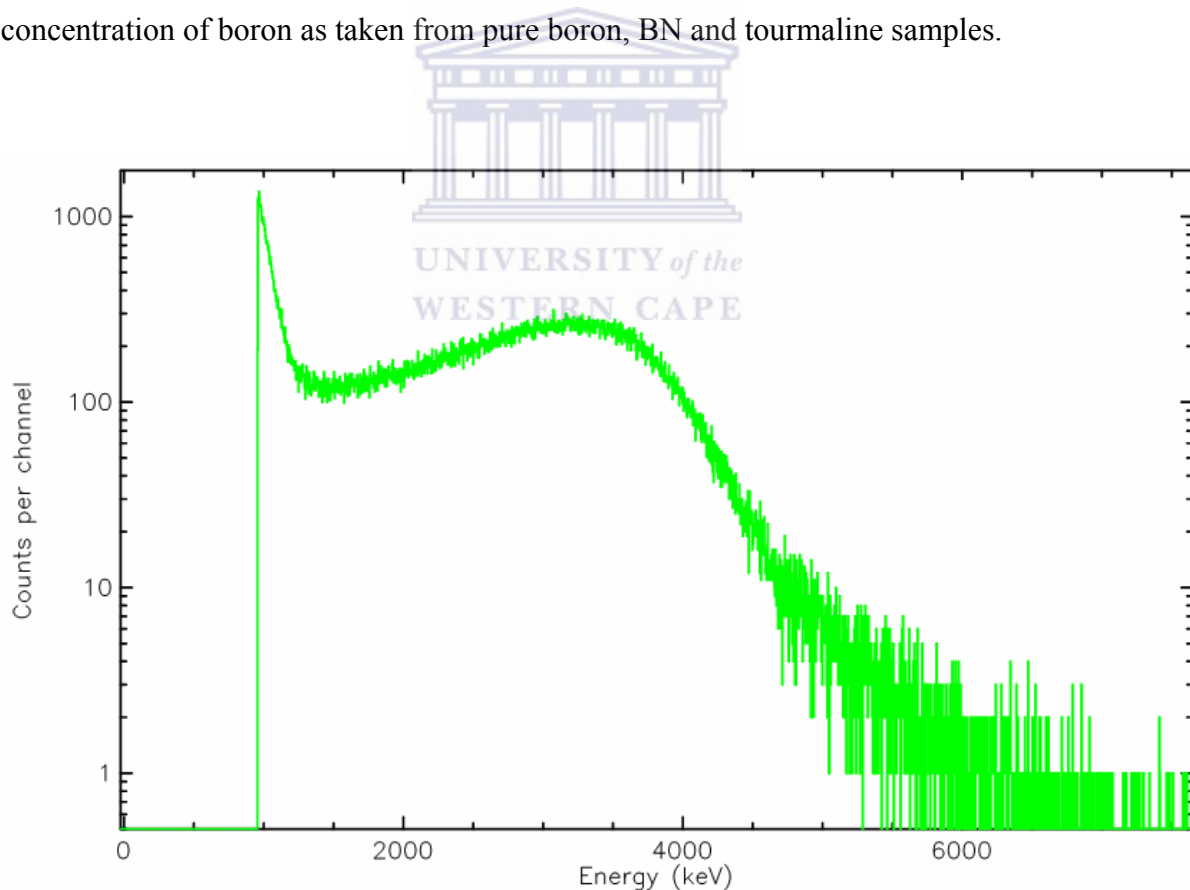

**Fig. 4.12:** The energy spectrum from the PIN diodes obtained from a BN as target.
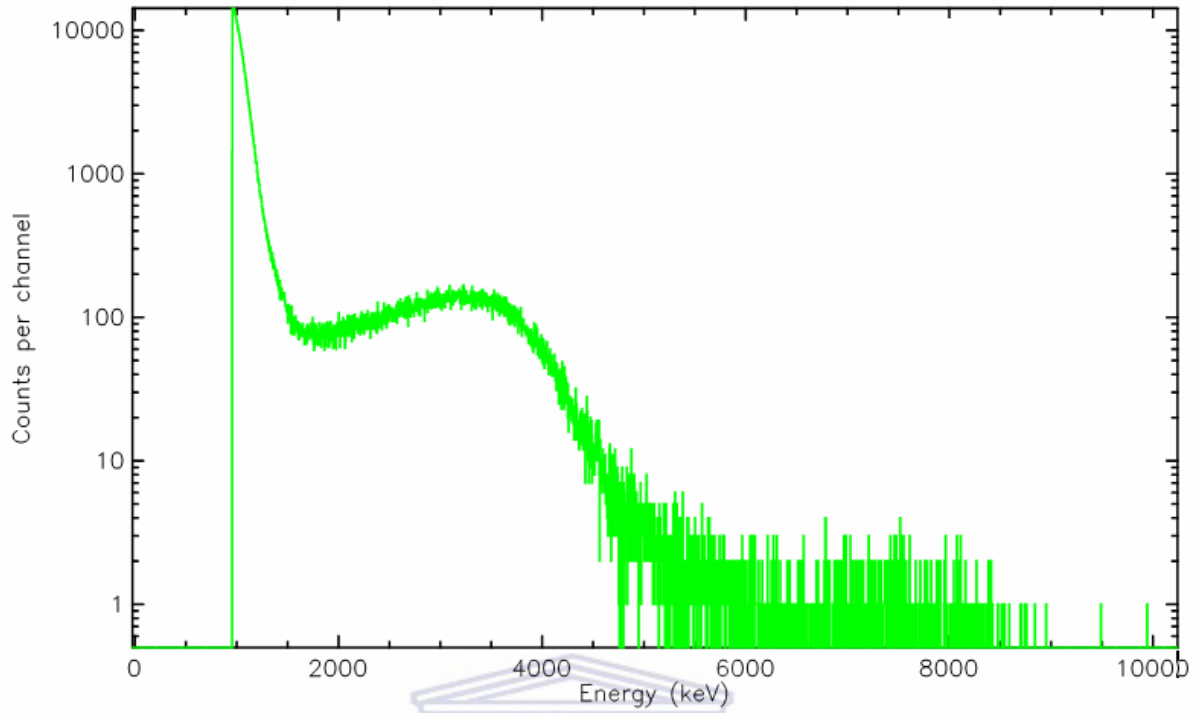
Fig. 4.13: The energy spectrum from the PIN diodes obtained from a tourmaline as target
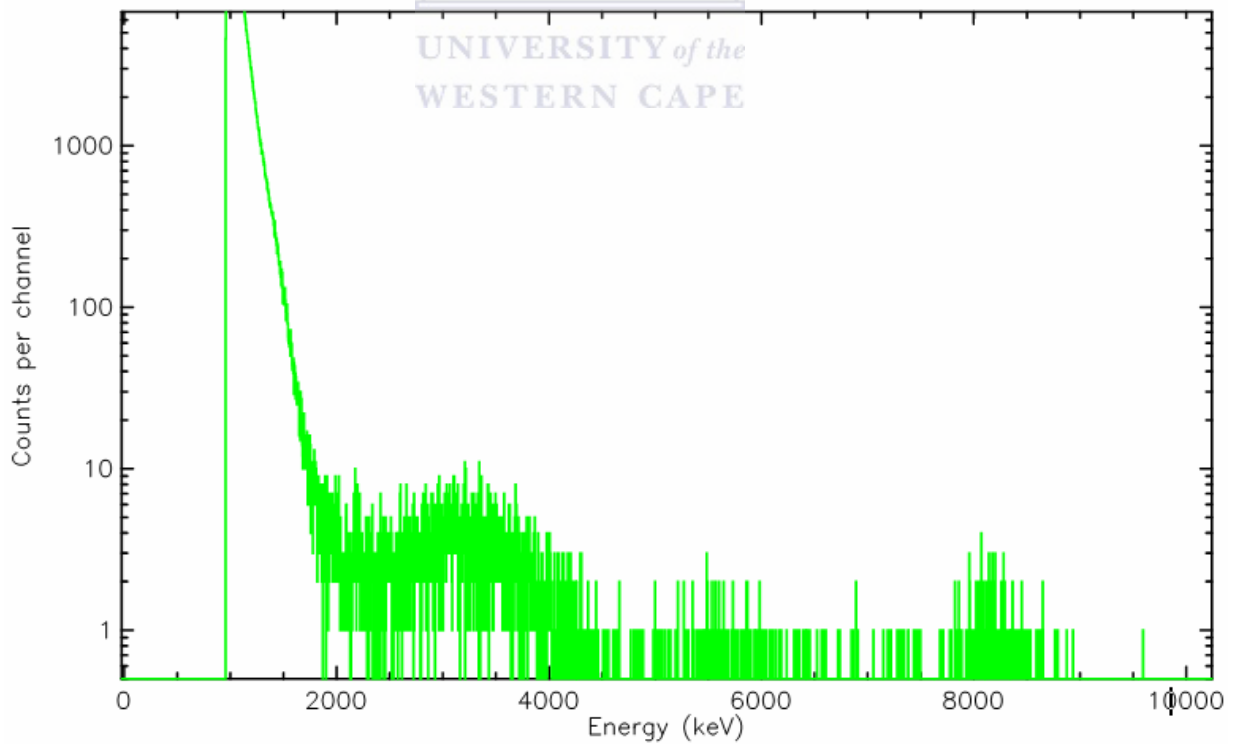

Fig. 4.14: The energy spectrum from the PIN diodes obtained from a NIST 611 as target.

To the right of Fig. 4.13 beyond 7000 keV, we expect the occurrence of lithium from a tourmaline sample. To confirm this energy range we consider the range on Fig. 2.11 by Lapppalain *et al*. had determined boron in the band 0-6 MeV while lithium signal was obtained above 7 MeV **[17]**.

Fig. 4.14 shows that the spectrum of NIST 611 has much lower counting statistics as compared to the previous spectra. This is due to the fact that the boron concentration from this standard is far lower than in B, BN and tourmaline standards. The high peak developed on the left may be related to the counts emitted from oxygen (see Fig. 4.20). A relative high level of noise results in an unclear broad peak of boron.

4.2.3 Boron analysis from unknown samples

In order to obtain the concentration of boron from unknown materials, energy scans on the standard targets were made to measure the boron yield curve (Fig. 4.10).The obtained linear regression (Fig. 4.10) was used to calculate the concentration from the unknown samples. The detection limit for the analysis of boron was calculated using the two points calibration curve. The observed spectra from Mts+Tu 950 unknown samples were analyzed (Figs. 4.15-4.19). The characteristic broad peak used for boron detection in the spectrum (selected area in Fig. 4.11) is due to the fact that the alpha particles in the reaction belong in fact to several groups: the α_1-particles which have 3.63 MeV and the α_{11}- and α_{12}- particles with energies varying from 4.48 MeV to 6.2 MeV. In fact the 3α particles are detected together **[4]**. This increases the overlapping of the α-peaks from different elements such as nitrogen and fluorine. With a suitable choice of bombarding

energy and absorbers it is possible to optimize the α-particles yield and separate overlapping peaks of several elements. As a result of all these factors, there is an optimum value for proton energy at which the highest sensitivity can be achieved. The energy range where alpha particles from the reaction $^{11}B(p, \alpha)^{8}Be$ are detected. The background issue has been previously investigated and was proven negligible [17]. In this study the background issue was not considered.
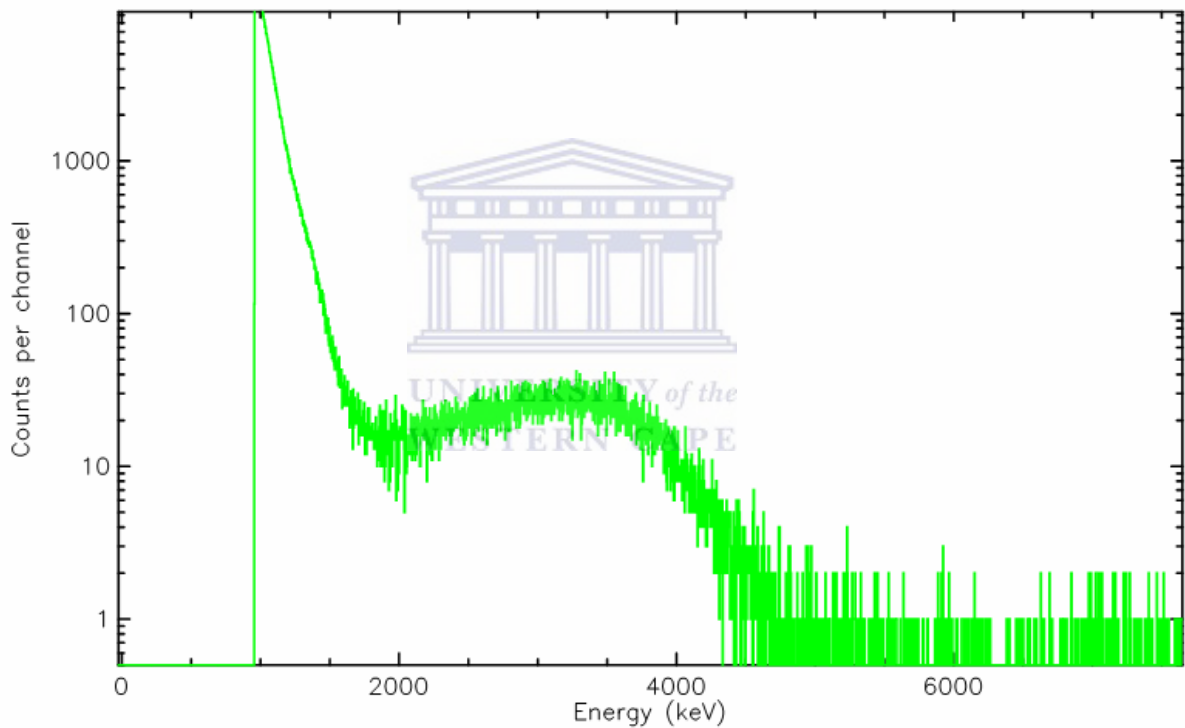

Fig. 4.15: The energy spectrum from PIN diodes obtained with Mts+Tu 950 (glass) sample.

Fig. 4.15 is a typical energy spectrum from Fig. 4.1A of Mts+Tu 950 sample. When analysis were done in single point mode the amount of boron in this region was found to be 1.05 wt %. The analysis measurements were also done by scanning the proton beam across Fig. 4.1B and the obtained spectrum is shown in Fig. 4.16 and the concentration of boron in this region was 0.67 wt %.
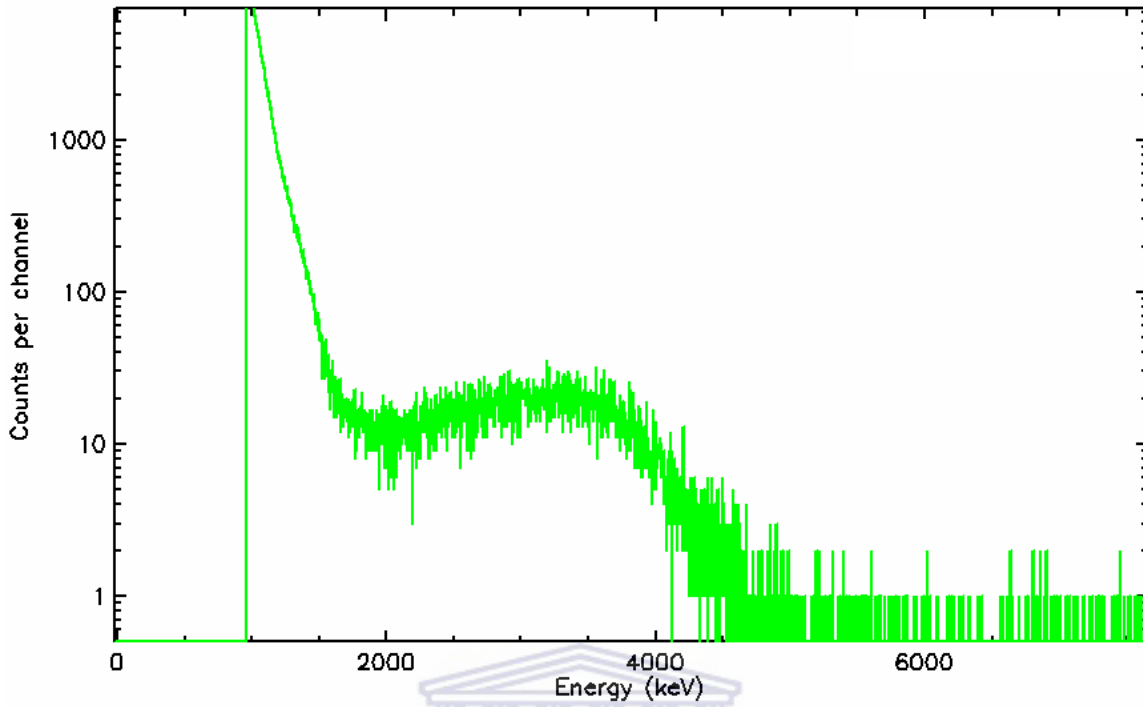
Fig. 4.16: The energy spectrum from PIN diodes obtained with Mts+Tu 950 (glass) sample.
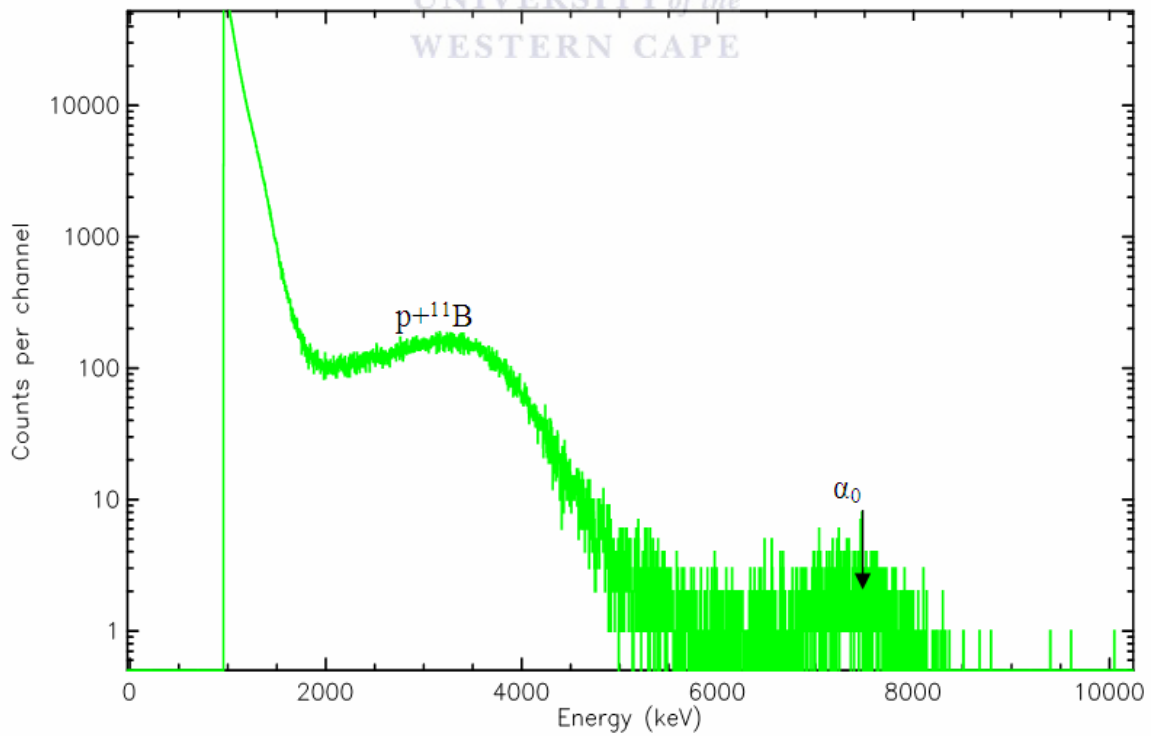

Fig. 4.17: The energy spectrum from PIN diodes obtained with Mts+Tu 950 (glass) sample.

Fig. 4.17 above displays the spectrum obtained by reducing the scan size in Fig. 4.1A. From this spectrum there is α_0 peak from (p, α_0) reaction developed to the right. Even though this peak is less interesting due to its low sensitivity and low cross section, it can be used for depth profiling at higher incident proton energy as it is well isolated from other alphas [4]. A Li peak is expected in the range between 7000-8000 keV, but the peak is not resolved in the present state of the curve. We can conclude that in this area of the sample, there is a tourmaline mineral. As shown in Fig. 4.26c, the tourmaline maps display the distribution of counts (a) below B, (b) B and (c) Li ranges. This means that by principle we can analyze both B and Li simultaneously.
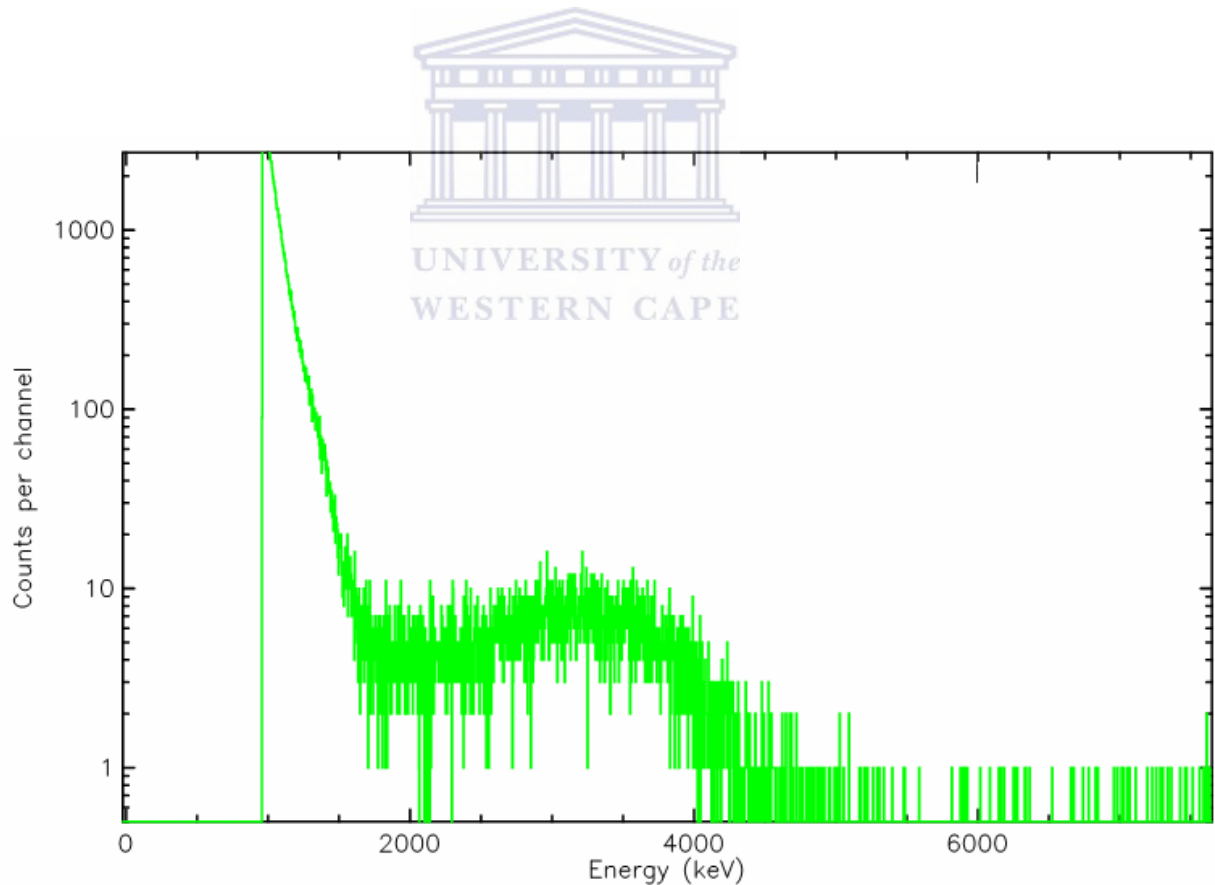

**Fig. 4.18:** The energy spectrum from PIN diodes obtained with Mts+Tu 950 (glass) sample.
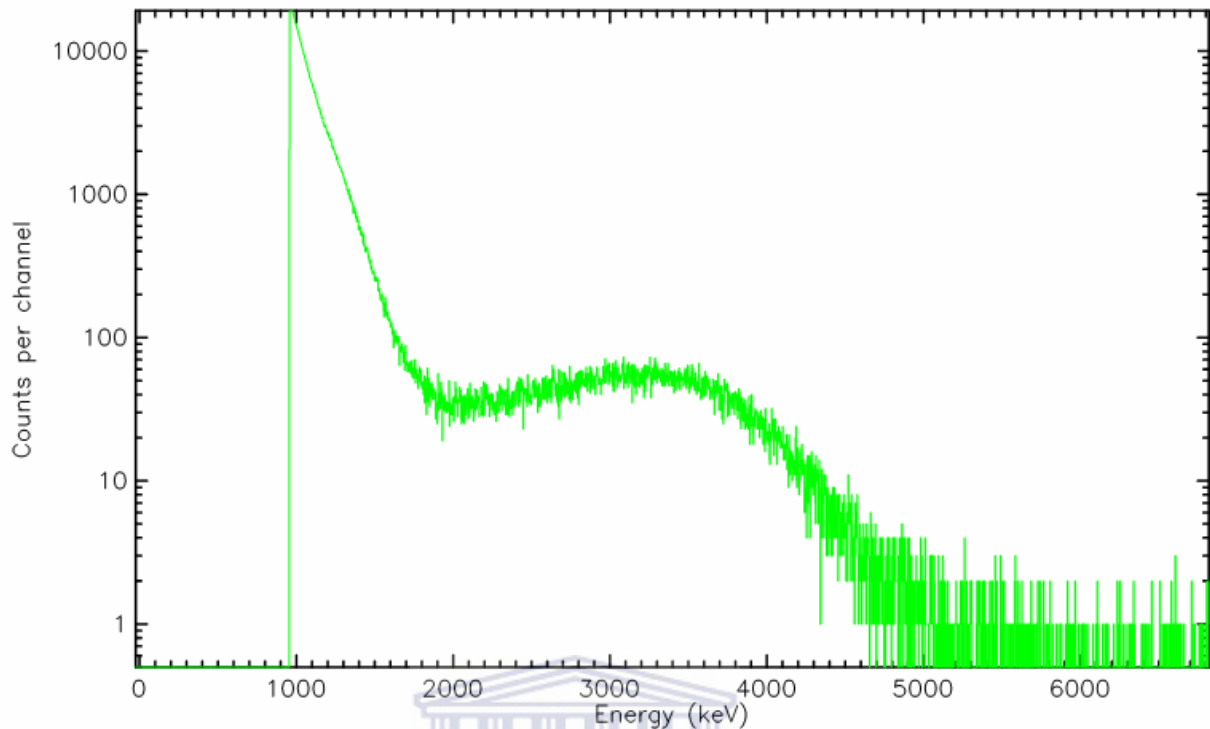
Fig. 4.19: The energy spectrum from PIN diodes obtained with Mts+Tu 950 (glass) sample.
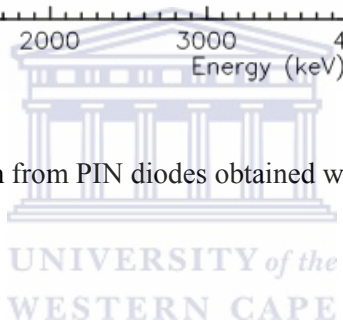
The spectrum in Fig. 4.18 was obtained by scanning part C of Fig. 4.1.This spectrum shows fewer counts of α-particles emitted from this region as compared to other spectra in the same sample. The spectrum in Fig. 4.19 was obtained by reducing the scan size on Fig.4.1 C and the counting statistics is improved. The amount of boron in this region was 0.81 wt %. The calculated concentrations of B in these samples are in Table 4.5. Figs. 4.15-4.19 show that the boron counts in this sample are not the same. This relates to different types of minerals within the sample. This means that the beam was focused on the region where the minerals have less amount of boron (Fig. 4.16 and Fig. 4.18) and also where the amount of boron was higher (Fig. 4.15, Fig. 4.17 and Fig. 4.19). Since there where cracks and holes in the samples, these might have also affected these results.
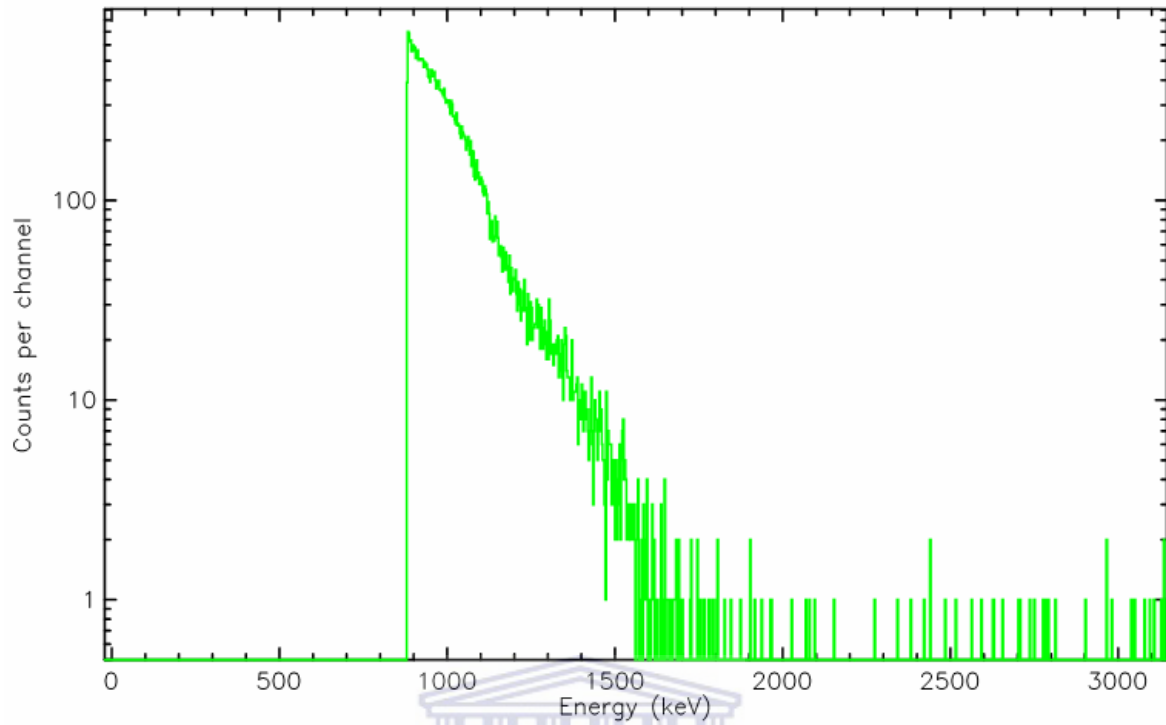
Fig. 4.20: The energy spectrum from PIN diodes obtained with quartz sample.
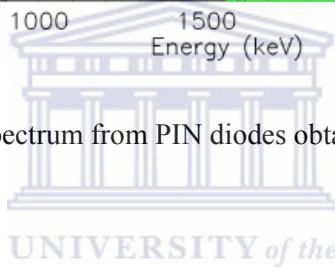
The energy spectrum from a quartz target (Fig. 4.20) shows the energy range (900-1600 keV) of oxygen. This measurement was made to avoid the influence of oxygen when selecting the energy window for boron, since the lower part below the selected energy range of the above spectra to the left is the α-particles from oxygen and is neglected **[3]**. The energy range of beryllium from beryllium standard (Fig. 4.21) is between 900-1200 keV. These energy ranges were made following the NRA analysis procedure as applied to all the measurements.
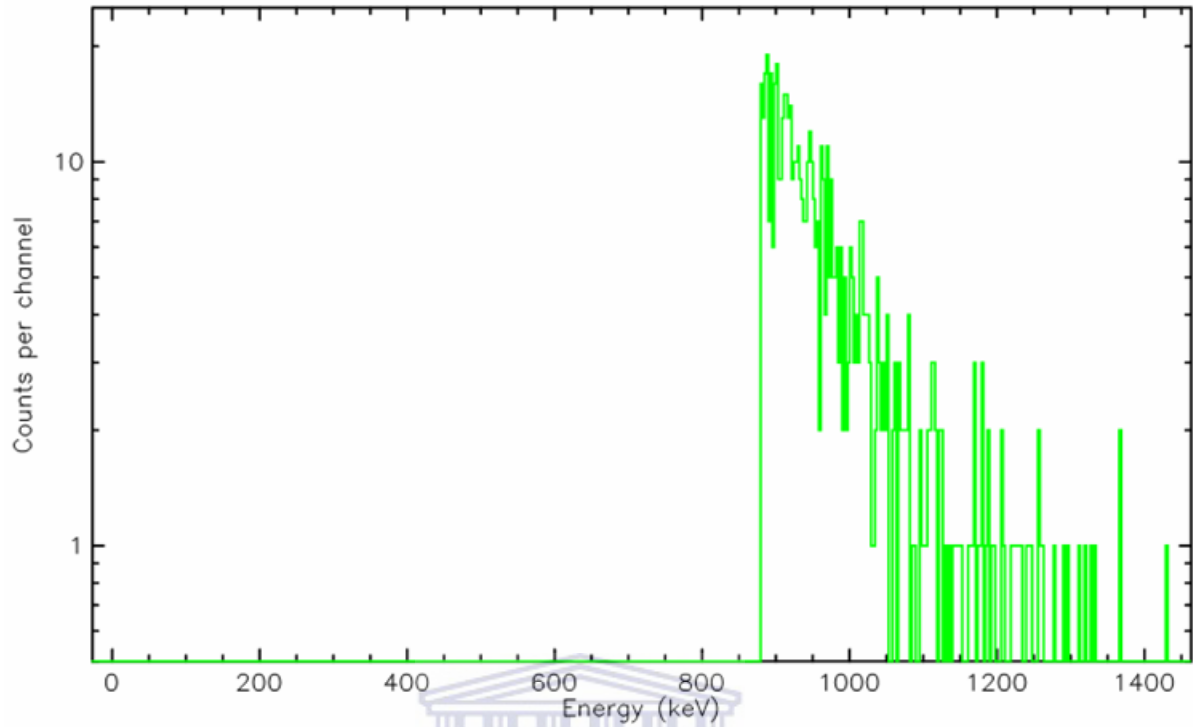
Fig. 4.21: The energy spectrum from PIN diodes obtained for pure Be spectrum.

Table 4.4: NMP B acquired data using NRA from Mts+Tu 950 (glass) samples.

Minerals	Area(counts) ×10⁴	Charge(μC)	B yield (counts/μC) ×10⁴
Region 1	1.73±0.014	0.141±0.0001	12.3±0.62
Region 2	1.31±0.012	0.168±0.0001	7.79±0.39
Region 3	0.457±0.007	0.068±0.0001	6.76±0.35
Region 4	1.48±0.013	0.229±0.0001	6.46±0.33
Region 5	1.21±0.011	0.182±0.0001	6.63±0.34
Region 6	1.29±0.012	0.184±0.0001	7.00±0.36
Region 7	12.12±0.03	1.560±0.0001	7.77±0.39
Region 8	1.67±0.013	0.220±0.0001	7.6±0.38

The elemental maps shown in the figures below were acquired in NAC XSYS-VAX data acquisition format and data were reduced at iThemba LABS NMP facility. The maps are used to identify the position of the samples, the elements in the sample and their distribution within the sample. They also help to extract the region of interest to see what you can find in that region. The standards and glass samples were scanned using the nuclear microprobe to test the capability of the set-up in producing elemental maps and identifying the phases where boron resides. The distribution of energy range below boron (O-keV) range, boron (B-keV) and lithium (Li-keV) elements in these samples recorded by NMP, NRA technique and PIN photodiodes detector are illustrated in Figs. 4.22-4.30. After extracting the region of interest we obtained the B yield (counts/charge).


(a)   (b)
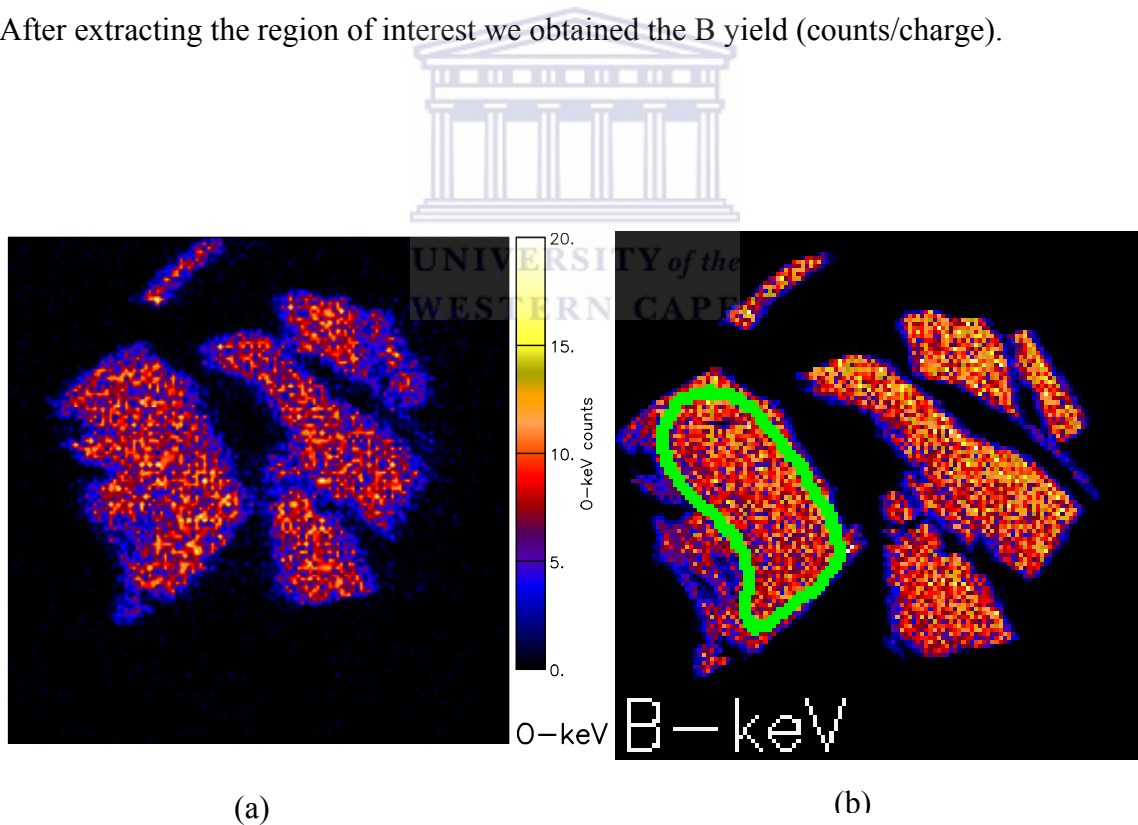
Fig. 4.22: The distribution of energy range (a) below B range and (b) boron maps from pure B standard obtained before realignment of the setup.

Fig. 4.22 and Fig. 4.24 show the distribution of energy range below B range and boron maps obtained from pure boron and BN standards before the realignment of the experimental setup, with the good energy calibration (Fig. 4.4). These maps are comparable with maps obtained after the realignment (Fig. 4.23 and Fig. 4.25) and do not show any difference in distribution. This shows that the electronic noise is not a prohibitive factor in quantitative analysis of boron.
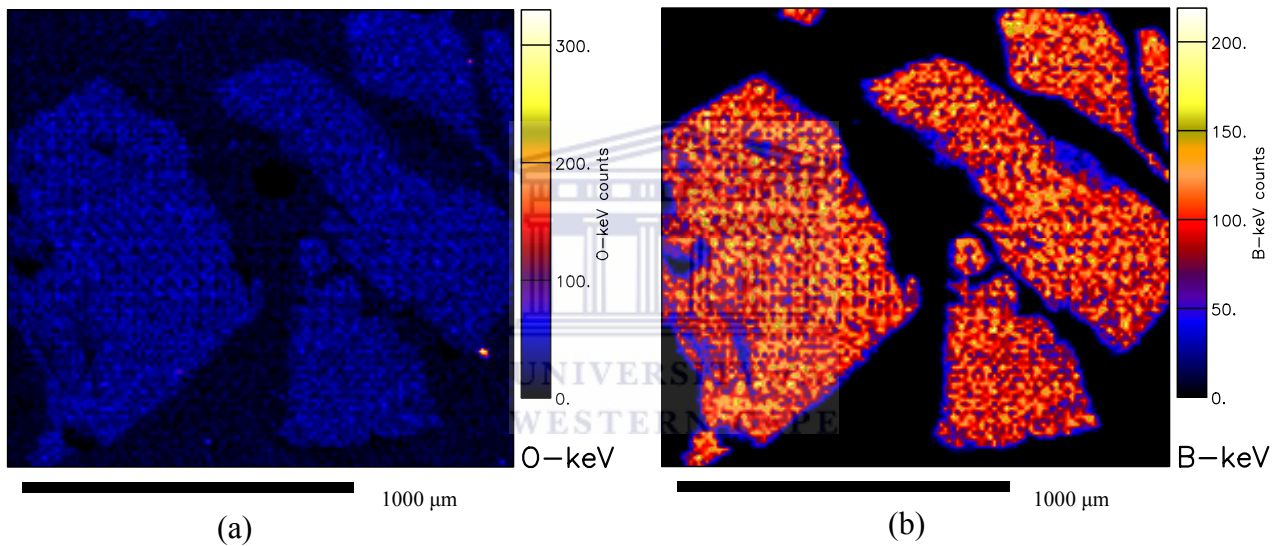

Fig. 4.23: Distribution of energy range (a) below B range and (b) boron maps from pure boron standard.

Fig. 4.23 (a) represents a distribution of counts in the energy range below B range and (b) boron maps from the pure boron standard respectively as obtained with the electronic noise inside the experimental chamber (Fig. 4.6). The shape and the position of the sample can be clearly seen from the above maps. Since it is a pure boron standard we expect 99.9% amount of boron.

Fig. 4.24 shows the maps A and B obtained by the surface barrier detector (SBD) and PIN photodiodes detector from BN standard respectively. The map A shows fewer counts that the map B which means the PIN diodes detector was more effective than the SBD. Fig. 4.25 show the distribution of counts in (a) the energy range below B range and (b) boron maps obtained when scanning the beam over the BN standard respectively. The maps clearly define the position and shape of BN target sample. From these maps we select a region (as indicated from Fig. 4.24B) with high boron content and obtain the boron yield (counts/charge) for calibration purposes.
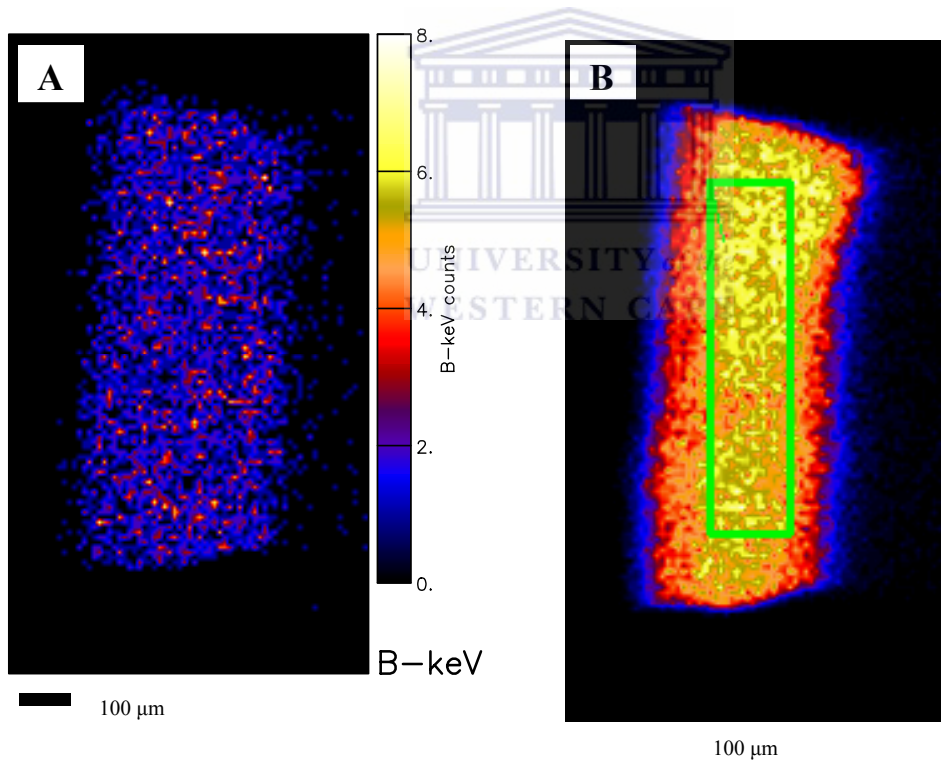

Fig. 4.24: Distribution of boron from BN maps

(A) Obtained by a SBD

(B) Obtained by a PIN diodes detector

B−keV

100 μm

(a)

O−keV

100 μm

(b)

B−keV

100

(a)

O−keV

100

(b)
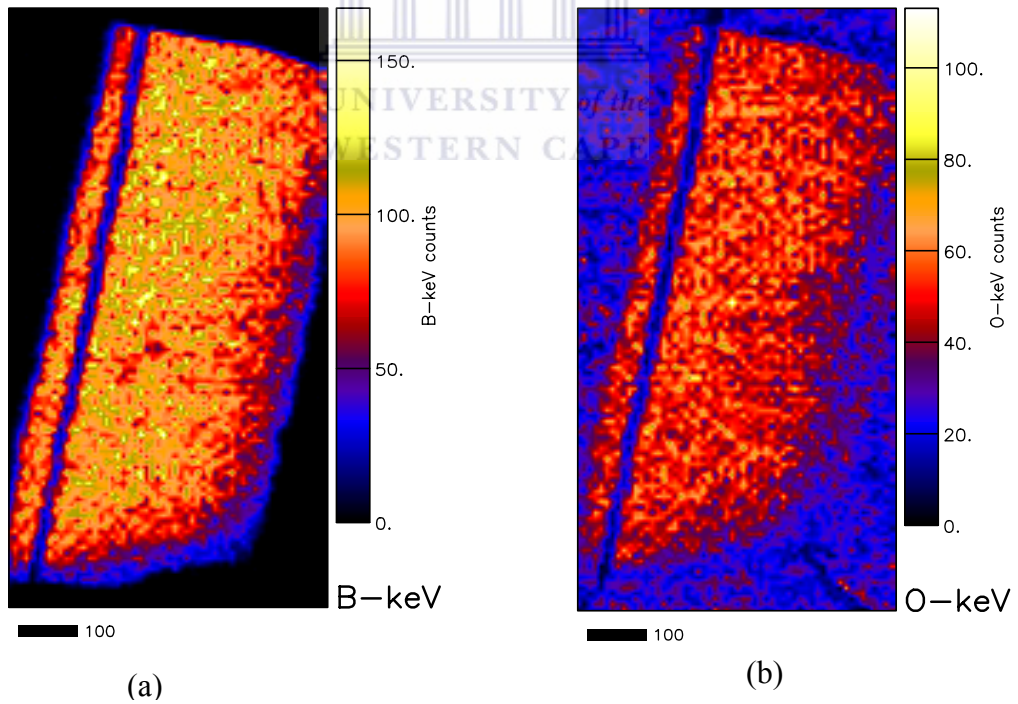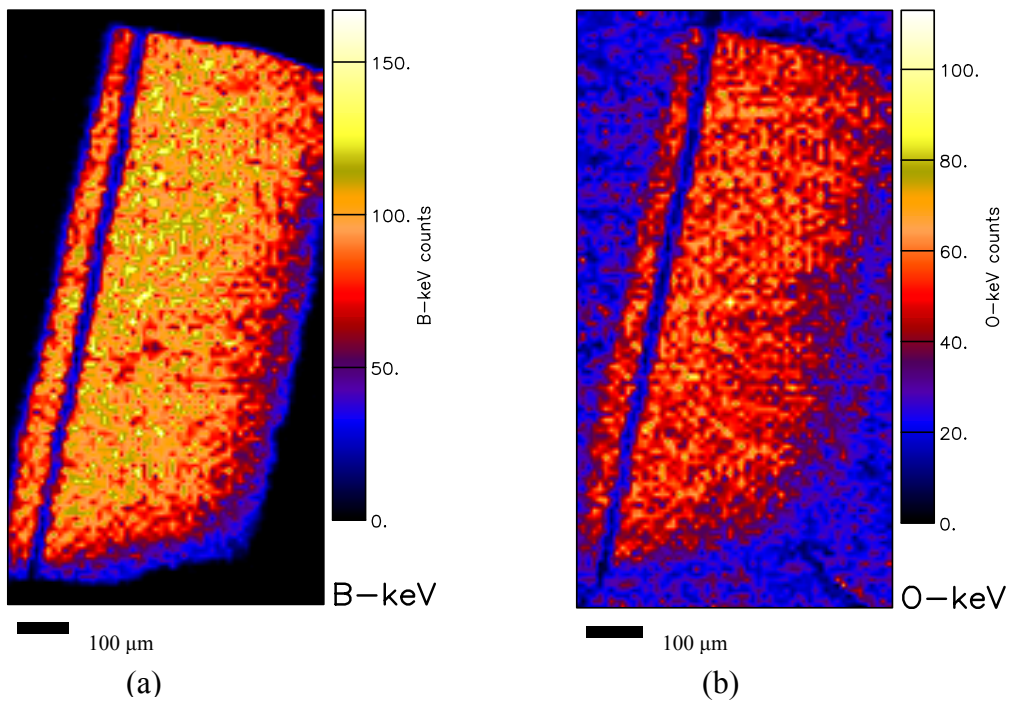
Fig. 4.25: Distribution of counts in the energy range (a) below B range and (b) boron from BN maps of standard.
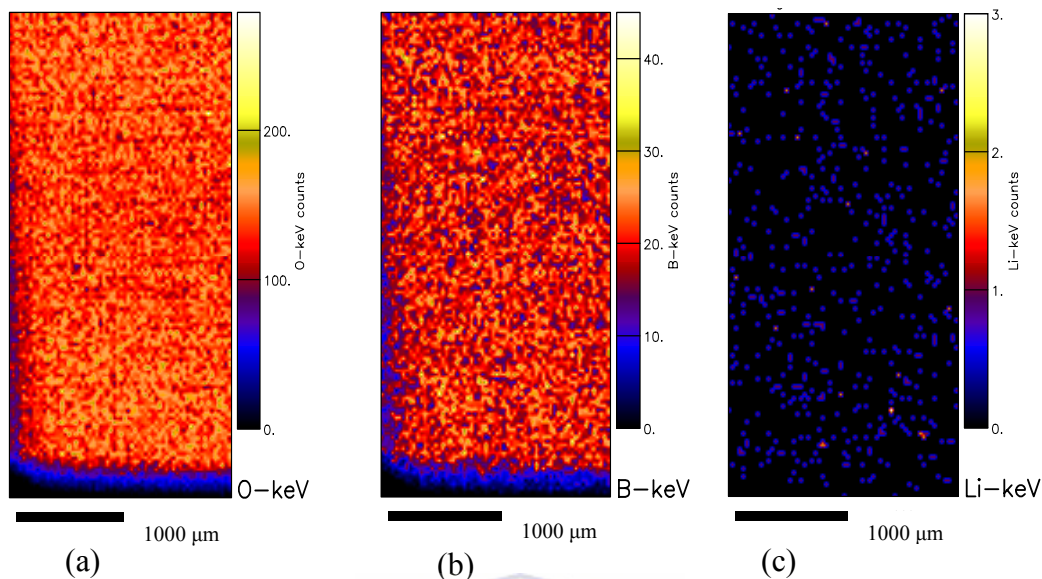
Fig. 4.26: Distribution of counts in the energy range (a) below B range, (b) boron and (c) lithium maps from tourmaline.

The maps of the distribution of counts in (a) the energy range below B range, (b) boron and (c) lithium from tourmaline sample are presented in the Fig. 4.26. These maps display a homogenous boron distribution within tourmaline sample. In tourmaline we observed some lithium counts as seen from the above map. The boron yield (counts/charge) was then obtained from both the above standards and the unknown samples. The obtained boron yield with the concentration from the standards was used to obtain the linear regression curves in Fig .4.9 and Fig. 4.10. The linear regression was used with the B yield from the unknown samples to obtain the concentrations and the detection limit of boron.
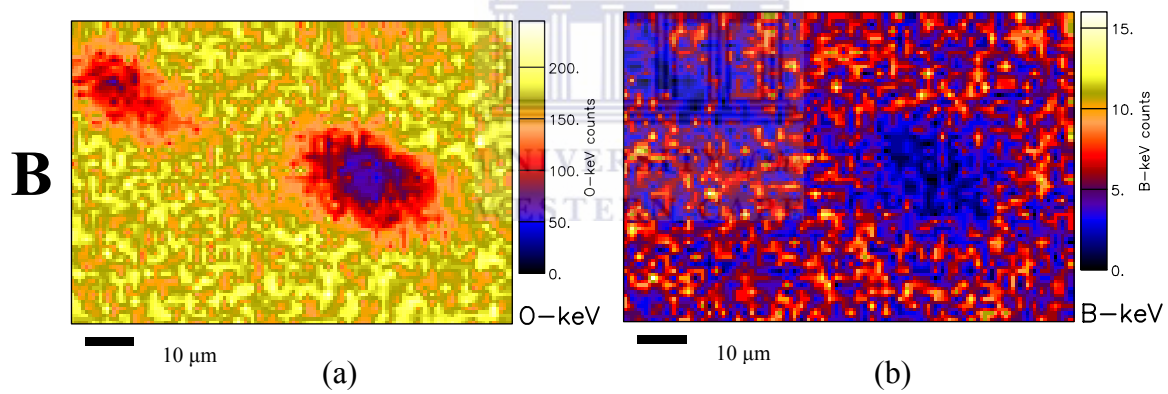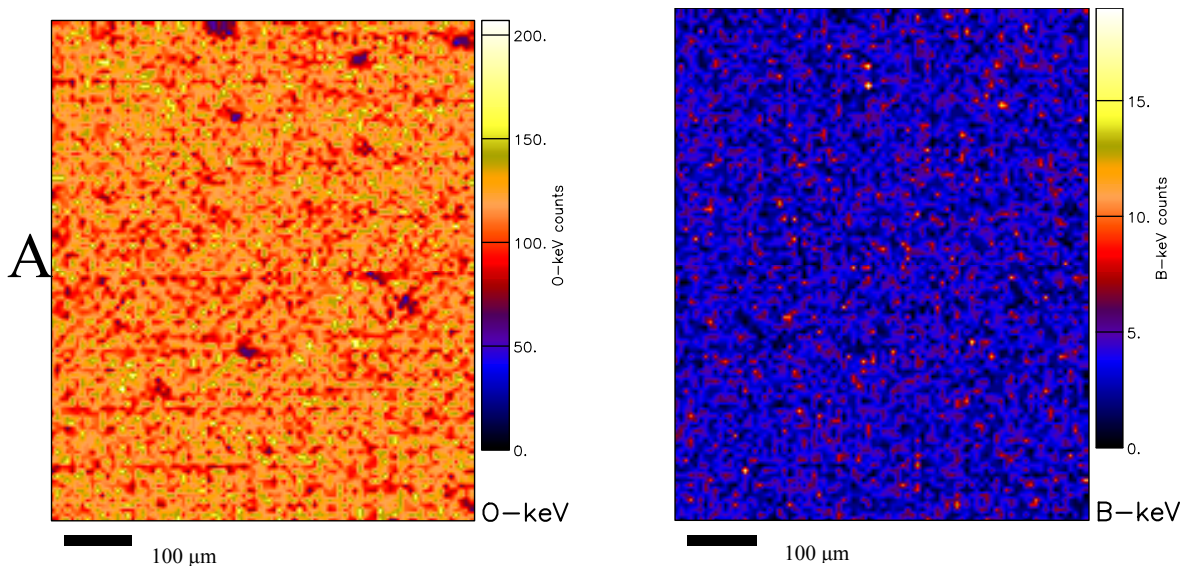
Fig. 4.27: Distribution of counts in the energy range (a) below B range and (b) boron maps from Mts+Tu 950 (glass) sample.
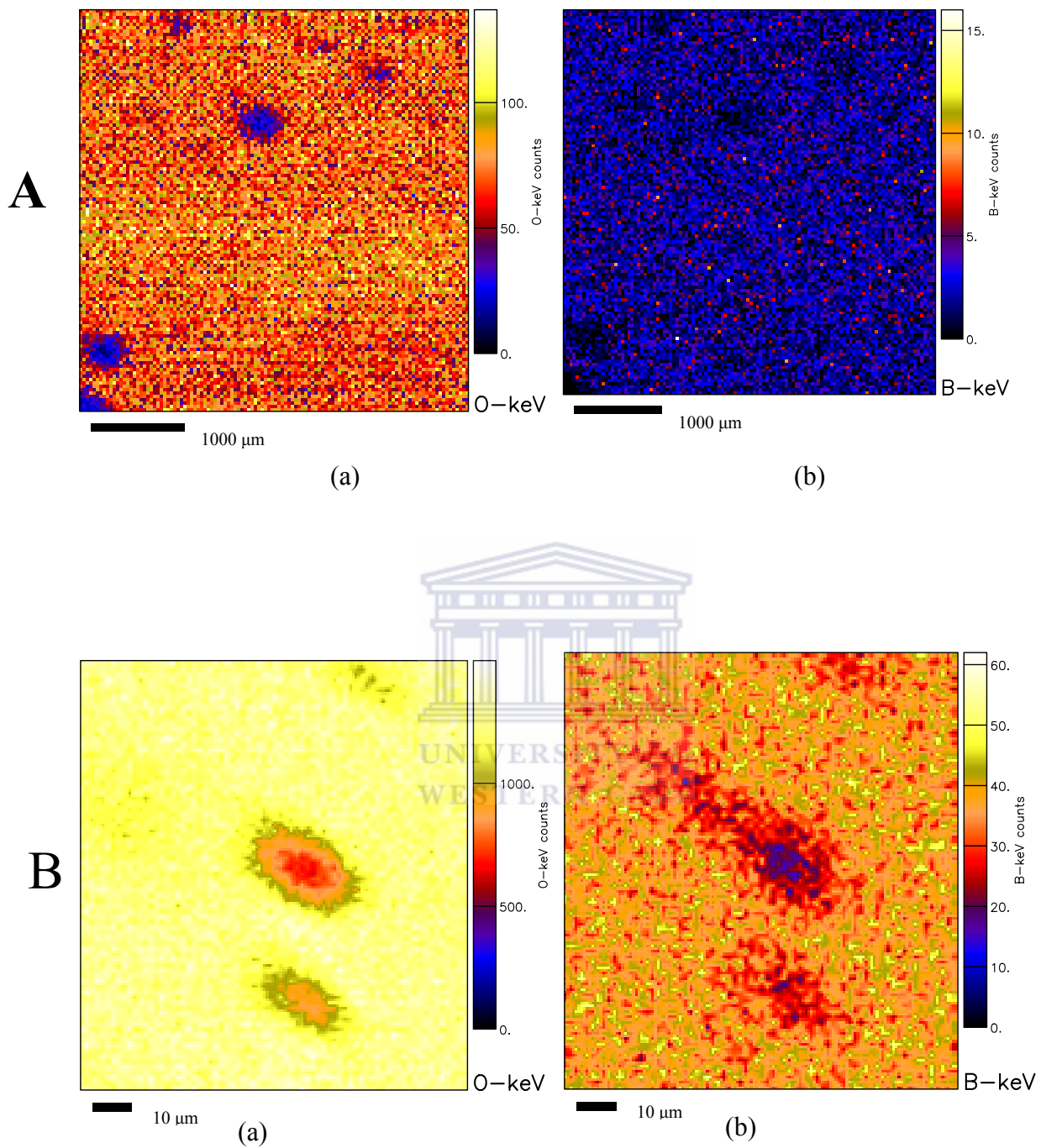
Fig. 4.28: Distribution of counts in the energy range (a) below B range and (b) boron maps from Mts+Tu 950 (glass) sample.
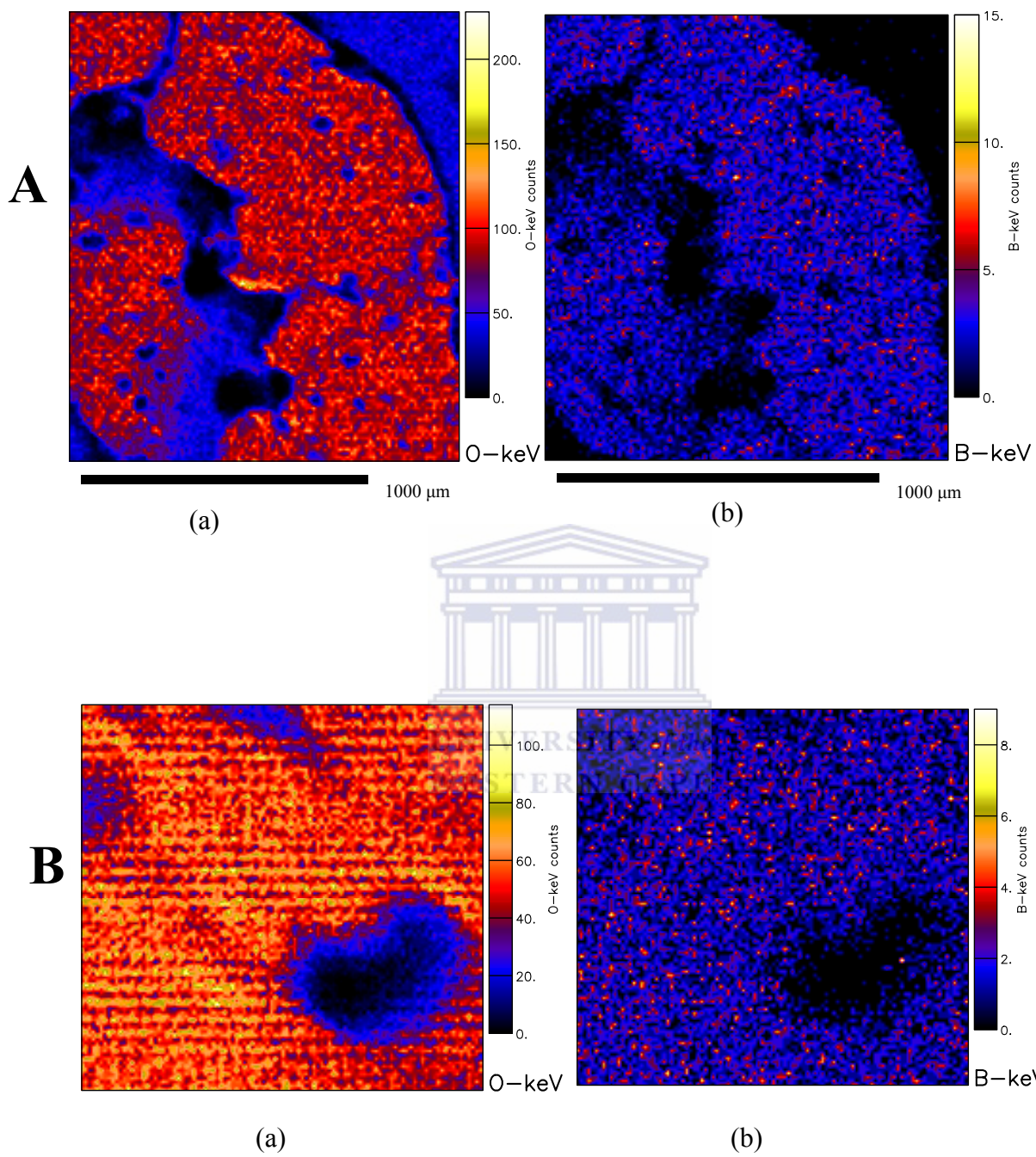
Fig. 4.29: Distribution of counts in the energy range (a) below B range and (b) boron maps from Mts+Tu 950 (glass) sample.
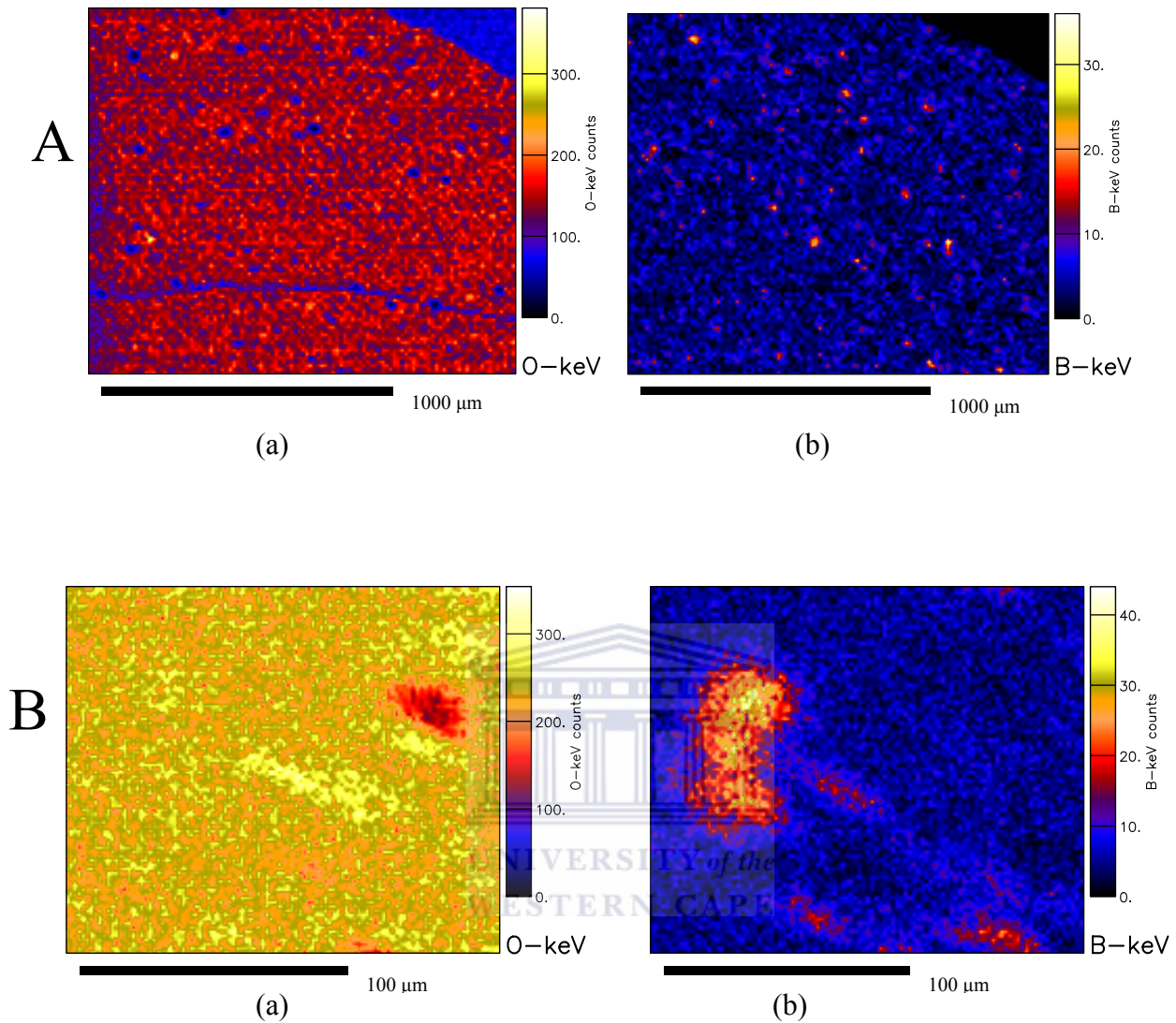
Fig. 4.30: Distribution of counts in the energy range (a) below B range and (b) boron maps from Mts+Tu 950 (glass) sample.

In order to demonstrate the capability of the set-up to produce elemental maps, distribution of energy range below B range and boron maps were also recorded for Mts+Tu 950 glass samples which have a low boron concentration. The maps of Mts+Tu 950 glass samples are presented in Figs. 4.27-4.30 respectively. These maps were obtained by first scanning the proton beam across the whole sample and then extracting

small region within the sample, i.e. by reducing the scan size to a small size. This was done so that we can select the correct region of boron and not to analyze the surroundings of the materials, since we were not certain about the location and distribution of boron within the glass sample.

Fig. 4.27 A was obtained by scanning part A2 of Fig. 4.1. The scan size was reduced to a small size and map in Fig. 4.27 B was then obtained. The concentrations of boron in these regions were 1.05 and 1.02 wt % respectively. Fig. 4.27 A shows homogeneous distribution of the elements while Fig. 4.27 B shows that the distribution of elements is homogeneous except in some small areas where there are holes (dark circles) in the sample. Fig. 4.28 A was obtained by scanning the region of A1 of Fig. 4.1 and after reducing the scan size to obtain the map in Fig. 4.28 B with boron concentration of 0.67 and 0.61 wt % respectively.

Fig. 4.29 A was obtained by scanning B2 in Fig. 4.1 and the concentration was 0.58 wt %. The reduced scan size produced the map in Fig. 4.29 B with 0.49 wt % of boron concentration. Fig. 4.30 A was obtained by scanning C on Fig. 4.1 and the boron concentration there was 0.56wt %; and then the scan size has been reduced (C1 of Fig. 4.1) to produce Fig. 4.30 B with 0.81 wt % boron concentration. The concentration with bigger scan sizes yielded higher concentration except on part C of Fig. 4.1. These maps show that the concentrations were low and comparable within the Mts+Tu 950 glass samples (see Table 4.5).

Table 4.5: The boron yield (counts/µC) and B concentration (%) from Mts+Tu 950 (glass) samples.

Minerals	B yield (counts/µC) ×10^4	B conc. (wt %)
Region 1	12.3±0.62	1.05±0.05
Region 2	7.79±0.39	0.67±0.03
Region 3	6.76±0.35	0.58±0.03
Region 4	6.46±0.33	0.56±0.03
Region 5	6.63±0.34	0.57±0.03
Region 6	7±0.36	0.60±0.03
Region 7	7.77±0.39	0.67±0.03
Region 8	7.6±0.38	0.67±0.03

CHAPTER 5

Summary and conclusion

5.1 Summary

The aim of this study was to perform microanalysis of boron by NRA method and to reach the developmental phase in which routine, non-destructive boron analysis would be possible below 5ppm using the $^{11}B(p, \alpha)^8Be$ nuclear reaction. In order to demonstrate the effectiveness of the $^{11}B(p, \alpha)^8Be$ reaction with an incident proton beam of energy 670 keV, five set of standards and unknown samples with different boron concentrations were analyzed. The standards were used to calibrate the boron yield with respect to concentration in order to determine the concentrations of boron from the unknown specimen and the detection limit. The ^{228}Th source was used for energy calibration of the detector. The experiment was carried out with 6MV Van de Graaf accelerator at iThemba LABS nuclear microprobe (NMP). The beam of protons from the accelerator was directed to the target sample in the experimental chamber. The interaction of the proton beam with target sample leads to a nuclear reaction where α-particles are emitted. These α-particles were detected by PIN photodiodes detector. The results were analyzed using NRA technique by GeoPIXE software. Before the nuclear microprobe measurements, we took images of the Mts+Tu 950 (glass) samples with light microscopy and SEM technique to find the position of the sample in the specimen chamber. Due to electronic noise during the experiment, a new approach was adopted; the noise level has been significantly reduced by placing the insulator between the turbo-molecular pump and the

experimental chamber. We have conducted measurements on the samples after we optimized the new conditions; however the noise level again increased after realignment of the experimental setup. The results obtained from the standards and the unknown samples do not fall in the same concentration range. The elemental maps were also taken by scanning the proton beam across the samples with the beam scan size of 3×3 μm^2. The maps were used to extract the region of interest (boron region) to obtain the boron yield (counts/charge) by GeoPIXE software in the samples. The obtained boron yields from the standards with a known concentration of boron were used for the linear calibration curve of the detector. The linear trend obtained with the five set of standards (Fig. 4.9) show one standard BN plotted slightly up the linear trend. It was not used for the determination of detection limit, but instead was used to obtain the boron concentration from unknown specimen. The possible detection limit of boron ~ 8.6 ppm was obtained using the two points calibration. It has been shown in Tables 4.4 and 4.5 that different regions of Mts+Tu 950 glass samples were comparable. As seen from the above mentioned tables, the Mts+Tu 950 (glass) samples have very low boron concentrations.

5.2 Conclusion

It is adequate to use one boron standard for calibration purpose to achieve the detection limit of boron in the present study. The NRA technique with $^{11}B(p, \alpha)^8Be$ reaction at 670 keV is a suitable IBA method for the determination of Boron concentrations and some other light elements such as Li. In principle we can measure boron and lithium simultaneously, but we couldn't get the standard of lithium for calibration. The technique

was efficient in producing elemental maps with a good lateral resolution. Our NRA measurements have in fact been in agreement with previous studies that display a broad peak for boron analysis. The concentration of boron from the measured unknown samples was ranging between 0.17-1.05%. The aim of the study was not reached, but we managed to get the possible lowest detection limits (LDL) of 8.6 ppm for 100 counts per 1μC of accumulated charge, by using a two points calibration curve. The results obtained from the nuclear microprobe have proved that the NRA technique with $^{11}B(p, α)^{8}Be$ reaction is indeed a technique capable of microanalytical method for boron analysis. We have noticed that the obtained results were not affected that much by the noise level in the chamber.

5.3 Recommendations

❖ Before starting with the measurements eliminate the electronic noise first because it can affect the measurements.

❖ Make sure not to touch the connection of the experimental set-up when running the experiment.

❖ For this kind of measurements, consider long time run or higher beam current to acquire good statistics in energy spectrum.

APPENDIX

Energy resolution obtained from PIN photodiode detector using [228]Th source and were used for the energy calibration in Fig. 4.8.

Channel	Energy (keV)
1953.75	5423.33
2041.44	5685.56
2261.7	6288.29
2435.68	6778.5
3138.34	8784.37

Acquired NMP data for Mts+Tu 950 (glass) samples.

Minerals	Area (counts) ×10^4	Charge(μC)
Region 9	0.178±0.005	0.058±0.0001
Region 10	0.866±0.01	0.073±0.0001
Region 11	1.58±0.013	0.210±0.0001
Region 12	9.90±0.032	1.393±0.0001
Region 13	0.286±0.006	0.055±0.0001
Region 14	0.328±0.006	0.058±0.0001
Region 15	0.635±0.008	0.114±0.0001
Region 16	3.45±0.02	0.369±0.0001

The boron yield (counts/µC) and B concentration (wt %) from Mts+Tu 950 (glass) samples.

| Minerals	B yield (counts/µC) ×10⁴	B conc. (wt %)
Region 9	3.08±0.17	0.17±0.01
Region 10	11.8±0.61	0.61±0.05
Region 11	7.54±0.38	0.38±0.03
Region 12	7.11±0.36	0.36±0.03
Region 13	5.23±0.28	0.28±0.02
Region 14	5.67±0.30	0.3±0.02
Region 15	5.56±0.29	0.29±0.02
Region 16	9.35±0.47	0.47±0.04
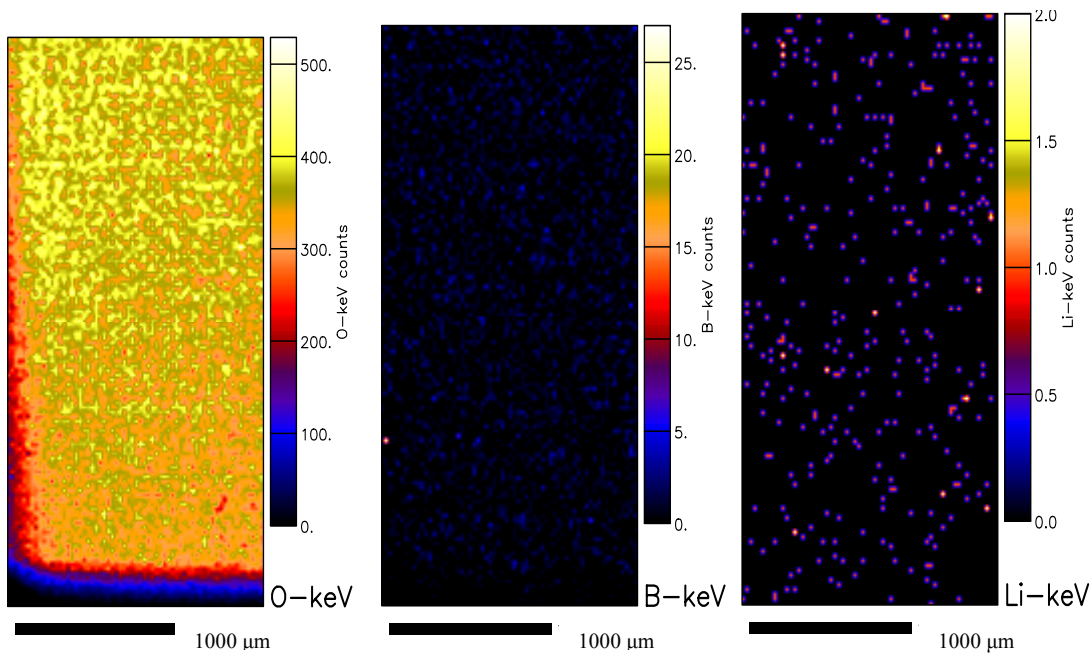
(a)   (b)   (c)

Distribution of counts in the energy range (a) below B range, (b) boron and (c) lithium maps from NIST 611

(a)

(b)
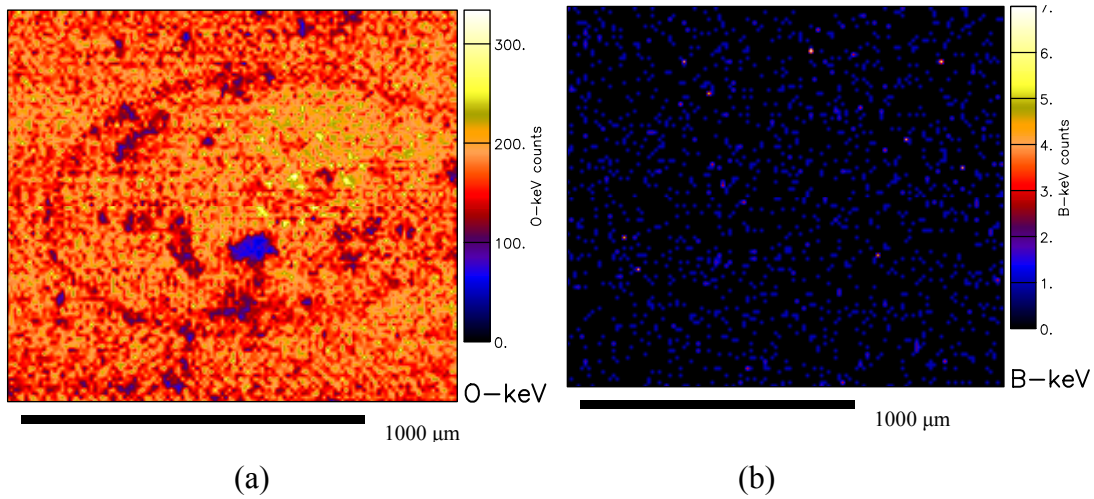
Distribution of counts in the energy range (a) below B range and (b) boron maps from NIST 612.
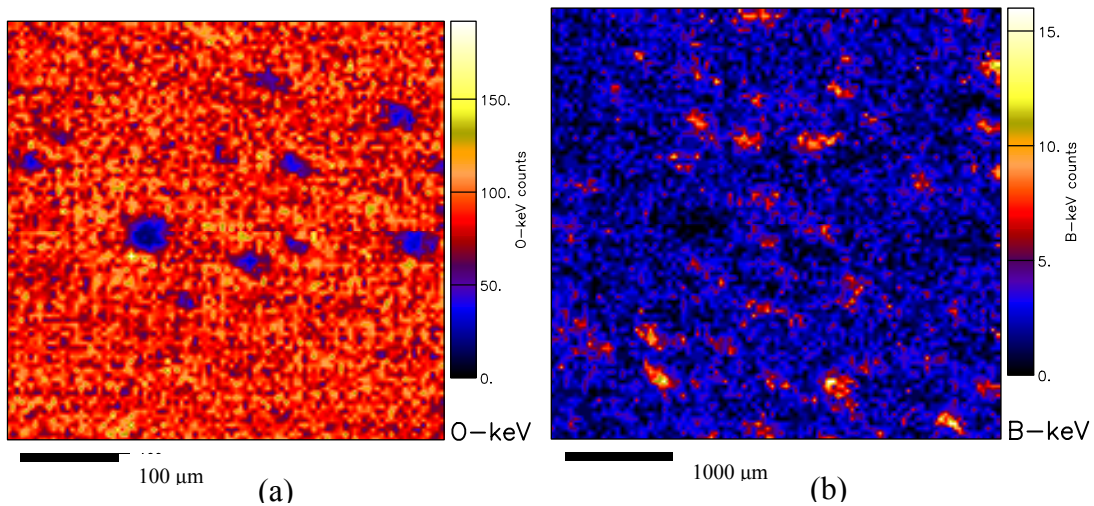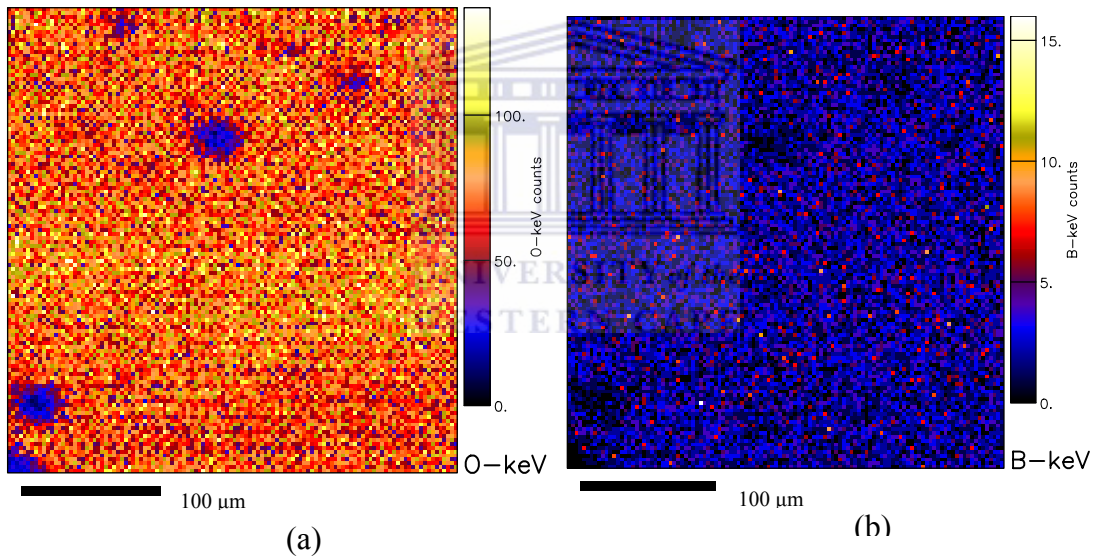
(a)

(b)

(a)

(b)

The maps of counts in the energy range (a) below B range and (b) boron maps from Mts+Tu 950 (glass) samples.
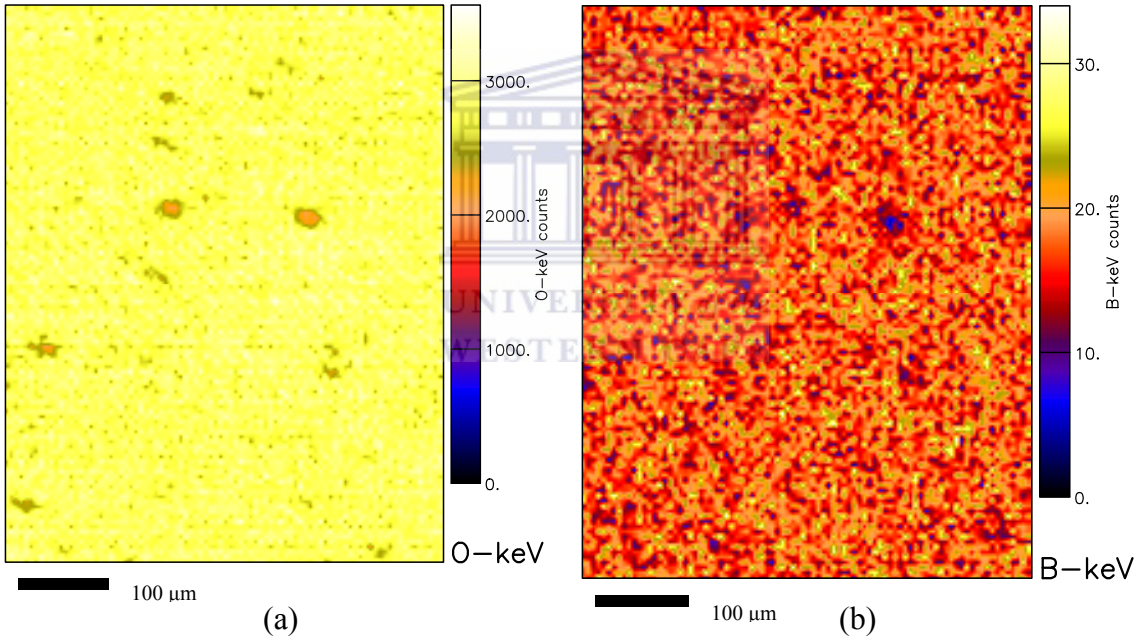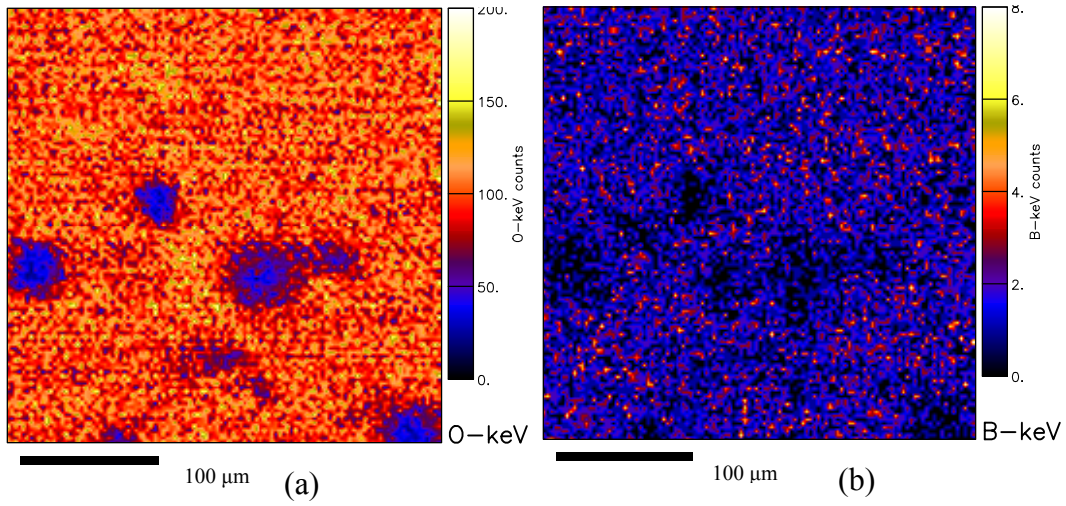
The maps of counts in the energy range (a) below B range and (b) boron maps from Mts+Tu 950 (glass) samples.
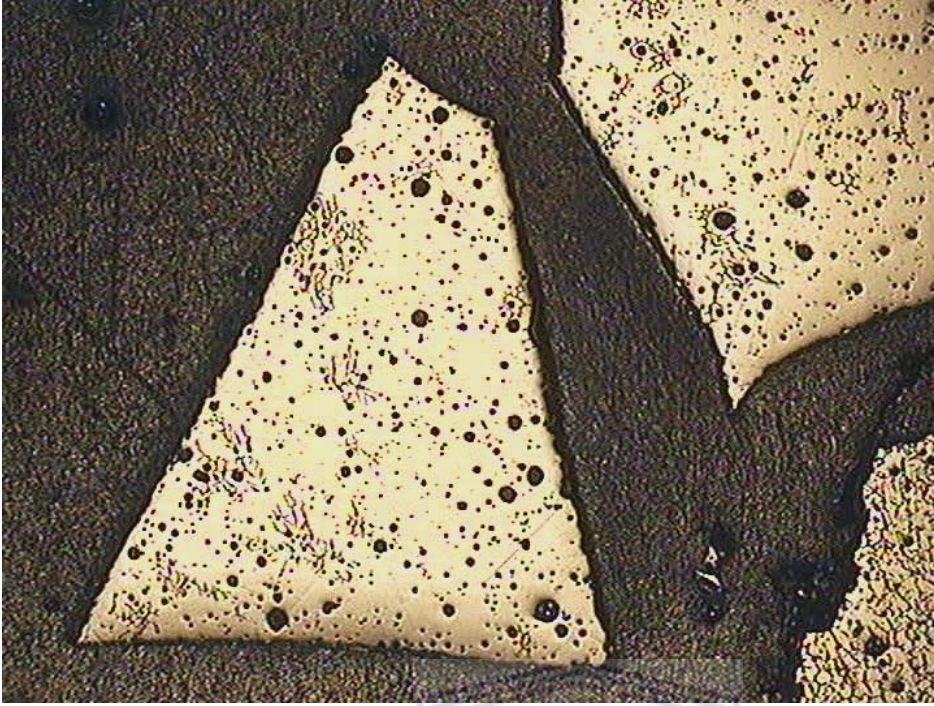
Optical light microscopy images of Mts+Tu 950 (glass) samples.
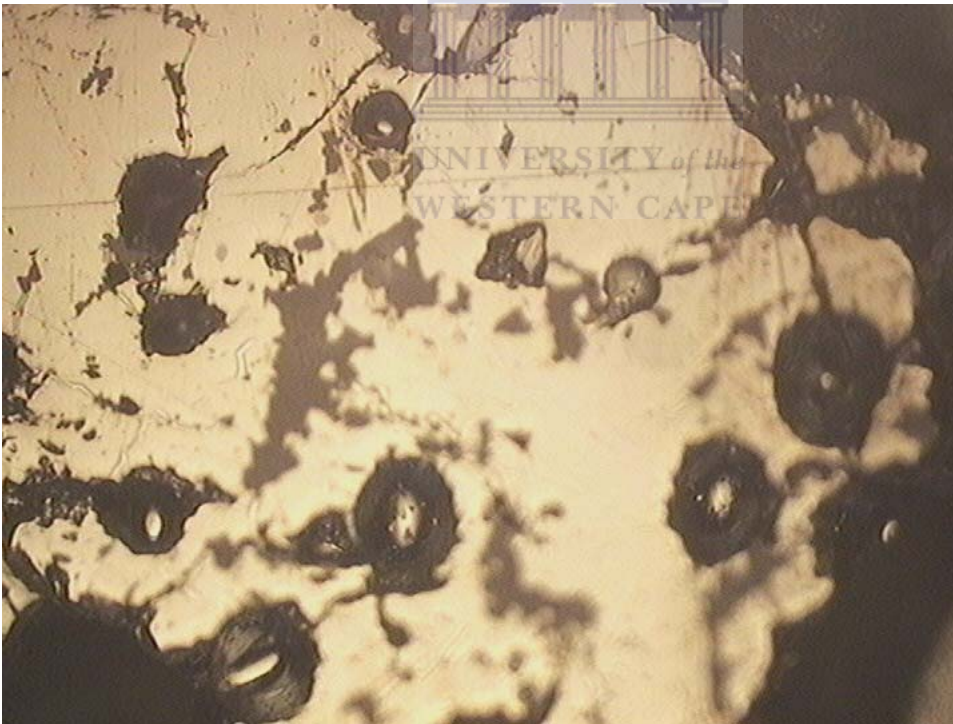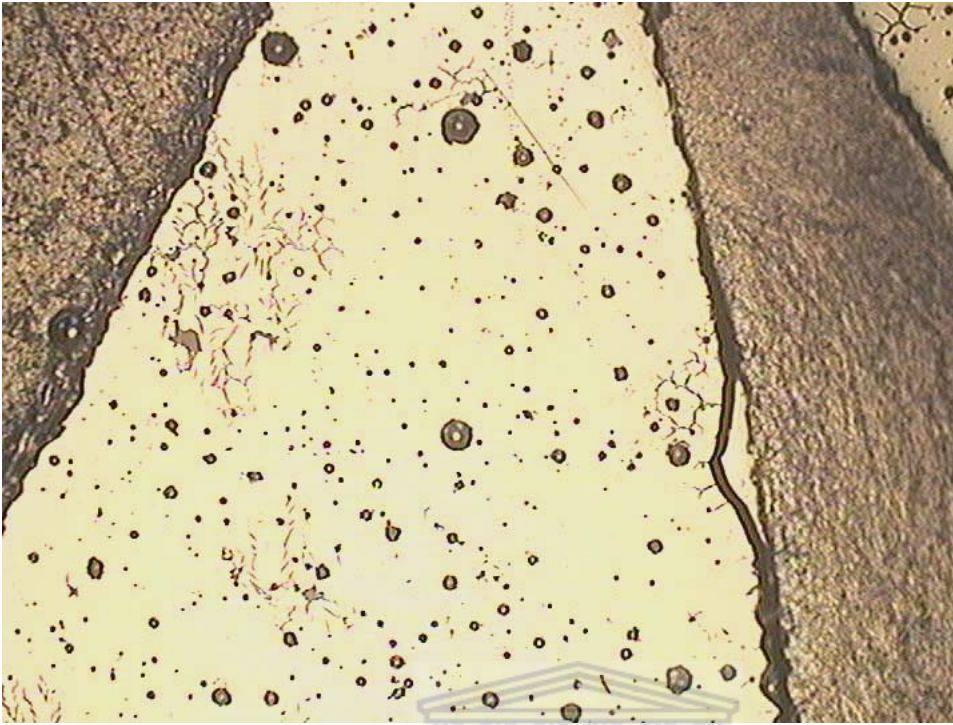
Optical light microscopy images of Mts+Tu 950 (glass) samples.

REFERENCES

[1] L. M. Anovitz and E. S Grew. Boron. Mineralogy, Petrology and Geochemistry. Review in mineralogy. Vol. 33 (1996) 1

[2] W.P. Leeman and V.B. Sission, (1996) Geochemistry of boron and its implications for crustal and mantle processs. Grew, E.S and Anovitz, L.M, Eds. Boron –Mineralogy, Petrology and Geochemistry, 33,805-820. Review in Mineralogy, Mineralogical Society of America, Washington D.C.

[3] Henrik Skogby, Per Kristiansson, and Ulf Hålenius. An assessment of nuclear microprobe analyses of B in silicate minerals. American Mineralogist Vol. 88 (2003) 1601-1604

[4] N. Moncoffre. Analysis of boron by charged particle bombardment. Nucl. Instr. and Meth. In Phys. Res. B66 (1992) 126-138

[5] Liu Jiarui, Lu Xinming, Wang Xuemei, Chu Wei-Kan. Cross-sections of 11B(p,α)8Be reaction for boron analysis. Nucl. Instr. and Meth. In Phys. Res B 190 (2002) 107-111

[6] P.J Scanlon, M.C Ridgeway and H.H. Brongersma. Detection of surface accumulation of dopants in rapid-thermally-annealed, shallow-implant silicon. Nucl. Instr. and Meth. In Phys. Res B45 (1990) 615-617

[7] Li Fuhe, K Marjorie, Balazs and Raymond Pong. Total dose measurements for ion implantation using laser ablation ICP-MS[†]. J. Anal. At. Spectrum. 2000, 15, 1139-1141.

[8] P.J. le Roux P, S.B Shirley, L. Benton, E.H. Hauri, T.D. Mock. In situ, multiple-multiplier, laser ablation ICP-MS measurement of boron isotopic composition ($\delta\,^{11}B$) at the nanagram level. Chemeical Geology 203 (2004) 123-138

[9] M. Mayer, A. Annen, W. Jacob, S. Grigull. The 11B(p,α0)8Be nuclear reaction and 11B(p,p)11B backscattering cross-sections for analytical purposes. Nucl. Instr. and Meth. In Phys. Res B 143 (1998) 244

[10] Liao Changgeng, Jian Hui, Wang Yongqiang, Zheng Zhiahao. Boron depth profiles in Silicon and simulation α-spectra layer. Nucl. Instr. And Meth. In Phys. Res B 95 (1995) 97-101

[11] M. Vollmer, J. D. Meyer, R. W. Michelmann, K. Bethge Boron detection using the nuclear reaction ^{11}B(p, α)2α. Nucl. Instr. and Meth. In Phys. Res B 117 (1996) 21-25

[12] Yong Joon Park, Pyo Hyung Yeal, Kyuseok, Chul Song Byoung, Yong Jee Kwang, and Won-ho Kim. Determination of Boron isotopic Ratio by Using an Alpha Track Technique. Bull. Korean Chem. Soc. 2006, Vol.27, No.10 1609-1612

[13] P. Kristiansson, U. Hålenius, H. Skogby, M. Elfman, K. Malmqvist, J. Pallon. Boron distributions in single crystals investigated with nuclear rection microanalysis. Nucl. Instr. And Meth. In Phys. Res B158 (1999) 562-567

[14] P. Kristiansson, S. Al-Suhaili, M. Elfman, K.G. Malmqvist, J. Pallon, K.A. Sjöland. Photo-tagged nuclear reaction analysis-evaluation of the technique for a nuclear microprobe. Nucl. Instr. and Meth. In Phys. Res B 136-138 (1998) 362-367

[15] N. Toulhoat, P. Courel, P. Trocellier and J. Gosset. Stability and distribution of lithium and boron in minerals. Nucl. Instr. and Meth. In Phys. Res. B77 (1993) 436-443

[16] S. Rio, N. Métrich, M. Mosbah, P. Massiot, Lithium, boron and beryllium in volcanic glasses and minerals studied by nuclear microprobe. Nucl. Instr. and Meth. In Phys. Res B 100 (1995) 141-148

[17] J.D. Robertson, and MD. Dyar, (1996). Nuclear methods for analysis of boron in minerals. In Grew, E.S and Anovitz, L.M, Eds., Boron –Mineralogy, Petrology and Geochemistry, 33,805-820. Review in Mineralogy, Mineralogical Society of America, Washington D.C.

[18] R. Lappalainen, J. Räisänen and A. Anttila. Analysis of boron using (p,α) reaction.Nucl. Instr. and Meth. In Phys. Res. B9(1985) 55-59

[19] N. Moncoffre, N. Millard, H. Jaffrezic, and J. Tousset, Boron analysis of thin layers using prompt nuclear techniques. Nucl. Instr. and Meth. In Phys. Res B 45 (1990) 81

[20] K.A Sjöland, P. Kristiansson, P. Tallone. Nuclear reaction analysis of boron for microbeam analysis of medical samples. Nucl. Instr. and Meth. In Phys. Res B 104 (1995) 255-260

[21] W. J. Trompetter, A. G. Reyes, I. C. Vickridge, A Markwitz. Lithium and boron in geological samples. Nucl. Instr. and Meth. In Phys. Res B 158 (1999) 568-574

[22] F. Watt and G.W. Grime, eds in: Principles and applications of high-energy ion microbeams. (1987)

[23] V. Prozesky, M., W. J. Przybylowicz, E. van Achterbergh, C. L. Churms, C. A. Pineda, K. A. Springhorn, J. V. Pilcher, C. G. Ryan, J. Kritzinger, H. Schmitt, T. Swart. The NAC nuclear microprobe facility. Nucl. Instr. and Meth. In Phys. Res B 104 (1995) 36

[24] S. A. E. Johansson, L. J. Campbell, K. G. Malmqvist, eds in; Particle Induced X-ray Emission Spectroscopy Vol. 133. 1995 John Wiley & Sons, Inc

[25] K. Strijkmans. Charged particle activation analysis. Chemical analysis by nuclear methods edited by Alfassi Z.B.,© 1994 John Wiley and Sons Ltd. 215-216

[26] U. Hålenius, P. Kristiansson, H. Skogby. Boron subtitution in diopside evaluated through 11B nuclear reaction reaction analysis. Phys. Chem. Minerals, 27 (2000) 681-688

[27] Micharl Sanborn and Kelvin Telmer. The spatial resolution of LA-ICP-MS line scans across heterogeneous materials such as fish otoliths and zoned minerals. J. Anal. At. Spectrom., 2003,18,1231-1237

[28] G. Dearnaley, G.A. Dissanaike, A.P. French, and G. Lindsay Jones. Study of B11 + p reactions. Physical Review, Vol. 108, Number 3, November 1, 1957

[29] A Anttila., R. Hänninen and J Räisänen. Proton-induced thick- target gamma-ray yields for the elemental analysis of the Z=3-9, 11-21 analysis. Journal of Radioanalytical chemistry, Vol. 62, No. 1-2 (1981) 293-306

[30] B. Nsouli, T. Darwish, K. Zahraman, A. Bejjani, M. Roumié, J.P. Thomas. Total boron assessment in soil samples from dry Mediterranean region using the thick target-particle induced gamma ray emission technique. Nucl. Instr. and Meth. In Phys. Res B 249(2006) 566-570

[31] Z. Elekes, Á. Kiss, I. Biron, T. Calligaro, J. Salomon.Thick targets γ-ray yields for light elements measured in the deuteron energy interval of 0.7 – 3.4 MeV. Nucl. Instr. and Meth. In Phys. Res B 168 (2000) 305

[32] K. A. Sjöland, P. Kritiansson, M. Elfman, K. Malmqvist, J. Pallon, R.J. Utui, C. Yang. The new nuclear reaction analysis facility at the Lund nuclear microprobe. Nucl. Instr. and Meth. In Phys. Res B 130 (1997) 20-24

[33] O. Beckman, T. Huus, and Č. Zupančič†. Excitation Curve for α Particles from B11 Bombarded with Protons. Physical Review, Vol. 91, Number 3, November 1, 1953

[34] P. Courel, P. Tocellier, M. Mosbah, N. Toulhoat, J. Gossset, P. Massiot and D. Piccot. Nuclear reaction microanalysis and electron microanalysis of light elements in minerals and glasses. Nucl. Instr. And Meth. In Phys. Res B 54 (1991) 429-432

[35] Sylvan Rubin. Elastic Scattering of Protons from [11]B and N[14†] . Physical Review, Vol. 103, Number 1, March 23, 1956

[36] J.C Overley and Ward Whaling. Highly Excited State in C11. Elastic Scattering of Proton by B[10†]. Physical Review, Vol. 128, Number 1, May 21, 1962.

[37] E.C. Lightowlers and A.T Collins. Determination of boron in natural semiconducting diamond by prompt particle nuclear microanalysis and Schottky barrier differential-capacitance measurement. J. Phys. D: App. Phys., Vol. 9, 1976

[38] C. Olivier, H.A Ras, M Peisach. Simultaneous determination of boron-10 and boron-11 under prompt bombardment. Journal of Radioanalytical Chemistry. Vol. 70, No. 1-2 (1982) 311-327.

[39] C. Olivier and M Peisach. Determination of [10]B by prompt proton spectrometry. Journal of Radioanalytical Chemistry. Vol. 12 (1972) 313-322.

[40] C. Olivier, H.J Morland, B.S. De Wet. Determination of lithium by boron spiking and proton irradiation. Journal of Radioanalytical and Nuclear Chemistry. Vol. 123, No. 2 (1988) 443-460

[41] C. Olivier and T.B. Pierce. The determination of boron in steels by measurement of the alpha-particles emitted during charged-particle irradiation. Radiochem. Radioanal. Letters Vol. 17, 5-6 (1974) 335-342
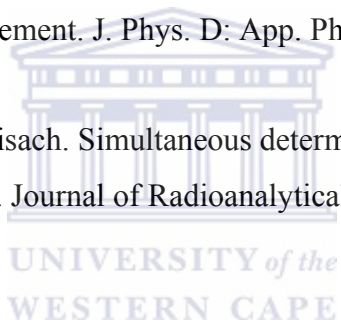
[42] J.G. Pearce Nicolas, T. Parkins William, A. Westgate John, P. Gordon Michael, E. Jackson Simon, R. Neal Clive and P. A Chenery Simon. Compilation of New and Published Major and Trace Element Data for NIST SRM 610 and NIST SRM 612 glass reference materials. Geostandards Newsletter. The journal of Geostandards and Geoanalysis. Vol. 21-no.1, p. 115-144

[43] C.G. Ryan 2000. Quantitative trace element imaging using PIXE and the nuclear microprobe. Int. J. Imaging Syst. Technol. 11:219-230

[44] M. Mayer, SIMNRA User's Guide, Report IPP9/113, Max-Plank-Institute für Plasmaphysik, Garching Germany, 1997

[45] Gusztáv Sziki, Erik Dobos, Zsófia Kertész, Zita Szikszai, Imre Uzonyi, Árpád Zoltán Kiss. A PIN detector array for the determination of boron using nuclear reaction analysis at a microprobe. Nucl. Instr. and Meth. In Phys. Res B 219-220 (2004) 420-424

[46] P. Kristiansson, G. Bengt Martinsson. Photo-tagged nuclear reaction analysis for trace element determination. Nucl. Instr. and Meth. In Phys. Res B 132 (1997) 159-176

[47] Lloyd A. Currie. Limits for qualitative detection and quantitative determination. Analytical Chemistry Division, National Bureau of Standards, Washington, D.C. 20234. Vol. 40, No. 3, March 1968, 587-593.

[48] D. Mookodi. The development of a micro-NRA setup for boron analysis. Master of Science in Applied Radiation Science and Technology, North West University, Mafikeng, 2006

[49] R.L. Hervig, (1996). Analysis of geological materials for boron by secondary ion mass spectrometry. In Grew, E.S and Anovitz, L.M, Eds. Boron –Mineralogy, Petrology and Geochemistry, 33,789-809. Review in Mineralogy, Mineralogical Society of America, Washington D.C.

[50] http://www.nac.ac.za/public/matservices.htm. Accessed 2007/05/23

[51] http://www.irb.hr/en/str/zef/z3labs/liis/metode. Accessed 2007/06/22

[52] http://nmp.csiro.au/ion-NRA.html. Accessed 2007/06/23

[53] http://mrw.interscience.wiley.com. Accessed 2007/12/07

[54]http://www.ansto.gov.au/environment/capabilities__and__facilities/secondary_ion_mass_spectrometry_sims/how_does_sims_work.htm. Accessed 2008/07/30

[55] http://www.cameca.fr/html/sims_technique.html. Accessed 2007/10/25

[56] [http://web.uvic.ca/~icpmslab/diag1.html. Accessed 2008/05/10

[57] http://web.uct.ac.za/depts/geolsci/facilities/icpms/lectures/lec4.html. Accessed 2008/05/10

[58] http://mse.iastate.edu/microscopy/whatsem.html. Accessed 2007/12/03

[59] http://mse.iastate.edu/microscopy/beaminteractions.html. Accessed 2007/12/03

[60] http://www.unl.edu/CMRAcfem/semoptic.htm. Accessed 2007/12/03

[61] http://nmp.csiro.au/GeoPIXE.html/ . Accessed 2007/12/03

[62] http://www.sales.hamamatsu.com/. Accessed 2007/06/04